UNIVERSITÀ DI SIENA 1240

Department of Experimental and Clinical Biomedical Sciences

University of Florence

Doctorate in Genetics, Oncology and Clinical Medicine

(GenOMeC)

XXXV Cycle (2019-2022)

Coordinator: Prof. Francesca Ariani

Optimization of Extracellular signal-regulated kinase5 (ERK5) targeting in melanoma

PhD candidate Zoe Lombardi

Tutor
Prof. Elisabetta Rovida

Supervisor
Prof. Barbara Stecca

Academic Year 2021/2022

Table of Contents

ABBREVIATIONS

AKT: Protein Kinase B (PKB)

AJCC: American Joint Committee on Cancer

AP-1: Activator Protein 1

ATCC: American Type Culture Collection

ATM: Ataxia-Telangiectasia Mutated

ATR: Ataxia Telangiectasia and Rad3-related

BAD: BCL-2 Antagonist of Cell Death

BCL-2: B-cell Lymphoma 2

BDNF: Brain Derived Neurotrophic Factor

BMK-1: Big Mitogen Activated protein Kinase

BMP: Bone Morphogenetic Proteins

BP: Bipartite

BRD: Bromodomain-containing Protein

BSA: Bovine Serum Albumin

CCLR: Clear Cell Renal Carcinoma

CD: Common Docking

CDC: Cell Division Cycle 37

CDK: Cyclin-Dependent Kinase

CDKN2A: Cyclin-Dependent Kinase Inhibitor 2A

c-Jun: Jun N-terminal Kinase

CML: Chronic Myeloid Leukemia

CRC: Colon Rectal Cancer

CSC: Cancer Stem Cells

CSF-1: Colony-Stimulating Factor 1

CTLA-4: Cytotoxic T-Lymphocyte Antigen 4

CXCR2: C-X-C Motif Chemokine Receptor 2

DDR: DNA-Damage Response

DENV: Dengue Virus

DMEM: Dulbecco's Modified Eagle's Medium

DMSO: Dimethyl Sulfoxide

DUSP: Dual-Specificity Protein Phosphatase

E2F: E2 Transcription Factor

ECM: Extracellular Matrix

EGF: Endothelial Growth Factor

EMT: Epithelial-Mesenchymal Transition

EOC: Epithelial Ovarian Cancer

ERK: Extracellular signal-Regulated Kinase

FAK: Focal Adhesion Kinase

FBS: Fetal Bovine Serum

FDA: Food and Drug Administration

FGF: Basic Fibroblast Growth Factor

GRO: Growth-Related Oncogene

HCC: Hepatocellular carcinoma

HEK-293T: Human Embryonic Kidney 293

HIF 1α: Hypoxia Inducible Factor 1α

HIV: Human Immunodeficiency Virus

HP1: Heterochromatic Protein 1

HSP: Heat Shock Protein

IBB: Importin-β1 Binding domain

IL-2: Interleukin 2

IL-6: Interleukin 6

IVM: Ivermectin

JNK1, 2, 3: c-Jun N-terminal Kinases 1, 2, 3

KPNB1: Karyopherin Subunit beta 1

LRRK2: Leucine-Rich Repeat Kinase 2

MAPK: Mitogen-Activated-Protein-Kinase

MC1R: Melanocortin-1 Receptor

MDM2: Murine Double Minute 2

MEF: Myocyte Enhancer Factor

MITF: Microphthalmia-associated Transcription Factor

MMPs: Metalloproteases

MP: Monopartite

MSCs: Melanoma Stem Cells

MSH: Melanocyte Stimulating Hormone

mTOR: Mammalian target of rapamycin

NLK: Nemo-Like Kinase

NES: Nuclear Export Signal or sequence

NF1: Neurofibromin 1

NF-κB: Nuclear Factor Kappa-light-chain-enhancer of activated B cells

NGF: Nerve Growth Factor

NGS: Next-Generation Sequencing

NLS: Nuclear Localization Signal or sequence

NPC: Nuclear Pores Complex

OIS: Oncogene-Induced Senescence

OS: Overall Survival

PD-1: Programmed cell Death protein 1

PDGF: Platelet-Derived Growth Factor

PML: Promyelocytic Protein

PR1/PR2: Prolin Rich Domain

PTEN: Phosphatase and Tensin Homolog

PTHrP: Parathyroid Hormone-related Protein

RAC1: Ras-related C3 botulinum toxin substrate 1

RB: Retinoblastoma Protein

ROS: Reactive Oxygen Species

RTK: Receptor Tyrosine Kinase

RSK: Ribosomal S6 Kinase

SA: Senescence Associated

SASP: Senescence-Associated Secretory Phenotype

SCF: Stem Cell Factor

SD: Standard Deviation

SEM: Standard Error of Mean

SDS-PAGE: Sodium Dodecyl Sulphate Polyacrylamide Gel Electrophoresis

SREBP: Sterol Regulatory Element-binding Protein

TAD: Transactivation Domain

TERT: Telomerase Reverse-Transcriptase

TGF-β: Transforming Growth Factor β

TNF-α: Tumor Necrosis Factor-α

TNM: Tumor-Nodes-Metastasis

US: United States

UV: Ultraviolet

VEGF: Vascular Endothelial Growth Factor

WHO: World Health Organization

YAP: Yes-Associated Protein 1

INTRODUCTION

1. MELANOMA

Malignant melanoma is one of the most aggressive types of cancer and is characterized by an abnormal proliferation of melanocytes. In the recent decade the incidence of cutaneous melanoma is strongly increasing worldwide. Globally in 2020 (Figure 1), 324 635 cases of melanoma were diagnosed and over 55 000 melanoma-associated deaths were reported, according to the World Health Organization (WHO). The American Cancer Society estimated that 99 780 new cases of melanoma will be diagnosed in the United States (US) in 2022 (57 180 for males and 42 600 for females) with 7 650 estimated deaths. Since the 1960s, the incidence of this cancer has increased in the Caucasian populations and melanoma has become one of the most common cancers in fair-skinned populations (Rastrelli *et al.,* 2014). Incidences were highest in New Zealand (35·8 per 100 000 person-years) and Australia (34·9 per 100 000 person-years). The incidence was 10·2 per 100 000 person-years in the EU and 13·8 per 100 000 person-years in North America (Schadendorf *et al.,* 2018). Currently, in the United States melanoma is the fifth most common cancer in men and the sixth most common in women. In Italy, about 14 900 new diagnoses of melanoma have been registered in 2020 (8 100 for men, 6 700 for women), with an increase of 20% compared to 2019, where 12 300 (6 700 for males and 5 699 for females) cases had been registered (https://www.aiom.it/i-numeri-del-cancro-in-italia).

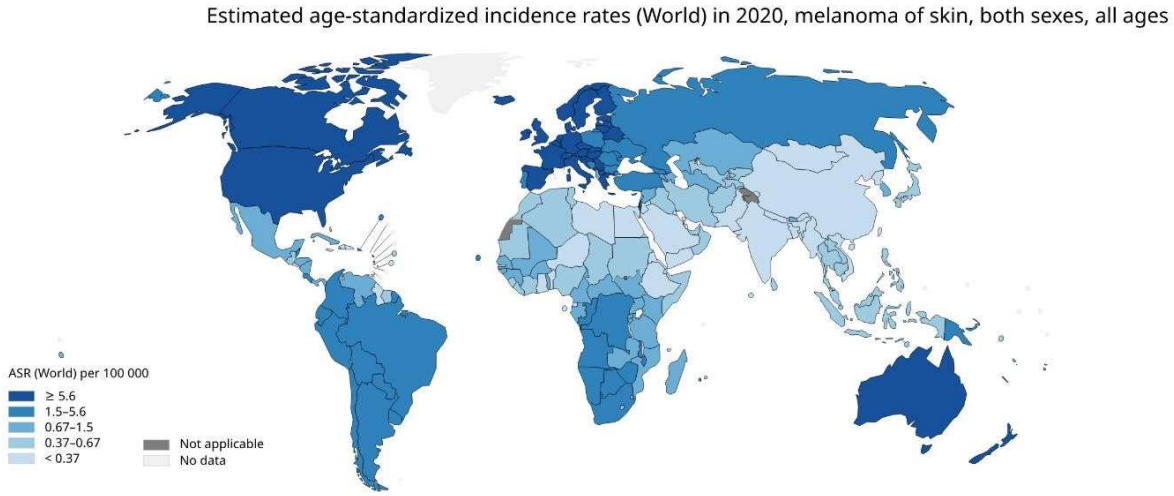

Figure 1. Incidence rate of melanoma worldwide. World Health Organization (WHO).

1.1 Risk Factors

The development of melanoma is due to both host and environmental factors, similarly to what happens in other types of cancer. The incidence of melanoma is strongly affected by ultraviolet (UV) exposure, pigmentation of the skin, geographic parameters (latitude and altitude), presence of congenital or acquired nevi, immune deficiency and genetic predisposition. The primary cause of cutaneous melanoma is the excessive exposure to UV rays from the sun and tanning lamps (especially in the first 35 years of life). It is established, indeed, that UV-elicited damage drives genomic instability, mutagenesis, and carcinogenesis and elicits the malignant transformation of melanocytes into melanoma (Filipp *et al.,* 2018). Exposure to sunlight can be intermittent (short and intense) or chronic (continuous over time): the intermittent exposure to UV rays and any related burns seem to represent one of the major risk factors in the onset of melanoma, conversely, the chronic pattern of exposure is more associated with actinic keratosis and non-melanomatous skin cancers (Rastrelli *et al.,* 2014). The UV spectrum is subdivided by wavelength into UVA (320-400nm), UVB (280-320nm) and UVC (100-280nm) rays. UVA and UVB radiations are responsible for the UV-induced skin damage, while exposure to UVC rays is prevented by the stratospheric ozone layer. Due to different electrophysiological properties of UVA and UVB, it is known that UVA radiation causes indirect DNA damage through the generation of reactive oxygen species, while UVB light causes direct DNA damage (Miller *et al*., 2008). Concerning the host risk factors, melanocytic nevi are benign accumulations of melanocytes or nevus cells and may be congenital or acquired. Approximately 25% of melanoma cases arise from a pre-existing nevus, so that the number of total nevi positively correlated with melanoma risk: patients with more than 100 nevi have a 7-fold increased risk of developing melanoma. Furthermore, the presence of atypical nevi (see below) is associated with a significantly higher risk of melanoma. An atypical nevus is usually large (larger > 5 mm) or giant (>20 cm), with variable pigmentation, irregular asymmetric outline, and indistinct borders (Rastrelli *et al.,* 2014). Phenotypic characteristics such as red hair, fair skin, numerous freckles, light eyes, sun sensitivity and an inability to tan, raise the risk of developing melanoma by approximately 50% (Titus-Ernstoff L *et al.,* 2005). Finally, it has been reported that approximately 10% of melanomas occur in a familiar context, in which the most common genetic abnormalities are mutations in cyclin-dependent kinase inhibitor 2A (CDKN2A or p16), in cyclin-dependent kinase 4 (CDK4) (Rastrelli *et al*., 2014) and in the master gene of melanocyte homeostasis microphthalmia-associated transcription factor (MITF).

1.2 Clinical Classification

Melanoma can be classified into 4 main clinical subtypes: superficial spreading melanoma (the most common type, representing about 70% of melanoma cases, that may arise de novo or in association with a nevus), nodular melanoma (representing 5% of melanomas and being more common in males than females; it is more aggressive and invasive than the other types, and is often related with the intermittent exposure to the sun), lentigo maligna melanoma (4%-15% of cutaneous melanomas, it arises with long-term sun exposure and increasing age) and acral lentiginous melanoma (uncommon in white people, whereas it is the most common type of melanoma among Asian, Hispanic and African patients; it affects especially female and elderly patients) (Markovic SN *et al.,* 2007). The universally accepted staging of cutaneous melanoma used in most scientific literature and international guidelines, is that of the American Joint Committee on Cancer (AJCC) which defines the stages of melanoma on the basis of the TNM (Tumor-Nodes-Metastasis) classification system. The TNM classification takes into consideration: the “thickness of the tumor" (calculated using the Breslow staging), lymph node involvement and any presence of metastases. According to TNM Classification, melanomas are currently categorized into six stages, stage 0 (no evidence of/or unknown primary tumor), Tis (the earliest stage, melanoma in situ), T1, T2, T3 and T4. Some of these are in turn divided according to the presence/absence of ulcerations using the capital letters A and B. The letter A means no ulceration while the letter B highlights its presence (Keung EZ and Gershenwald 2018).

1.3 Melanoma Progression

The development of malignant melanoma from normal melanocytes is characterized by some histological changes schematized in the Clark model (Clark *et al.,*1984). The first event described in this model event is the proliferation of normal melanocytes leading to benign nevi (step 1). In these cells the growth is limited by control mechanisms and a nevus rarely progresses to cancer, indeed the melanocytes are destined in most instances to follow a programmed pathway of differentiation that leads to disappearance of the nevus. However, if the pathway of differentiation is not followed, some nevi can acquire additional molecular lesions (these are the formal histogenetic precursors of melanoma and they occur after this aberrant differentiation) that abolish growth restraints by inducing the constitutive activation of signalling pathways involved in the enhancement of cellular growth, thus resulting in the

transformation into dysplastic nevi (step 2). The morphology of these dysplastic nevi may be characterized by asymmetry, increased diameter and irregular borders. The step 3 is termed radial-growth phase, where melanocytes can proliferate as isolated cells or arranged in small nevi, confined at the epidermis or papillary dermis. This phase can last for a few months to years, and such melanomas are not associated with metastasis and are characterized by the absence of aggressive behaviour and good prognosis. To acquire competence for metastasis melanoma must advance to the next step (step 4) of tumor progression: the vertical growth phase. In this step the cells within the tumor mass acquire the ability to invade the dermis and are capable of expansion, widening the papillary dermis as an expanding nodule. They acquire autonomous proliferation capacity and cohesive growth, with aggregate or nodule formation extending to the reticular dermis or subcutaneous tissue. The cells of the vertical growth are those that give rise to metastasis, so that this phase is responsible for the metastatic phenotype and therefore for a worse prognosis (Clark *et al.,*1984). The last step (step 5) of tumor progression is metastasis: metastatic melanoma develops when tumor cells dissociate from the primary lesions, migrate through the stroma, and invade lymphatic and blood vessels to form a tumor at a distant site (Haass *et al.,* 2005) (Figure 2). The acquisition of a metastatic phenotype is due to alterations in melanoma cell adhesion, such as decreased expression of E-cadherin and overexpression of N-cadherin, αVβ3 integrin and matrix metalloproteinase 2 (MMP-2). N-cadherin increased expression is a characteristic of invasive malignancies and enables metastatic spread through the interaction between melanoma cells and other N-cadherin-expressing cells, such as dermal fibroblasts and vascular endothelium (Hsu *et al.,* 2000). The αVβ3 integrin mediates interaction between melanoma cells and the components of the extracellular matrix such as fibronectin, collagens, as well as laminin, and induces the expression of prosurvival gene BCL-2 and stimulates the motility of melanoma cells through the reorganization of the cytoskeleton. MMP-2 is a metalloprotease enzyme that induces the degradation of the components (i.e., collagen) of the extracellular matrix, thus favoring tumor cell infiltration and spreading through the bloodstream (Hoffmann *et al.,* 2000). Recent studies suggest that cancer may arise from a cancer stem cell (CSC), a tumor-initiating cell that has properties similar to those of stem cells. CSCs have been identified in several malignancies and Fang and colleagues demonstrated that they are essential for melanoma progression (Fang *et al.*, 2005). Other studies support the role of CSC in initiation and progression, therapeutic failure and chemoresistance in human malignant melanoma (Grichnik *et al.*, 2006; Monzani *et al.,*2007). Moreover, stem progenitor cell-associated proteins have been identified in melanoma, and include Notch receptors (Balint *et al.,* 2005), bone morphogenetic proteins

(BMP) (Rothhammer et al., 2007), Wnt proteins (Weeraratna et al., 2002) or the CD133, CD166, CD34, nestin, or c-kit stem cell antigens (Hendrix *et al.,* 2003). Recent findings of melanoma subsets with increased tumorigenic potential further suggest the existence of malignant melanoma stem cells, which may contribute to natural progression and therapeutic failure in this disease.

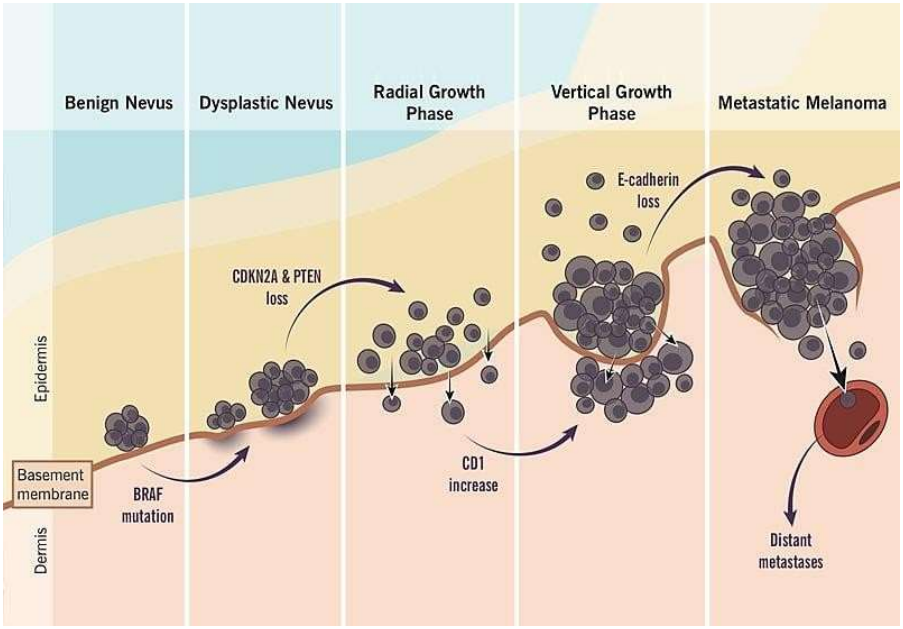

Figure 2. Proliferation of melanocytes at different stages of melanoma (https://www.google.com/search/melanoma/progression).

1.4 Melanoma Genetic Alterations

Metastatic melanoma progression is the result of a complex process that involves exogenous and endogenous factors as well as tumor-intrinsic and immune-related elements. As mentioned above, when melanocyte proliferation increases, there is an increase of gene copy-number alterations and point mutations, and benign nevi start to acquire additional molecular alterations that drives towards a malignant and invasive melanoma stage. Recent years have seen unprecedented growth in the understanding of genetic and genomic changes in melanoma. Much of the information become from next-generation sequencing (NGS), in particular exome sequencing, that has been essential in the discovery of new cancer driver genes. These NGS studies have corroborated the previously identified frequent somatic mutations in BRAF, NRAS and neurofibromin1 (NF1), and revealed new melanoma mutations in multiple genes and pathways involved in important cellular processes, such as proliferation, apoptosis,

senescence and response to DNA damage (Krauthammer *et al.,* 2015). The mutations involved in the BRAF melanoma subtype are the most common genetic alterations in melanoma (about 50% of all melanoma cases). Most BRAF mutations occur in the kinase activation loop, 74% of them consist of a single-base missense substitution that changes the amino acid valine to a glutamic acid at codon 600 (known as V600E). That substitution creates a constitutively active BRAF molecule with elevated kinase activity (BRAFV600E), leading to the subsequent activation of MEK1/2 (mitogen-activated protein/ERK kinase) and ERK1/2 (extracellular signal-related kinase) independently of upstream RAS activation. 20% of BRAF mutations determines the replacement from valine 600 to lysine (V600K) and finally 6% is represented by aminoacidic substitution in positions other than 600 (D594G, G469E, and G469A) endowed with low kinase activity (Smalley *et al.,* 2012). NF1 is a tumor suppressor gene that is mutated in 10-15% of cases of cutaneous melanoma. Loss of function mutations of NF1 results in hyper-activation of RAS proteins and therefore in the hyper activation of the MAPKs cascade and of the PI3K/AKT pathway. The NRAS melanoma subtype is the second most common subtype after BRAF, with about 25% of cases belonging to this category. In this case, missense mutations at the level of codons 12, 13 or 61 are the most frequent, accounting for 80% of all NRAS mutations present in melanoma cases, and lead to the hyper activation of NRAS. The most common mutation is a substitution of a Glutamine with Arginine, Lysine or Leucine at codon 61, exon 2 (Ellerhorst *et al.,* 2011). These mutations result in the constitutive activation of the protein which no longer requires ligand-binding to upstream RTK for its activation, and lead to enhanced signaling through the MAPK pathway, followed by promotion of proliferation, invasion, survival, and angiogenesis of melanoma. The PI3K/AKT pathway, which might be activated in melanoma cells by additional mechanisms besides those indicated above, has a key role in cell proliferation and in apoptosis, through the inhibition of many pro-apoptotic proteins, such as BAD (antagonist of BCL-2, which hinders the mechanisms of cell death) and the activation of MDM2 (responsible of p53 degradation). Key components of the PI3K signaling cascade are the p110a catalytic subunit (PIK3CA), the Phosphatase and Tensin homolog (PTEN) tumor suppressor, the downstream effector serine/threonine kinases (AKT), and the mammalian target of rapamycin (mTOR). It has been discovered that the PI3K/AKT pathway is deregulated in advanced melanoma stage. In fact, in about 37% of melanoma, PTEN is inactivated through somatic mutations (loss of function), so its negative regulatory function is abolished, allowing p110a to activate Akt in an unchecked manner. Activated Akt can stimulate cell proliferation by activating downstream effectors like mTOR and can inhibit apoptosis by mechanisms such as MDM2-mediated p53 degradation and Bcl-2-associated death

promoter (BAD) phosphorylation., thus supporting melanoma progression (Shull *et al.,* 2012). Furthermore, it is well known that the PI3K/AKT signalling regulates epithelial mesenchymal transition (EMT), promoting the expression and activity of factors involved in cell motility, such as RAC1, and the degradation of basal laminae components, such as the metalloproteases MMP-9, inducing melanoma cells invasion (Larue *et al.,* 2005). Other frequent genetic alteration observed in melanomas include mutations in the cyclin-dependent kinase-inhibitor 2A (CDKN2A) which is mutated in approximately 40% of melanoma cases. CDKN2A locus is located on chromosome band 9p21 and encodes two distinct tumor suppressor proteins, $p16^{INK4A}$ and $p14^{ARF}$ (which are translated in alternate reading frames, from alternatively spliced transcripts). $p16^{INK4A}$ forms binary complexes with the cyclin-dependent kinases 4 and 6 (CDK4/6) to inhibit Cdk4/6-mediated phosphorylation of the retinoblastoma protein (Rb). In the unphosphorylated state, Rb binds and represses the E2F transcription factor and prevents G1 to S phase transition in cell cycle. On the other hand, $p14^{ARF}$ directly prevents p53 degradation by the inhibition of E3 ubiquitin protein ligase MDM2 (Mouse Double Minute 2) (Nelson *et al.,* 2009). In physiological conditions, CDKN2A appears to play a central role in preventing cancer formation by mediating a senescence-like state upon oncogenic stress. In melanoma, the loss of $p14^{ARF}$ and $p16^{INK4A}$ activity promotes sustained proliferation of tumor cells. Interestingly, activating mutations of BRAF and loss of functional $p16^{INK4A}$ and $p14^{ARF}$ were detected in the majority of melanomas. Although, mutations in the p53 are lowest in melanomas compared to other cancers. Indeed, only 1-5% of primary and 11-25% of metastatic melanoma show mutations or deletions of TP53. However, p53 inactivation may be due to $p14^{ARF}$ mutations (Regad *et al.,*2013). Finally, mutations in the telomerase reverse-transcriptase (TERT) promoter and in genes involved in the pigmentation of the skin, such as MC1R (Melanocortin-1 Receptor) and MITF (Microphthalmia-associated Transcription Factor) have been reported (Shain *et al.,* 2015; Huang *et al.,* 2013). MC1R is a seven trans-membrane G protein coupled receptor that activates adenylate cyclase (Fig. 2) after the binding with the α-MSH (α-melanocyte stimulating hormone) (Garcia-Borron *et al.,* 2005). The subsequent increase in cAMP levels promotes the activity of MITF, that controls the transcription of genes involved in melanin production. Some MC1R genetic variants are not able to stimulate an appropriate production of melanin, whose job is to defend the skin against the ultraviolet rays damage. The presence of these MC1R variants in combination with intermittent exposure to solar ultraviolet rays is considered to be responsible for BRAF oncogenic activation by increasing intracellular AMP cyclic levels (Tsao *et al.,* 2012). MITF is overexpressed in 20% of melanoma patients and represent a negative prognostic factor. MITF controls genes involved

in cell cycle regulation, such as CDK2, or antiapoptotic genes belonging to the BCL2 family, which are amplified in 30% of melanomas. MITF targets include the hypoxia-inducible factor 1 (HIF1α) whose expression is increased in the presence of MITF amplification, and promotes survival, angiogenesis and metastasis (Dahl *et al.,* 2007).

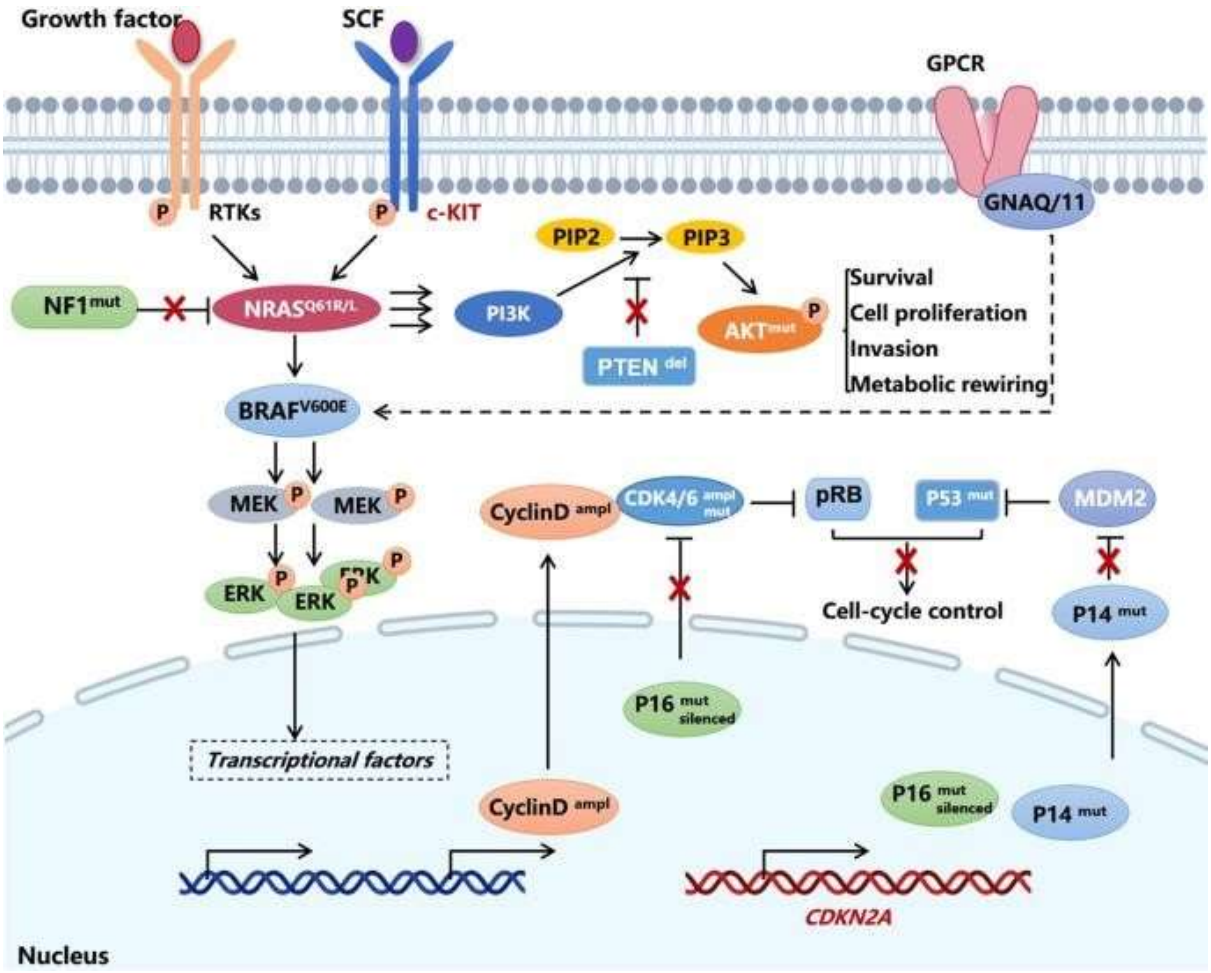

Figure 3. Mutated driver genes and downstream signal pathways in melanoma. Guo *et al.,* 2021.

1.5 Therapy

The efficacy of melanoma treatment depends on tumor stage at diagnosis. While early-stage melanoma can be successfully treated through surgery, patients with metastatic melanoma have a poor prognosis. Usually, in the presence of metastases, the treatment used until the last few years is the conventional chemotherapy, based on the use of dacarbazine, an alkylating agent that binds to DNA and causes mismatched or broken strands that generate errors during DNA duplication, finally resulting in the blockage of tumor proliferation. However, the overall

survival of patients following dacarbazine treatment is reported to be about 5-11 months. Over the last few years, the use of targeted therapies has greatly improved the prognosis of patients with metastatic melanoma so that chemotherapy is used much less frequently. Indeed, the identification of melanoma molecular alterations and of the strategy used to block specific targets allowed a better therapeutic approach. More than 50% of metastatic melanoma cases express the mutated form of BRAF protein, and BRAFV600E has become a key target for molecularly tailored therapy in melanoma. Starting from that, several BRAF inhibitors have been developed for melanoma treatment, among the others vemurafenib, an ATP-competitive BRAFV600E inhibitor, was approved by the FDA in 2011 (Chapman *et al.,* 2011). Recently, also new ATP-competitive BRAF inhibitors dabrafenib (GSK2118436) and encorafenib allowed the selective inhibition of metastatic BRAFV600-mutated melanoma (Cosgarea *et al.,* 2017). In particularly, vemurafenib selectively inhibited V600E, but is also active against V600D and V600R mutant cell lines (Yang *et al,* 2010) and dabrafenib against V600E, V600D and V600K (King et al., 2013), whereas both drugs are ineffective in cells expressing wild type BRAF or non- BRAFV600- mutations (Yang *et al.,* 2010; Gentilcore *et al.,* 2013). Conversely, encorafenib targets V600E and V600K mutants and it has been found to induce inhibitory effect also on wild type BRAF (Delord *et al.,* 2017). The BRAF inhibitors clinical efficacy in patients with BRAFV600E melanoma represented the success of oncogene-targeted cancer therapy, but the duration of clinical benefit is limited by the emergence of drug resistance disease (Das Thakur et al 2013). In particularly, there are two types of resistance termed primary/intrinsic resistance or secondary/acquired resistance. In the first case, BRAF inhibitors are totally ineffective in patients, while in the second one patients initially respond to therapy and then show disease progression (Patel *et al.,* 2020). The mechanisms involved in the occurrence of primary resistances include: the loss of the tumor suppressor PTEN (lost in 10-35% of melanomas), thus leading to the upregulation of the PI3K/AKT pathway whose activation can explain tumor resistance; the overexpression of cyclin D1 (found amplificated in about 20% of BRAF mutated melanomas) together with mutated CDK4 (Smalley et al., 2008); the loss of NF1 (mentioned above); RAC1 mutations (present in 9% of melanomas, a key regulator of motility and proliferation cells and a GTPase effector of RAS). Concerning the secondary resistance mechanisms, they are mainly associated with the reactivation of the MAP kinase pathway at or to the activation of parallel signaling pathways including that of PI3K/AKT (Manzano *et al.,* 2016). These mechanisms included: NRAS and NF1 mutations that drive MAPK activation; the overexpression or hyperactivation of receptor tyrosine kinase (RTK) likely platelet derived grow factor receptor beta (PDGFRβ) and insulin-like grow factor I

receptor (IGF-1R) that drives the activation of RAS pathway in a non-ERK dependent manner, after BRAF inhibitors treatment (Nazarian *et al.,* 2010); amplification of BRAF and alternative splicing of mutant BRAF (Corcoran *et al.,* 2010), resulting in overexpression and leading to reactivation of ERK independently of RAS. Over the last few years, combination therapies have become a valid approach to improve the efficacy of BRAF inhibitors in melanoma, delaying the onset of resistance. Recently, the Food and Drug Administration (FDA) approved the treatment with MEK1/2 inhibitors (i.e Cobimetinib, Trametinib) in combination with the BRAF inhibitors as a strategy to bypass acquired BRAF inhibitor mechanism of resistance to therapy (Voskoboynik *et al.*, 2014). Furthermore, also the final MAPK of MEK1/2 pathway, ERK1/2, has been used for targeted therapy combined with BRAF inhibitors against melanoma. In fact, it has been developed a potent and selective ERK1/2 inhibitor that blocks both ERK1/2 kinase activity and its phosphorylation by MEK1/2 (SCH772984). SCH772984 resulted in a high efficacy in BRAF, KRAS and NRAS mutant tumors, reducing tumor progression and cell proliferation at nanomolar concentrations also in resistant tumor cells (Morris *et al.,* 2013). Immunotherapy is another effective approach for the treatment ofmetastatic melanoma. The most common immunotherapy treatment for melanoma includes interleukin 2 (IL-2), a cytokine that promotes the clonal expansion of specific T lymphocytes against antigens of cancer cells. However, it was demonstrated that treatment with IL-2 showedclinical effect only in a small percentage of patients (6%) and induced high toxicity. For this reason, over the last few years, other immuno-therapeutic treatments have been preferred against melanoma progression. Among the others, the most effectives are represented by the immune checkpoint inhibitors, including treatments that exploit the use of anti-programmed cell death protein 1 (PD-1) antibodies (nivolumab, pembrolizumab) and anti-cytotoxic T- lymphocyte-associated antigen 4 (CTLA-4) antibody ipilimumab (Davis *et al.,* 2019). Although these types of inhibitors have been a breakthrough for cancer therapy and have revolutionized the treatment of metastatic melanoma, it has been observed that a significant number of patients doesn't respond to these drugs or develop resistance.

2. MITOGEN-ACTIVATED PROTEIN KINASES

Mitogen-activated protein kinases (MAPKs) are a group of highly conserved proteins in eukaryotes with Serine/Threonine kinase activity. The members of the MAPK family regulate a variety of fundamental cellular processes, including cell proliferation, differentiation, survival, transformation, and migration. Numerous extracellular stimuli, such as growth factors, mitogens and cytokines determine a sequential activation of the MAPK cascade members, thus resulting in the consequent activation of molecular effectors able to induce a specific intracellular response (Savoia *et al.,* 2019). The importance of MAPK is underlined by the abnormal signaling conveyed by members of MAPK family in several human diseases, including Parkinson's disease, inflammatory disorders and cancer (Kim *et al.,* 2009, Kim *et al.,* 1999). In mammals, 14 MAPKs have been found, which have been organized into four families: the extracellular signal-regulated kinases (ERK) 1 and 2, the best characterized among the classical MAPK, are activated mainly by growth factors, and are primarily involved in the transmission of proliferative signals; the c-Jun N-terminal kinases (JNK1, 2 and 3) and the stress-activated protein kinases (α, β, γ and δ p38), activated mainly by inflammatory cytokines, are primarily involved in adaptation to stress, apoptosis and differentiation; and the least characterized classical MAPK ERK5 (Cargnello *et al.,* 2011). ERK5 is activated by both growth and stress stimuli and plays critical roles in a number of cellular processes, including proliferation, differentiation and migration. The relevance in important cellular functions make this kinase an interesting target for future therapeutics interventions. In particular, it is well established that this pathway is involved in the pathogenesis of different types of cancer, including melanoma. Moreover, the MAPK family also includes four atypical MAPK: ERK3, ERK4, ERK7 and the nemo-like kinase (NLK) (Coulombe *et al.,* 2006). MAPK pathways are characterized by a three-tiered MAPK signaling cascade starting with a MAPK kinase kinase (MAPKKK, including BRAF and MEKK2/3 proteins) which, upon activation by upstream signals, phosphorylate and activate a MAPK kinase (MAPKK, including MEK1/2 and MEK5). Once activated, these enzymes phosphorylate the MAPK (among this ERK1/2 and ERK5) on specific residues of Threonine and Tyrosine (Figure 4). These residues are found within the T-X-Y sequence of an activating domain highly preserved in MAPKs.

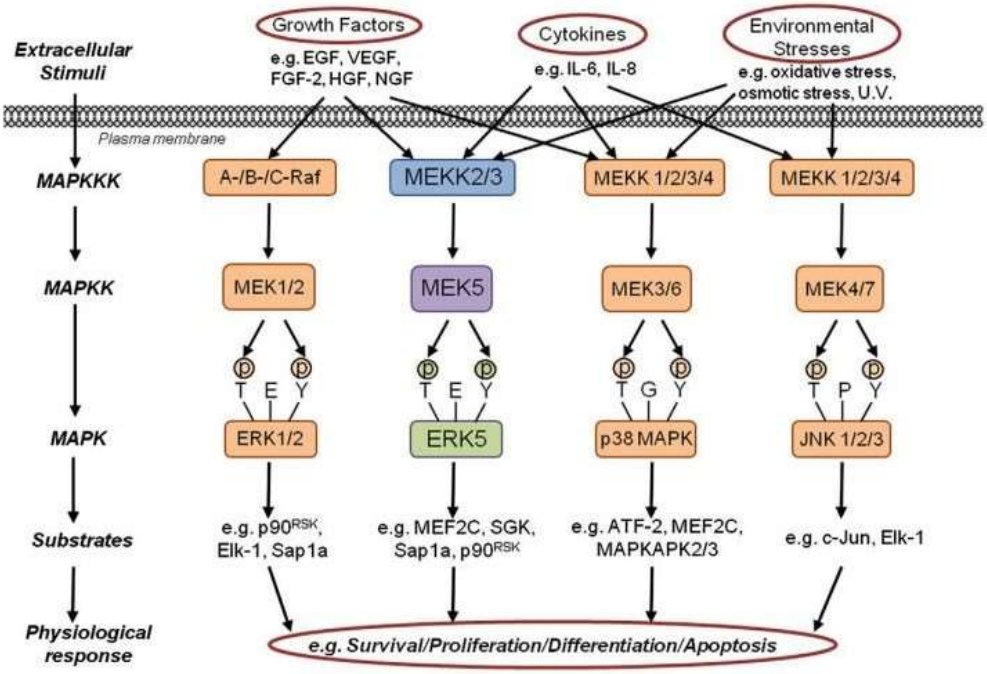

Figure 4. MAPK signaling cascade in mammalian cells (Nithianandarajah-Jones et al., 2012).

2.1 Extracellular Signal-Regulated Kinase 5 (ERK5)

The Mitogen-Activated Protein Kinase ERK5, also named BMK1 (Big MAP Kinase1) because it is two times longer than the other MAPK family members, is expressed in many tissues, including heart, skeletal muscle, placenta, lung and kidney (Lee *et al.,* 1995; Zhou *et al.,* 1995). ERK5 is also expressed in several cancer cell lines, including those of human melanoma, and supports melanoma cell proliferation (Tusa et *al.,* 2018), the latter event being strictly linked to ERK5 nuclear localization (Gomez *et al.,* 2016). ERK5, discovered in 1995 by two independent research groups, it is encoded by the *MAPK7* gene and contains 816 amino acid residues. ERK5 possesses an N-terminal kinase domain (amino acids 1-406) highly homologous to that of ERK1/2, and a unique long C-terminal tail (410 aa), which contains a transcriptional transactivation domain and a nuclear localization signal (NLS) (Buschbeck & Ullrich, 2005) (Figure 5). In particular, the N-terminus (amino acids 1-406) contains a region required for cytoplasmic targeting (a.a. 1-77), followed by a kinase domain (a.a. 78-406) which shares 66% sequence identity to the kinase domain of ERK2. Furthermore, the kinase domain can be separated into a region essential for the association with the upstream kinase MEK5 (a.a. 78-139), an oligomerisation domain (a.a. 140-406) and a common docking (CD) domain, consisting of a short sequence of negatively charged amino acid residues (a.a. 350-358), which

allows ERK5 to associate with certain docking (D)-domain-containing substrates (Nithianandarajah-Jones *et al.,* 2012). Within the C-terminal domain, in addition to the NLS region (a.a. 505-539), there are two proline-rich (PR) domains termed PR1 (a.a. 434-465) and PR2 (a.a. 578-701) which are considered to be potential binding sites for Src-homology 3 (SH3)-domain-containing proteins and a myocyte enhancer factor 2 (MEF2)-binding region (Yan *et al.,* 2001). It has been identified a transcriptional activation domain (a.a. 664-789), which undergoes auto-phosphorylation, thus enabling it to directly regulate gene transcription, an ability which is unique of ERK5 amongst the conventional MAPKs (Morimoto et al.2007). Furthermore, it has been shown that truncation of these C-terminal tail gives rise to increased kinase activity of ERK5, suggesting that the tail has an auto-inhibitory function (Buschbeck & Ullrich, 2005). ERK5 C-terminal domain presents different residues which undergo both auto phosphorylation by activated ERK5 itself or phosphorylation by other kinases (see below). Phosphorylation in this region is crucial for ERK5 nuclear localization and transcriptional transactivation activity.

The sole upstream MAPKK that can directly activate ERK5 is MEK5. Encoded from MAP2K5 gene, MEK5 is a 448 amino acid protein, with a PB1 domain, a protein interaction module, consisting of residues 19-97, and a kinase domain (residues 166-448) (Zhou *et al.*, 1995). MEK5 is activated by upstream kinases MEKK2 and MEKK3 in two specific Ser311/Thr315 residues. MEKK2 and MEKK3 also contain PB1 domains in their N-terminal regions. The PB1 domain of MEKK2 or MEKK3 specifically interacts with the PB1 domain of MEK5 (Nakamura *et al.*, 2003).

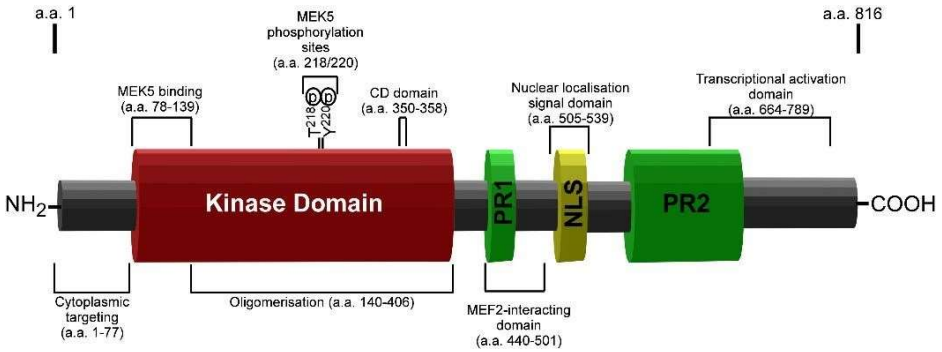

Figure 5. ERK5 structure and functional domains (Nithianandarajah-Jones et al., 2012).

2.2 ERK5 nuclear translocation

Under basal conditions, ERK5 is localized in the cytoplasm of the cell, in an unphosphorylated inactive folded form, where the N- and the C-terminal domains are bound to each other, so that the NLS is hidden, and nuclear translocation is prevented (Yan *et al.,* 2001). This conformation is stabilized by ERK5 interaction with the co-chaperone CDC37 and the chaperone HSP90, the latter ensuring cytosolic anchorage of ERK5 protein. Moreover, in the inactive structure, the C-terminus masks the CD domain of the N-terminus, inhibiting ERK5 interaction with its substrates. ERK5 kinase activation is achieved through the phosphorylation of Thr228/Tyr220 by MEK5 in the kinase domain, the latter event leading to ERK5 auto-phosphorylation in the C-terminus and the subsequent release of HSP90 from the trimeric complex (ERK5-Hsp90-CDC37). Following this event, ERK5 may assume an open conformation, exposing the NLS sequence that allows ERK5 nuclear translocation (Gomez *et al.,* 2016). Once in the nucleus, ERK5 acts as a co-activator for gene transcription by phosphorylating transcription factors or, in a kinase-independent manner, by interacting with transcription factors through the TAD domain. Regarding the activation of ERK nuclear translocation, it has been reported that a mutated form of ERK5 that cannot be phosphorylated by MEK5, ERK5-AEF, where TEY has been mutated to AEF, is unable to translocate into the nucleus upon stimulation (Buschbeck & Ullrich, 2005). Thus, MEK5-dependent phosphorylation of ERK5 seems necessary for nuclear translocation, under certain conditions. Recently, it has been found that ERK5 SUMOylation at residues Lys6 and Lys22 supports ERK5 nuclear translocation promoting ERK5 transcriptional activity and cancer cell proliferation. Erazo and colleagues showed that SUMOylation is a necessary, but not sufficient, per se, for the MEK5-mediated ERK5 nuclear shuttling. In fact, the ERK5 kinase inactive mutant (D200A) is SUMOylated following MEK5 activation, but it does not translocate into the nucleus and ERK5 K6/22R SUMO-deficient mutant did not show transcriptional activity (Erazo *et al.,* 2020). Recently, accumulating evidence it has also been proposed a MEK5-independent mechanism of ERK5 nuclear translocation. Indeed, ERK5 shuttling from the cytoplasm to the nucleus is avery complex process in which many events are involved (Figure 5). Beyond ERK5 nuclear translocation driven by MEK5-dependent phosphorylation, other mechanisms have been recently described. Among these, the overexpression of CDC37 in cancer cell lines induces HSP90 dissociation from ERK5, and nuclear translocation of wild type ERK5 as well as of a kinase-inactive form (D200A) which retains transactivation activity (Erazo *et al.,* 2013). As stated above, ERK5 nuclear shuttling is driven by phosphorylation at the C-terminal domain, an event that may be promoted by ERK5

itself or by other kinases. It has been reported that four residues (S753, T732, S773, S706) of ERK5 C-terminal half may be phosphorylated during mitosis in a cyclin-dependent kinase (CDK)1-dependent manner, and that this phosphorylation is important for ERK5 nuclear localization (Diaz-Rodriguez *et al.,* 2010). Conversely, this study could not conclude that CDK1 is the unique kinase phosphorylating ERK5 during mitosis, as only two out of the four identified phosphorylated ERK5 residues, S706 and T732, are followed by a proline and are CDK1 consensus target sites. CDK5 is an unusual member of the CDK family, endowed with functions not related to cell cycle control. CDK5 is involved in tumorigenesis in several types of cancer, such as breast, pancreas and neuroendocrine thyroid carcinomas and has been recently demonstrated to directly phosphorylate ERK5 in T732, inducing ERK5 nuclear accumulation and modulating the oncogenic ERK5-AP1 axis in colorectal cancer (Zhuang *et al.,* 2016). Moreover, it has been reported that a constitutively active RAS mutant (RASV12) resulted in ERK5 phosphorylation at T732. The involvement of ERK1/2 in this process was suggested by the fact that treatment with a MEK1/2 inhibitor (U0126) reduces ERK5 phosphorylation at T732. This event induces ERK5 nuclear localization and promotes ERK5-dependent transcription, without affecting the phosphorylation status at TEY or at other (S769/S773/S775) C-terminal residues (Honda *et al.,* 2015). Along this line, it has been recently demonstrated by our group that the overexpression of mutated BRAF (BRAFV600E) in melanoma cells increases the total amount of ERK5 and of its phosphorylated (S753 and T732) condition status as well as the nuclear amount of ERK5. Moreover, BRAFV600E increased ERK5 fraction bound to chromatin and enhanced its ability to induce transcription activity of MEF2, demonstrating that BRAF can also influence the latter ERK5 function (Tusa *et al.,* 2018). All these MEK5-independent mechanisms induce the nuclear translocation of ERK5 which wields a transcriptional transactivation activity independently of its kinase activity.

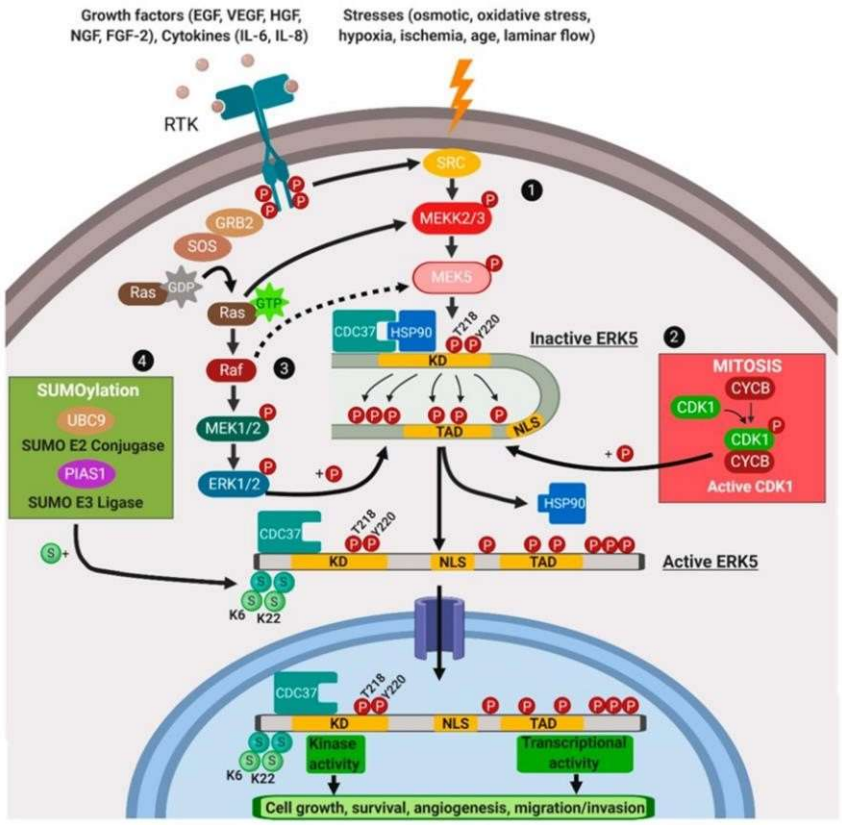

Figure 6. ERK5 nuclear translocation. In the inactive state, HSP90 and CDC37 are bound to ERK5, that resides in the cytosol in a close conformation. (1) Upon MEK5-mediated phosphorylation and subsequent activation, ERK5 auto-phosphorylates itself inducing a conformational change resulting in the dissociation from HSP90, exposition of the NLS, and nuclear translocation. MEK5-independent mechanisms of ERK5 and nuclear translocation include: (2) phosphorylation by CDK1 in mitosis; (3) MEK1/2-ERK1/2-dependent mechanism, under growth factors stimulation and/or oncogene activation. (4) Regulation of ERK5 nuclear shuttling by SUMOylation. Tubita, Lombardi, Tusa, Dello Sbarba and Rovida. Int J Mol Sci. 2020.

2.3 ERK5 and cancer

In physiological conditions ERK5 is ubiquitously expressed in mammalian tissues and cell types, where it is activated by extracellular stimuli, including several growth factors and cellular stresses. During development, ERK5 is involved in the formation of cardiac tissue and blood vessels. In fact, it has been demonstrated that the ERK5 pathway is critical for endothelial function and for maintaining blood vessel integrity (Hayashi *et al.,* 2004). In adults, ERK5 plays an essential role in the regulation of proliferation and survival, especially in endothelial and immune system cells. ERK5, in addition to oxidative stress and osmotic stress, can be activated by many growth factors such as: VEGF (vascular endothelial growth factor), EGF (epithelial growth factor) (Kato *et al.,*1998), nerve growth factor (Shao *et al.,* 2002), FGF-2 (fibroblast growth factor) (Kesavan et *al.,* 2004), colony-stimulating factor 1 (CSF-1) (Rovida, *et al.,*

2008)and PDGF (platelet-derived growth factor) (Rovida, *et al.,* 2008). In addition to these, also sometrophic factors of neurons, such as neurotrophic factor derived from the brain (BDNF) and some pro-inflammatory cytokines (such as Interleukin-6), have a stimulating action on the activity of ERK5. Furthermore, physiological and pathological conditions including laminar shear-stress, ischaemia and hypoxia are also able to activate ERK5 (Abe *et al.,* 1996; Sohn *et al.,* 2002; Yan *et al.*, 1999).

Over the last few years, the MEK5/ERK5 pathway has been shown to play an important role in the process of carcinogenesis and neoplastic progression (Lochhead *et al.,* 2011). Alterations in the MEK5/ERK5 pathway are in fact present in many types of cancer including breast, prostate, lung, colorectal brain and skin cancer. Cancer represents a progression from normal cellular homeostasis to a neoplastic condition with the cellular acquisition of a number of defined hallmarks (schematized in Figure 7): sustained proliferative signalling, evading growth suppressors, resisting cell death, enabling replicative immortality, inducing angiogenesis, activating invasion and metastasis, reprogramming energy metabolism and evading immune destruction (Hanahan *et al.,* 2011). ERK5 is responsible for proliferative signaling, which is necessary to sustain tumor development through the regulation and induction of cell cycle regulators, including cyclin D1, c-MYC, N-MYC, SGK, RSK2 and NF-kB. Moreover, through phosphorylation of MEF2 transcription factors, ERK5 has been shown to regulate the expression of c-JUN, a proto-oncogene essential to cell growth. In addition, ERK5 can also represent a mediator of a survival signal used by tumor cells to escape apoptosis (Pi *et al.,* 2004). Within cancer cells ERK5 interacts with the promyelocytic protein (PML) and inhibits its oncosuppressive activity. ERK5-mediated phosphorylation of PML induces MDM2 dissociation, down-regulating p53 expression (Yang *et al*., 2013). This suppression enables the cells to overcome the G1-S transition checkpoint in cell-cycle progression, thereby reducing inhibition of tumour cell proliferation (Nithianandarajah-Jones *et al.,* 2012). It has been shown that genetic or pharmacological inhibition of ERK5 is able to delay cell cycle progression and to reduce proliferation in several types of cancer. Upregulation and overexpression of ERK5 have been reported in several tumor types, in which they are associated with advanced stage, metastases and worse overall survival (Monti *et al.,* 2022). In fact, it has been reported that the MEK5/ERK5 pathway is involved in cellular motility and play a role in EMT, one of the key processes in tumor progression towards a metastatic phenotype. Indeed, it has been demonstrated that transcription of some key genes in EMT (such as Twist, ZEB, Snai2) is under the control of the MEK5/ERK5 pathway (Drew *et al.,* 2012). In breast cancer it has been observed that an overexpression of MEK5 due to the constitutive activation of STAT, promotes

metastasis through the EMT. Furthermore, in breast cancer, the overexpression of MEK5/ ERK5 correlates with the presence of bone metastases (Liu *et al.,* 2017). Moreover, ERK5 is able to form complexes with the αvβ3 integrin and to interact with focal adhesion kinase (FAK) to regulate the organization of the cytoskeleton, thus participating in adhesion and motility processes (Sawhney *et al.,* 2009). Invadopodia and podosomes are dynamic, actin-based protrusions of the plasma membrane that are involved in cell attachment to the extracellular matrix (ECM). They also contain matrix metalloproteases (MMPs) that degrade the ECM and facilitate cell motility/invasion. In this context, ERK5 is known to regulate the expression of MMP2 and MMP9 and the degradation of synthetic ECM in vitro promoting the migration and metastasis of tumor cells. Indeed, it has been demonstrated that ERK5 is involved in the formation of invadopods, cellular cell protrusions that allow migration during metastasis in A375 melanoma cells and in prostate cancer cells (Ramsay *et al.,* 2011). In addition, it has been shown that ERK5 is involved in chemoresistance in breast cancer cells raising the possibility that ERK5 may play a role in drug-resistance in cancer treatment (Weldon *et al.,* 2002). Furthermore, our group recently found that the MEK5/ERK5 pathway genetic inhibition reduces the growth of CML-patient-derived cells and cell lines in vitro (Tusa *et al.,* 2018). It has been recently showed that the constitutive activation of MEK5/ERK5 pathway induces colon cancer cells proliferation and that in colon cancer patients high ERK5 expression levels correlate with worse overall survival (Pereira et al., 2016), as well as in clear cell renal carcinoma (CCRC) (Arias-González *et al.,* 2013). Moreover, ERK5 is found overexpressed in approximately 50% of primary hepatocellular carcinomas (HCC) and our group showed that ERK5 amount in the nucleus of cells from HCC samples is higher compared with normal liver tissue. Moreover, genetic or pharmacological inhibition of ERK5 reduces proliferation, migration and invasiveness of HCC cells. Moreover, ERK5 silencing decreases the growth of HCC xenografts (Rovida *et al.,* 2015). Finally, as mentioned above, our group has recently shown that ERK5 is expressed in human melanomas and genetic silencing and pharmacological inhibition of the ERK5 pathway reduce growth of melanoma cells and xenografts harboring wild-type (wt) or mutated BRAF (V600E). Interestingly, the combination of MEK5 or ERK5 inhibitors with the BRAFV600E inhibitor vemurafenib is more effective than single treatments in decreasing colony formation and proliferation of BRAFV600E melanoma cells and growth of melanoma xenografts (Tusa *et al.,* 2018). Indeed, the MEK5/ERK5 pathway represents one of the alternative pathways that come reactivated in cancer cells following treatments with chemotherapeutic agents. In fact, recent studies have shown that ERK5 phosphorylation is increased in melanoma cells treated with the

combination of BRAF and MEK1/2 inhibitors (CBIM), which is the current therapeutic approach. Additionally, ERK5 genetic (shRNAi) or pharmacological (XMD8-92) inhibition impaired not only the acquisition of resistance to CIBM, but also the proliferation of CIBM resistant cells, sensitizing cancer cells to targeted therapy, restoring the antiproliferative effect of the chemotherapy. Further kinome-scale siRNA screening demonstrated that SRC\MEK5 cascade promotes the phospho-activation of ERK5 inresponse to CIBM (Song *et al.*, 2017).

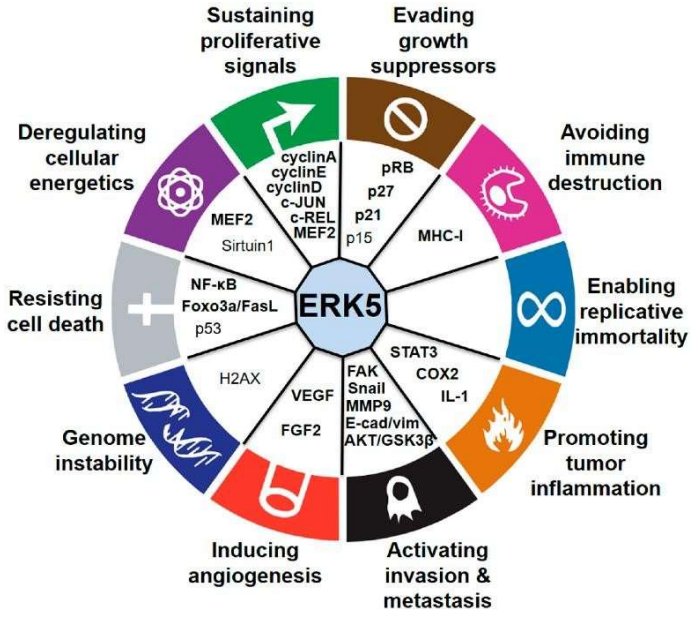

Figure 7. Impact of ERK5 on the hallmarks of cancer (Stecca and Rovida, 2019).

2.4 ERK5/MEK5 pathway inhibitors

Due to the role of ERK5 in tumorigenesis and in drug resistance described above, many small-molecule compounds targeting ERK5 (including XMD8-92, XMD17-109, JWG-071, AX15836, BAY-885) or MEK5 (BIX02188, BIX02189) have been developed over the last few years (Yang *et al.,* 2010; Wang *et al.,* 2018; Lin *et al.,* 2016; Deng *et al.,* 2013; Nguyen *et al.,* 2018). BIX02188 and BIX02189 (indolinone-6-carboxamides) are the first small-molecule compounds developed for the inhibition of both MEK5 and ERK5. These inhibitors compete for the ATP binding site in the MEK5 catalytic domain, blocking its kinase activity with IC50 4.3 and 1.5 nM, respectively and block ERK5 phosphorylation without affecting activation of ERK1/2, p38 MAPK, or JNK (Tatake *et al.,* 2008). It has been demonstrated that BIX02189 induces a more potent suppression of ERK5 kinase activity, with an IC50 of 59 nM, compared to that of BIX02188 (810 nM). Both these two MEK5 inhibitors inhibited the transcriptional activity of MEF2, a downstream substrate of the MEK5/ERK5 signaling cascade, in a dose-dependent manner. Later on, the small-molecule compound XMD8-92 (benzopyrimido-diazepinone), a competitive inhibitor of the ATP-binding site in ERK5 kinase domain, has been developed. This compound induces the inhibition of ERK5 kinase activity, that can no longer phosphorylate either its cellular substrates or itself at the level of the C-terminal domain (Yang *et al.,* 2010). In vivo experiment showed that administration of 50 mg/kg dose of XMD8-92 (twice daily) reduces tumor growth and inflammation with good pharmacokinetics, bioavailability and tolerability (Al-Ejeh *et al.,* 2014). However, it is worth point out that the clinical application of XMD8-92 and of its derivatives is compromised by the recently discovered role of them in the direct inhibition of bromodomain-containing protein (BRD), as off-target effect (Lin et al., 2016). Hence the need to generate new small molecule inhibitors to avoid possible unspecific effects. In this respect, JWG-045 and JWG-071 have been developed, both have selectivity over BRD4 but inhibit Leucine-rich repeat kinase 2 (LRRK2) and are classified as dual ERK5/LRRK2 inhibitors (Williams *et al.,* 2016). So, a second generation of ERK5 kinase activity inhibitors was obtained synthetizing derivatives of the XMD8-92 that show a 37 more potent inhibition of ERK5 with IC50 values ranging from 8 to 190 nM. The first ERK5i to be described were compound (cpd) 25 (XMD17-26) and cpd 26 (also known as XMD17-109 and ERK5-IN-1). Furthermore, AX15836, an analogue of XMD8-92, was engineered to lack bromo-domain activity and is a potent and selective inhibitor of ERK5 kinase activity. However, cell-based experiments showed that AX15836 does not phenocopy genetic ERK5 knockdown that results in the reduction of cell proliferation. Recently, Cook et al. have

found that cpd 26 (XMD17-109) and AX15836, cause a conformational change in the kinase domain of ERK5 which leads to exposure of the NLS and to paradoxical activation of the TAD, enabling ERK5 to regulate its downstream targets (Lochead *et al.*, 2020), thus resulting in the ineffectiveness in reducing cancer cell proliferation. None of these inhibitors, however, has been tested in humans so far. TG02, a dual ERK5/CDK inhibitor, has been tested in clinical trials for haematological malignancies following the promising results obtained in preclinical studies (Alvarez-Fernandez *et al.,* 2013; Ortiz-Ruiz *et al.,* 2014). Based on all above, concerted efforts should be pursued to develop therapeutically suitable MEK5-ERK5 inhibitors.

3. α/β IMPORTIN-MEDIATED NUCLEAR TRANSPORT

Regarding ERK5 nuclear translocation, several mechanisms of regulation have been recently reviewed in Tubita et al. 2020. However, despite several events have been identified, how ERK5 enters the nucleus still needs to be clarified. Based on the presence of a cNLS (classical nuclear localization signal) (Lu *et al.,*2021), it has been postulated that ERK5 shuttles into the nucleus through α/β1 importin (Flores *et al.,* 2019), but this hypothesis has not been demonstrated yet.

The first nuclear localization signal was identified through the analysis of simian virus 40 (SV40) mutants, whose NLS is composed of seven amino acids, Pro-Lys-Lys-Lys-Arg-Lys-Val (PKKKRKV) (Adam *et al.,* 1989). Afterwards, functional NLS sequences were identified in several other proteins that translocate from the cytoplasm to the nucleus within the cell. Over the last few years, several studies focused on novel NLS motifs and on the import proteins that recognize and bind them in order to find novel treatments against cancer and viral infection disease. It is well known that cNLS are divided into two categories: “monopartite” (MP) and “bipartite” (BP) NLS. MP NLS are made by a single cluster composed of 4-8 basic amino acids, which generally contains 4 or more positively charged residues, that is, arginine (R) or lysine (K).By contrast, BPNLS (505RKPVTAQERQREREEKRRRRQERAKEREKRRQERER539) are characterized by twoclusters of 2-3 positively charged amino acids that are separated by a 9-12 amino-acid linker region, which contains several proline (P) residues (Lu *et al.,* 2021). It has been demonstrated that a BP NLS of ERK5 is required for its nuclear translocation upon activation, and that this NLS itself is sufficient to drive GFP to the nucleus, indicating that the ERK5 BP NLS is biologically functional (Yan *et al.,* 2001, Erazo *et al.,* 2020).

3.1 α/β importin mediated NLS-proteins nuclear trafficking

It is well known that small proteins (less than approximately 50 KDa) can pass through the nuclear pores complex (NPC) by simple diffusion, while proteins with a high molecular weight (more than about 60 KDa), including some MAPKs, are actively transported into the nucleus by carrier proteins or transport factors. Many of these carriers belong to the β-karyopherin (β-Kap or importin-β, Impβ) superfamily. All β-Kap family members are characterized by tandem HEAT repeats, each of which contains ~ 40–45 amino acids that form two antiparallel α-helices (designated A and B) linked by a loop. HEAT repeats (see below) can form alpha solenoids, a type of solenoid domain found in a number of proteins involved in nucleocytoplasmic transport (Kobe *et al.,* 2000). The name "HEAT" is an acronym for four proteins in which this repeat structure is found: Huntingtin, Elongation factor 3 (EF3), protein phosphatase 2A (PP2A) and the yeast kinase TOR1. In this respect, it is well known that cNLS, the first nuclear targeting signal discovered and the best characterized, on cargo proteins is recognized by the importin-α (Impα) (karyopherin-α), which, in turn, is recognized by the importin β1 subunit. Importin-α is an adaptor protein that recognizes and links cNLS on the cargo protein and interacts via its importin-β1 binding domain (IBB) with the latter. Importin-β1 is able to interact with some NPC nucleoporins, so that the resulting cargo-α/β1 importin-trimer is imported into the nucleus (Christie *et al.,* 2016). Also, Importin-α is a solenoid protein, but is built from armadillo (ARM) repeats (Conti *et al.,* 2000) rather than HEAT ones. In humans, the importin α protein family contains 6 members, namely, importin α1, importin α3, importin α4, importin α5, importin α6 and importin α7. As mentioned above, the interaction of Impα with Impβ1 occurs through the N-terminal αIBB domain, made up of approximately 40 highly conserved residues and the Importin-β HEAT repeats 7-19, among which two main regions mediate interaction: HEAT repeats 7-11, which bind the N-terminal region of the αIBB domain (α11-α23), and HEAT repeats 12-19, which bind the C-terminal α-helical region of the αIBB domain (α24-α51) (Cingolani *et al.,* 1999). In humans, 20 members of β-Kap family have been discovered, 10 of which mediate transport of macromolecules into the nucleus, 7, including the best characterized one, importin-β1 (often termed importin β), translocate macromolecules from the nucleus to the cytoplasm, 2 have been shown to mediate translocation in both directions and 1 member remains to be characterized (Christie *et al.,* 2016). Importin-β1 effectively allows migration through the NPC, while the NLS/importin-α complex behaves as an inert cargo during import. Among the Impβs, importin-β1 is the only one that require the interaction with importin-α to bind the cNLS, instead it can directly bind cargo containing the

non-classical NLS allowing passage into the nucleus. After the cargo is released into the nucleus, importin-α and β1 must return to the cytoplasm and be available for new import cycles. This mechanism is regulated by an additional key component of nuclear transport event is the small GTPase Ran (Figure 8).

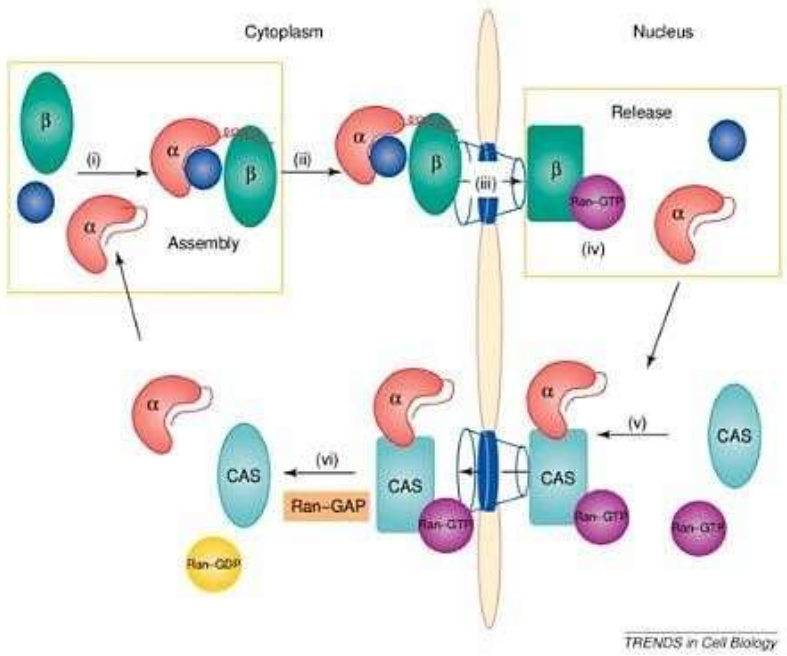

Figure 8. The nucleocytoplasmic shuttling cycle of importin α. (i) Importin α (α) forms a ternary complex with importin β (β) and a cargo protein (blue circles). (ii) The ternary complex reaches the nuclear-pore complex (NPC) and (iii) translocates into the nucleus. (iv) Ran-GTP binds the ternary complex leading to the dissociation of its components. (v) Importin α binds the exportin CAS-Ran-GTP complex to be exported to the cytoplasm. (vi) Ran-GAP-stimulated hydrolysis of GTP by Ran induces the dissociation of the exportin complex and the release of free importin α into the cytoplasm for another transport cycle. The recycling of importin β to the cytoplasm, and of Ran-GDP to the nucleus and its conversion to Ran-GTP are not shown. (Goldfarb et al.2004).

Ran can be in two different states: GDP- and GTP-bound states. These two different forms of Ran are asymmetrically distributed in the cell: RanGTP is enriched in the nucleus, whereas RanGDP is enriched in the cytoplasm. This compartmentalization allows Ran to impart directionality to nuclear transport, acting as a molecular switch that controls the compartment-specific binding and release of cargo proteins (Ayanlaja *et al.,* 2020). Importantly, importin α can interact, through its C-terminal region, with the nuclear export factor CAS, also known as Cse1, and nucleoporin 50 (Nup50), which catalyzes cargo dissociation allowing importin α to combine with RanGTP to be exported from the nucleus. First, the binding of importin α to the nucleoporin Nup153 (required for the anchoring of NPCs) promotes the translocation of the cNLS-cargo-importin α-importin β trimeric complex into the nucleus. Once the trimer complex

is inside the nucleus, RanGTP binding causes a conformational change in importin β, which releases the IBB region of importin α. This event, together with Nup50 and CAS interaction with importin α, facilitates cNLS dissociation and the delivery of the cNLS-cargo in the nucleus. After dissociation, importin α is exported from the nucleus by CAS in conjunction with RanGTP. The importin β-RanGTP complex returns to the cytoplasm, where GTP is hydrolyzed, leading to the dissociation of RanGDP from the importin, ready for reuse in the subsequent round of transport (Lu *et al.,* 2021).

Interestingly, it has been found that Imp-βs expression is altered (upregulated or downregulated) in several cancers (Table 1). Indeed, within tumor cells, the aberrant expression of Imp-βs should affect the localization of different proteins that might be involved in oncogenic processes (Kimura *et al.,* 2014).

β-member	**function**	**cancer type**	**reference**
importin-β/importin-β1	import	Cervical cancer, hepatocellular carcinoma, glioma	Van der Watt 2009; Yang 2015; Lu 2016
transportin-1/importin-β2	import		
transportin-2/importin-β2b	import		
importin-4	import		
RanBP5/importin-3/ importin-5	import	Esophageal cancer	Li Meiyu 2022
importin-7	import	Colorectal cancer, glioblastoma, prostate cancer	Li 2000; Xue 2015; Szczyrba 2013; Chen 2021
importin-8	import		
importin-9	import		
importin-11	import	Glioma	Hongzao 2021
transportin-SR/transportin3/ importin-12	import		
CRM1/exportin-1	export	Ovarian cancer, pancreatic cancer, glioma, osteosarcoma,	Noske 2008; Shen 2009; Yao 2009;

		cervical cancer	Van der Watt 2009
CAS/CSE1L/exportin-2	export	Hepatoma, lymphoma, colorectal, ovarian, breast, colon, endometrial cancer, urinary bladder urothelial carcinoma	Peiro 2002; Stawerski 2010 Lorenzato 2013 Shiraki 2006 Wellmann 1997 Alnabulsi 2012 Behrens 2001 Chang 2012
exportin-5	export	Bladder urothelial carcinoma	Han 2013
exportin-6	export		
exportin-7	export		
exportin-t	export	Breast cancer, HCC, promyelocytic leukemia	Vaidyanathan 2016; Lin 209; Suzuki 2006
RanBP17	export	head and neck squamous cell carcinoma	Mandic 2022
importin-13	bidirectional receptors	Endometrial carcinoma	Zheng 2012
exportin-4	bidirectional receptors	Hepatoma	Liang 2013
RanBP6	not characterized		

Table 1. List of β karyopherins and their role in nuclear transport. In the table there are indicated also thetumors in which each protein expression has been found to be deregulated.

3.2 Importin β1-mediated nuclear import

Impβ1 was the first member of the β-Kap family to be structurally characterized and it is often termed importin β. It has been reported that Impβ1 holds 19 HEAT repeats arranged in

a superhelix, making a convex face (formed by the A-helices of each repeat) and a concave face (formed by the B-helices each repeat). The majority of Impβ1 interactions with its cargoes take place on the concave (B-helix) face, and competition for these binding sites by Ran, Impα and other binding partners induces the mechanisms of assembly, disassembly and translocation. The structural flexibility of the Impβ1 structure is essential for its function. As stated above, a number of cargo proteins are recognized directly by Impβ1 without interaction with the importin-α adaptor. Cargo proteins that are recognized directly by Impβ1 are significantly different from each other and contain a non-classical NLS (Lee *et al.,* 2003). Examples include: the parathyroid hormone-related protein PTHrP (Cingolani *et al.,* 2002), the sterol regulatory element-binding protein SREBP2 (Lee et al.2003) and the zinc finger protein SNAI1 (Snail1) (Choi et al.2014), ribosomal proteins, CREB, the human immunodeficiency virus (HIV) Rev and Tat, the human T-cell leukemia virus type 1 (HTLV-1) protein Rex, cyclin B1, Smad3, TRF, and SRY (Marfori *et al.,* 2011). The regions on Impβ1 to which they bind overlap, implying that only one cargo can bind at a time. Interestingly, recent work has shown that KPNB1 expression is upregulated in several cancers, including cervical cancer (van der Watt *et al.,* 2009), hepatocellular carcinoma (Yang *et al.,* 2015) and glioma (Lu *et.,* 2016). Indeed, KPNB1 inhibition in cancer cells leads to apoptosis, mainly because importin β1 shuttles into the nucleus proteins related to proliferation and cancer progression. Intriguingly, inhibition of importin β1 expression in non-cancer cells has only a minor effect on cell viability (van der Watt *et al.,*2009), pointing to a potential use for KPNB1 as an anticancer therapeutic target (van der Watt *et al.,* 2013).

3.3 ERK 1/2 nuclear translocation

MAPK translocation from the cytoplasm to the nucleus is involved in the regulation of several cellular processes such as cell cycle progression, differentiation, and circadian clocks (Xu *et al.,* 2004). ERK1/2 possess a non-canonical NLS, called Nuclear Translocation Signal (NTS). Upon stimulating factors, ERK1/2 are phosphorylated on the regulatory Tyr and Thr residues, this activation induces a conformational change that releases ERK1/2 from anchoring proteins and leads to the exposure of two additional Ser residues within a unique nuclear translocation signal (NTS). The phosphorylation of ERK1/2 Ser residues induces the binding to importin-β7 (Imp7), through which ERK1/2 go into the nucleus via the nuclear pores. Similarly to what described above, once in the nucleus, the small GTPase Ran causes the

dissociation between ERK1/2 and Imp7, leading to an accumulation of the kinase in the nucleus and to the export of Imp7 back to the cytoplasm (Maik-Rachline *et al.,* 2019). Within the nucleus, ERK1/2 promotes cFos transcription and cell proliferation (Formstecher *et al.,* 2001). The characterization of ERK1/2 nuclear translocation has been essential to target this process as a therapeutic approach. In fact, the RAS-ERK pathway is activated mutated in cancer and several inhibitors have been developed to achieve its blockage. A few of these inhibitors are already in therapeutic use, but they are effective only in limited cancer types, and it has been reported that 2-18 months after administration resistances developed. For example, SCH772984 is a potent and selective ERK1/2 inhibitor that blocks both ERK1/2 kinase activity and its phosphorylation by MEK1/2. It has been reported that treatment with SCH772984 reduced tumor progression and cell proliferation at nanomolar concentrations in BRAF, KRAS NRAS mutant tumors (Morris *et al.,* 2013). However, a long-term exposure of cells to SCH772984 leads to acquired resistance (Jha et al., 2016). Resistance has been reported also for MEK1/2 inhibitors, such as Trametinib and UO126 (Das Thakur *et al.,* 2014) and for BRAF inhibitors mentioned above. To this purpose, Maik-Rachline and colleagues designed a synthetic peptide (EPE peptide), which specifically inhibits ERK 1/2 interaction with Imp7 and ERK 1/2 nuclear translocation. They showed that the peptide specifically induced apoptosis of mutated BRAF melanoma cells. Moreover, the peptide inhibited the proliferation of Vemurafenib (RAF inhibitor)- and U0126 (MEK inhibitor)-resistant melanoma cells and of several NRAS and NF1 mutant melanomas, also in combination with the MEK inhibitor trametinib, showing a synergistic effect in inhibiting proliferation of some NRAS mutant melanomas resistant to each drug alone. Importantly, EPE peptide resulted to be effective also in vivo, in xenograft models, inhibiting the growth of breast and colon cancer, and of melanoma, including the BRAF-mutated model (Maik-Rachline *et al.*, 2019).

3.4 α/β importin inhibitors

Small-molecule inhibitors of α/β importin have been designed and provided a promising approach to study the nuclear import in living cells (Figure 9). High Throughput Screening (HTS) using chemical compound libraries and recombinant proteins has been used to identify many small molecule inhibitors targeting IMPα/β. Among these, importazole specifically inhibits the function of importin-β by altering its interaction with RanGTP (Soderholm *et al.,* 2011), as well as Karyostatin 1A that binds importin β with high nanomolar affinity targeting

the molecular interaction between importin β and the GTPase Ran, thus resulting in the inhibition of α/β importin- mediated nuclear import at low micromolar concentrations in vitro and in living cells (Hintersteiner *et al.,* 2010). Additionaly, it has been designed the inhibitor of nuclear import-43 (INI-43) that specifically inhbits the binding between importin β and its cargo proteins NFAT, NF-κB, AP-1 and nuclear transcription factor Y (van der Watt *et al.,* 2016). Also, the inhibitor 2-aminothiazole derivative 1 specifically target importin β (Ha *et al.,* 2017). Finally, two peptides, Bimax1 and Bimax2, showed high affinity for importin α to inhibit importin α/β-dependent transport, but the therapeutic applicability of these peptide inhibitors has not been investigated yet (Kosyna and Depping 2018). Ivermectin (22,23-dihydroavermectin B, IVM), a dihydro derivative of Avermectin, is the best-studied among the α/β importin inhibitors. This compound is a macrocyclic lactone produced by the bacterium *Streptomyces avermitilis*, and it was initially developed as a broad-spectrum anti-parasite drug used to treat nematode infections. Wagstaff and colleagues investigated the effects of ivermectin treatment on the subcellular localization of proteins containing a nuclear localization sequence (NLS), demonstrating that ivermectin is a potent inhibitor of IMPα/β1-dependent transport, with no effect on proteins containing NLSs recognized by alternative nuclear import pathways (Wagstaff *et al.,* 2011). Hence, ivermectin started to be used as treatment against HIV and DENV (dengue virus) infection, due to its ability of inhibiting integrase nuclear import that rely on Impα/β1-dependent transport (Wagstaff *et al.,* 2012). Regarding the mechanism of action, it has been reported that ivermectin can dissociate the preformed importin α/β1 heterodimer, as well as prevent its formation, through binding to the IMPα ARM repeat domain (see above) to impact IMPα thermal stability and α-helicity that prevent binding to IMPβ1 (Yang *et al*,.2020). Recently, it has been demonstrated that ivermectin could have an antiviral action also against the SARS-CoV-2 clinical isolate in vitro, with a single dose able to control viral replication within 24-48 hours (Caly *et al.,* 2020). Since studies on SARS-CoV proteins revealed the involvement of IMPα/β1 during infection in signal-dependent nucleocytoplasmic shutting of the SARS-CoV Nucleocapsid protein 16-18, that may impact on host cell division. Over the last few years, many studies carried out with ivermectin have demonstrated its anticancer activity in several types of cancer, including colon cancer, ovarian cancer, melanoma and leukemia (Juarez *et al*., 2020). The molecular mechanisms underlying this anticancer effect are different, among the others it has been reported that ivermectin markedly inhibits the growth of breast cancer cells by stimulating cytostatic autophagy in vitro and in vivo, through the blockade of the PAK1-AKT-MTOR axis (Wang *et al.,* 2016). Ivermectin inactivates the oncogenic kinase PAK1 also in ovarian cancer cell lines, leading to the reduction of the PAK1-

dependent growth of human ovarian cancer and NF2 tumor cell line (Hashimoto *et al.*, 2009). Furthermore, it was demonstrated that ivermectin is able to induce apoptosis by the upregulation of cleaved poly (ADP-ribose) polymerase, of BAX expression, and of caspase-3 activity and by the downregulation of BCL-2 expression in the melanoma cell line Sk-Mel-28 (Deng *et al.,* 2018). It has also been reported that ivermectin suppressed the growth of gastric cancer cells in vitro and in vivo by inhibiting YAP1 expression (Nambara *et al.,* 2017). In addition, another investigation demonstrated that ivermectin induces apoptosis in glioblastoma and HeLa cells by enhancing cytochrome c release, upregulating Bax and p53 expression, downregulating Bcl-2 expression and decreasing the levels of cyclin E, cyclin D1, CDK2, CDK6 and CDK4 (Song *et al.,* 2019, Zheng *et al.,* 2018). Recently, it has been discovered that IVM significantly inhibits the motility of cancer cells in vitro and tumor metastasis in vivo. Mechanistically, ivermectin suppressed the expressions of migration-related proteins via inhibiting the activation of Wnt/β-catenin/integrin β1/FAK and the downstream signaling cascades in colorectal and breast cancer cell lines (Jiang *et al.,* 2022). Additionally, it has been reported that ivermectin inhibits growth, regulates the cell cycle, and induces apoptosis in human urothelial carcinomas (UC) cells (Tung *et al.,* 2022). Interestingly, in the last years ivermectin started to be used in combination with chemotherapeutic agents because of its capability to counteract chemoresistance mechanisms. For example, Nunes and colleagues demonstrated that the combination of Paclitaxel with Ivermectin showed the highest cytotoxic effect and the strongest synergism among many combinations tested in Paclitaxel resistant ovarian cancer cells (Nunes *et al.,* 2022). Furthermore, it has been recently reported that ivermectin and sorafenib showed synergistic effects in reducing the growth of hepatocellular carcinoma in vitro, and this was confirmed in vivo. Mechanistically, it emerged that IVM inhibited mTOR/STAT3 pathway and decreased EMT as shown by the increased expression of E-cadherin and decreased expression of vimentin, snail and slug after ivermectin treatment (Lu *et al.,* 2022). Recently, ivermectin was also used as an anti-cancer treatment due to its ability of importin α/β1-mediated transport. Indeed, it was reported that ivermectin has a KPNB1-dependent antitumor effect on multiple epithelial ovarian cancer (EOC) cell lines, where KPNB1 acts as an oncogene and supports cell proliferation. In the same study, it has also been found that the combination of ivermectin and paclitaxel produces a stronger antitumor effect on EOC cell lines than either drug alone (Kodama *et al.,* 2017) Furthermore, Ishikawa and colleagues showed that ivermectin interfered with the nuclear localization of NF-κB and AP-1 through importin β1 into adult T leukemia/lymphoma (ATLL) cells. Thus, the expression of NF-κB- and AP-1-target proteins involved in cell cycle was

reduced, resulting in the apoptosis increase and in the reduction of tumor growth (Ishikawa *et al.,* 2020).

Compound	Synonym	NTR	Type of Compound
cSN50.1	-	Imp α/β, Impβ	Peptide
58H5-6	-	Imp β	Small molecule (synthetic)
Karyostatin 1A	-	Imp β	Small molecule (synthetic)
Importazole	-	Imp α/β	Small molecule (synthetic)
Inhibitor of nuclear import-43 (INI-43)	-	Imp β	Small molecule (synthetic)
2-aminothiazole derivative 1	-	Imp β	Small molecule (synthetic)
M9M	-	Transportin	Peptide
Bimax 1/Bimax 2	-	Imp α	Peptide
Ivermectin	Stromectol	Imp α/β	Antibiotic
Mifepristone	Mifegyne	Imp α/β	Small molecule (synthetic)
N-(4-hydroxy-phenyl) retinamide (4-HPR)	-	Imp α/β	Small molecule (synthetic)

Figure 9. α/β importin-mediated nuclear import inhibitors. From "*Controlling the Gatekeeper: Therapeutic Targeting of Nuclear Transport*" Friederike K. Kosyna and Reinhard Depping, Cells 2018.

4. CELLULAR SENESCENCE

Human melanomas are frequently characterized by a loss or a reduced expression of the pathways supporting cellular senescence that would prevent tumor growth and progression. Cellular senescence is a permanent state of cell cycle arrest that occurs in response to various stimuli. The first description of this phenomenon dates back to the last century. In 1960, indeed, Hayflick and Moorhead observed that human diploid fibroblasts in culture could undergo a maximum number of cell divisions (between 40 and 60 times, known as the "Hayflick limit") before blocking their proliferation. This sort of biological clock was then discovered to be due to the progressive shortening of telomeres in every single replicative event and represents a physiological mechanism of the cell to prevent accumulation of DNA damage along multiple DNA replicative cycles, that could lead to neoplastic transformation. This phenomenon is currently defined as replicative senescence (Calcinotto *et al.*, 2019). However, cells can undergo senescence independently from the telomere shortening. In fact, senescence is also considered a cellular mechanism of response that occurs immediately after certain insults, such as oxidative stress, genotoxic stress or metabolic shock, mitochondrial dysfunction, treatments with chemotherapeutic agents, irradiation, and after aberrant activation of proliferative pathways, such as following the expression of activated oncogenes. Regarding the latter,

oncogene-induced senescence (OIS) has been identified in non-malignant human tissues as one mechanism of senescence tumor suppression. Indeed, it has been reported that the expression of oncogenic BRAF(V600E) in benign melanocytic nevi increases the expression of $p16^{INK4a}$ and promotes cell cycle arrest, as a protection mechanism against BRAF(V600E)-driven proliferation (Michaloglou *et al.,* 2005), may be an endogenous barrier to malignant transformation and that senescence in tumors may indicate a more benign or favorable outcome (Ewald *et al.,* 2010). Senescent cells are characterized by the presence of several features. First of all, cellular senescence is generally accompanied by significant morphological alterations: senescent cells become flat and enlarged due to rearrangement of the cytoskeleton. Moreover, lysosomal content and lysosomal enzyme senescence associated β-galactosidase (SA-β-gal) are highly upregulated during senescence, together with an increase in the expression of cycle inhibitory proteins such as the CDKi $p16^{INK4a}$, $p21^{CIP1}$ and p27. Another prominent feature that characterizes the senescent phenotype is the presence of senescence-associated heterochromatin foci (SAHFs), described for the first time in 2003 in the nuclei of senescent cells as punctate DNA-stained dense foci that can be readily distinguished from chromatin in normal cells (Narita *et al.*, 2003). SAHF are highly condensed and heterochromatic chromosomes that are proposed to enforce cellular senescence by suppressing the transcription of genes involved in proliferation (Di Micco *et al.*, 2011). These distinct chromatin structures are enriched with repressive epigenetic marks, such as methylated H3K9, heterochromatic protein 1 (HP1), and macroH2A1, that after their formation suppress the transcription of genes that promote cell cycle progression. Another feature of cellular senescence is the reduction of Rb phosphorylation. In fact, as mentioned above, the hypo-phosphorylated RB, binds the transcription factor E2F, preventing its binding to the promoters of genes regulating the G1/S phase transition and entry into the S phase of mitosis, ultimately halting the cell cycle. Furthermore, aberrant activation of signal transduction pathways and positive cell-cycle regulators during OIS can lead to the accumulation of DNA damage, involving the DNA-damage response (DDR) cascade and accumulation of H2AX foci. DNA damages recruit and activate the two protein kinases ataxia telangiectasia and Rad3-related (ATR) or ataxia-telangiectasia mutated (ATM), thus promoting the phosphorylation the histone H2AX (γH2AX), that recruits additional ATM complexes in a positive feedback loop, thereby increasing local ATM activity. The latter promotes the spread of γH2AX along the chromatin and the recruitment of a high number of DDR factors resulting in the formation of nuclear foci that contain multiple copies of the same protein (D'Adda di Fagagna 2008) Thus, despite DDR and γH2AX formation are typical features of replicative senescence and ageing, start to be

associated as markers of cellular senescence in general. In addition to these characteristics, senescent cells are able to secrete interleukins, cytokines, chemokines, extracellular matrix proteases and growth factors that are collectively responsible for the senescence-associated secretory phenotype (SASP). The SASP is a crucial mediator of the physio-pathological functions of senescent cells, and it has been reported that this secretory phenotype can have pro- as well as anti-tumorigenic effects, making cellular senescence a double-edged sword. For instance, it has been reported that senescent fibroblasts secrete amphiregulin and growth-related oncogene (GRO) α, which stimulate the proliferation of premalignant epithelial cells (Bavik et al., 2006; Coppé *et al.*, 2010). Moreover, senescent cells also secrete high levels of interleukin 6 (IL-6) and IL-8, which induces epithelial-mesenchyme transition and invasiveness in cultured premalignant epithelial cells (Coppé *et al.,* 2008). Furthermore, it has been showed that conditioned media from senescent fibroblasts stimulate angiogenesis (Coppé *et al.,* 2006). Finally, it has been reported that SASP of senescent hepatic stellate cells promotes the proliferation and malignancy of the neighboring cells in obese mice exposed to chemical carcinogens (Yoshimoto *et al.,* 2013). On the contrary, for example, it has been reported that SASP from senescent human fibroblasts induces paracrine senescence in neighboring normal cell (Acosta *et al.,* 2013). Moreover, Kuilman and colleagues showed that the expression of IL-8 correlated with a nonproliferative phenotype in colonic adenomas, supporting the possibility that these cytokines function in vivo to promote cell senescence in benign human tumors (Kuilamn *et al.,* 2008). Finally, Acosta and colleagues suggest that senescent cells activate a self-amplifying secretory network in which CXCR2 (C-X-C Motif Chemokine Receptor 2)-binding chemokines reinforce growth arrest Acosta *et al.,* 2008), These examples suggest that in some cases, the SASP cytokines could reinforce the senescence growth arrest, thus resulting in beneficial effects against cancer. Therefore, over the last few years, it has been shown that senescence could represent an important cellular response in many neoplasms with a suppressive function able to inhibit tumor growth and progression (Ewald *et al.,* 2010) and this effect has paved the way for pro-senescence therapy as a powerful and promising strategy for anticancer therapy.

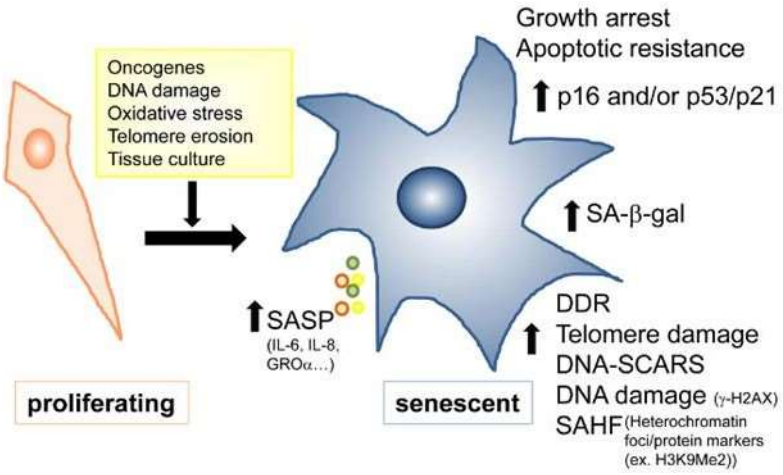

Figure 10. Features of cellular senescence (Hooten *et al.,* 2017. Techniques to Induce and Quantify Cellular Senescence).

AIMS

In the last few years, immunotherapy and targeted therapy have greatly improved the survival of melanoma patients, however they are still unsatisfactory due to resistance mechanisms and to lack of long-term benefits. Thus, there is an urgent need to identify novel targets critical for melanoma growth and progression. Considering that ERK5 is involved in the pathogenesis of different types of cancer, including melanoma as demonstrated from latest study (Tusa *et al.,* 2018), the final aim of this project was to deeply characterize the mechanisms involved in ERK5 regulation and signaling in melanoma cells in order to optimize the ERK5 targeting to counteract melanoma growth. In particular, this work addressed two major scientific issues:

- Aims 1. Melanoma is frequently characterized by the loss of the pathways supporting cellular senescence that would prevent tumor growth and progression. It has been previously showed by my research group that ERK5 inhibition reduces the growth of melanoma, determining a block of the cell cycle rather than inducing apoptosis (Tusa et *al.,* 2018). Because MAPK are frequently involved in cellular senescence (Munoz-Espín *et al.,* 2014, Anerillas *et al.,* 2020), we investigated the effects of ERK5 targeting on senescence with the aim to identify a novel therapeutic strategy for melanoma.

- Aim 2. Concerning the mechanism of ERK5 translocation from the cytoplasm to the nucleus, the actors involved in this process are still poorly characterized. Based on that, the second aim of this project was the elucidation of the mechanisms involved in ERK5 cytoplasmic-nuclear shuttling in order to identify new strategies useful to counteract melanoma progression.

MATERIALS AND METHODS

1. Cell Cultures

A375 melanoma cells, HEK-293T (CRL-3216) and HeLa cells (CRM-CCL-2) were obtained from ATCC (Manassas, VA, www.lgcstandards-atcc.org); SK-Mel-5 melanoma cells were kindly provided by Dr. Laura Poliseno (CRL-ISPRO, Pisa, Italy). SSM2c melanoma cells were kindly provided by Barbara Stecca (ISPRO, Firenze, Italy). HUH-7 hepatocellular carcinoma cells were kindly gifted by Prof. Fabio Marra (AOUC, Firenze, Italy). Cells were maintained in Dulbecco's modified Eagle's medium (DMEM) supplemented with 10% heat-inactivated fetal bovine serum (FBS), 2 mM glutamine, 50 U/mL penicillin, and 50 mg/mL streptomycin (EuroClone, Paignton, UK). Cell lines were yearly authenticated by cell profiling (Promega PowerPlex Fusion System kit; BMR Genomics s.r.l; Padova, Italy). The presence of mycoplasma was periodically tested by PCR.

2. Drugs

The α/β1 importin inhibitor Ivermectin (HY-126937) and the ERK5 inhibitor AX15830 (HY-101846) were from MedChemExpress LLC (Monmouth Junction, NJ, USA). The ERK5 inhibitors XMD8-92 (Yang *et al.,* 2010), JWG-045 (Williams *et al.,* 2016) and JWG-071 (Wang *et al.,* 2018) have been kindly provided by Nathanael Gray and Jinhua Wang, (Harvard Medical School & Dana-Farber Cancer Institute, Boston, MA, USA). MEK5 inhibitor BIX02189 (S1531), BRAFV600E inhibitor Vemurafenib (S1267) and MEK1/2 inhibitor Trametinib (S2673) were from Selleck Chemicals LLC (Selleckchem, Italy, www.selleckchem.com). Considering that ERK5 is positively regulated by FBS-contained growth factors, pharmacological treatments with ERK5 inhibitors were performed in low serum condition (2.5% fetal bovine serum). Serum deprivation is necessary to eliminate upstream activations of ERK5 due to all the factors that regulate the pathway. For the selection of lentiviral-infected cells (see below) we used puromycin (2μg/ml; Sigma-Aldrich, St. Louis, Missouri, USA).

3. Plasmids and transient transfections

pcDNA-HA-ERK5wt and pcMV5-MEK5DD-HA (a constitutively active form of MEK5) constructs were generously provided by Jiing-Dwan Lee (Scripps Institute, La Jolla, CA, USA). pcDNA3-HA-ERK5wt-HaloTag construct was made in our lab. HEK-293T or HeLa cells were plated in 100 mm diameter dishes and transfected after 24 hours with a total amount of 2μg of plasmid DNA. Transfection was performed in the reduced-serum media OptiMEM (Life Technologies, Carlsbad, CA, USA) using Polyethylenimine (jetPEI reagent, Polypus Transfection, Euroclone, Milan, Italy) as transfection reagent, added to the diluted DNA in a ratio of 3:1. Experiments were performed 48h after transfection.

4. ERK5 and p21 genetic knock-down

Lentiviral vectors for stable knockdown of ERK5 in melanoma cells were TRC1.5-pLKO.1-puro vector containing non-targeting sequence shRNA (LV-c), targeting human MAPK7 (NM_139032, NM_139034, NM_002749) clone ID: TRCN0000010262 (LV shERK5-1), clone ID: TRCN0000010275 (LV-shERK5-2). Lentiviral vectors for stable knockdown of p21 in melanoma cells were TRC1.5-pLKO.1-puro vector containing non-targeting sequence shRNA (LV-c), targeting human CDKN1A (NM_000389, NM_000389) clone ID: TRCN0000287021 (LV shp21-1), clone ID: TRCN0000287091 (LV-shp21-2). Lentiviral vectors have been prepared as previously reported (Rovida *et al.,* 2015). HEK293T cells were seeded in 100 mm diameter dishes (2×10^6 cells/dish) in DMEM supplemented with 10% FBS and 2 mM glutamine without antibiotics. After 24 hours (reached 40%–70% of confluence) medium was replaced with fresh complete medium. The plasmid mixture was prepared as follows: 8 μg of lentiviral vectors encoding for shRNA, 4 μg of pRSV-Rev, 4 μg pMDLg/pRRE and 4 μg pMDG.1-VSV and 150 mM NaCl (Polyplus Transfection, Euroclone, Milan, Italy) to a final volume of 250 μL. Transfection was performed using 40 μL of jetPEI reagent (Polyplus Transfection, Euroclone, Milan, Italy) following the manufacturer's protocol. Twenty-four hours after transfection, the medium was replaced with fresh complete medium. The following day culture media from HEK293T was collected and fresh complete medium added to the cells. Harvested medium was centrifuged at 1500 rpm for 5 min and filtered through a 0.45 μm filter and either directly added to melanoma cells or stored at −80°C for later use. This procedure was repeated 1 day after. For infection, melanoma cells were seeded in a 60 mm diameter dish (3×10^5 cells/dish). At an optimal confluence of 50%, 2 mL/dish of virus

supernatant was added in the presence of 5 μg/mL polybrene. Infected cells were selected with2 μg/mL puromycin for at least 72 hours.

Gene	Clone ID	shRNA	TRC Number	Sense sequence 5' to 3'
none	none	shNT	TRCN0000023236	CCGGCGACAATATCATCG CCATCAACTCGAGTTGAT GGCGATGATATTGTCGTT TTT
MAPK7	NM_139032	shERK5-1	TRCN0000010262	CCGGGCTGCCCTGCTCAA GTCTTTGCTCGAGCAAAG ACTTGAGCAGGGCAGCTT TTT
MAPK7	NM_139032	shERK5-2	TRCN0000010275	CCGGGCCAAGTACCATGA TCCTGATCTCGAGATCAG GATCATGGTACTTGGCTTT TT
CDKN1A	NM_000389	shp21-1	TRCN0000287021	CCGGCGCTCTACATCTTCT GCCTTACTCGAGTAAGGC AGAAGATGTAGAGCGTTT TTG
CDKN1A	NM_000389	shp21-2	TRCN0000287091	CCGGGACAGATTTCTACC ACTCCAACTCGAGTTGGA GTGGTAGAAATCTGTCTT TTTG

Table 1. List and sequences of the shRNA used in the present study.

5. HaloTag vector cloning strategy

ERK5 full length sequence was amplified from the pCDNA HA-ERK5 plasmid using the primers below: the forward (FW) primer allows the insertion of the Kozac consensus sequence; the reverse (RV) primer allows the amplification of the complete ERK5 sequence excluding the stop codon). The amplified sequence was cloned into the pcDNA3.1(+) plasmid by forced

cloning using the BamHI/NotI restriction sites. The obtained plasmid is termed pCDNA3.1 ERK5.

- ERK5 Kozac FW: CGGGATCCCCACCATGGCCGAGCCTCTGA

- ERK5 w/o stop RV: ATAAGAATGCGGCCGCGGGGTCCTGGAGGTCAGGC

HaloTag sequence, having at 3' the coding sequence for the 3xHA-Tag and the stop codon, was amplified from the plasmid pFC20A using the primers below. The amplified sequence was cloned into the pCDNA3.1 ERK5 vector by forced cloning using the XhoI/XbaI restriction sites. The obtained plasmid is termed pCDNA3.1 ERK5 Halo 3xHA.

- Halo w/o Kozac FW:

CCGCTCGAGGGGAAATCGGTACTGGCTTTCCA

- Halo w stop 3xHA RV:
GCTCTAGATTAAGCGTAGTCAGGTACGTCGTAAGGGTATTCCGCAGCGTA ATCCGGAACGTCGTACGGATATTCCGCCGCGTAGTCTGGAACGTCATATG GGTAACCGGAAATCTCCAGAGT

Agarose gel electrophoresis after the restriction enzyme digestion of the obtained plasmid was performed to verify the cloning accuracy.

6. CRISPR Assay

HUH-7 cells were knocked out for ERK5 expression using a MAPK7 human gene CRISPR/Cas9 knockout kit (reference KN200655) from Origene (Rockville, MD, USA) and a control CRISPR/Cas9 plasmid (reference sc-418922) from Santa Cruz Biotechnology following the manufacturer's protocol. KO-ERK5 cells were selected with 2 µg/mL puromycin and ERK5 levels were tested by Western blotting.

7. α/β1 importin siRNA genetic inhibition

A375 and HEK293T cells were removed by trypsinization, seeded in complete medium without antibiotics in p100 dishes in a number of 1 000 000 cells/dish, and incubated for 24 h until they reached 50% confluence. Transfection was then performed in the reduced serum media OptiMEM (Life Technologies, Carlsbad, CA, USA) using Lipofectamine 2000

(Invitrogen Life Technologies) as transfection reagent added to 100 nM of two different siRNA for KPNB1 (siKPNB1-1 and siKPNB1-2) or 100 nM non targeting siRNA (siNT) as a negative control following the manufacturer's instructions.

8. Cell lysis and Western Blotting

Total cell lysates were obtained by scraping cells in Laemmli buffer (62.5 mM Tris-HCl-pH 6.8, 10% glycerol, 0.005% bromophenol blue, SDS 2%) and incubating at 99°C for 10 min. Lysates were then clarified by centrifugation (13,000 rpm for 10 min at room temperature). Nuclear-cytoplasmic fractionation was obtained with a subcellular protein fractionation kit (ThermoFisher Scientific, Waltham, Massachusetts, USA), following manufacturer's instructions. Proteins were separated by SDS–PAGE and transferred onto Hybond™ PVDF (GE Healthcare, Illinois, USA) by electroblotting. Infrared imaging (Odyssey, Li-Cor Bioscience, Lincoln, NE, USA) was performed. Images were quantified with ImageJ software. Antibodies are listed in Table 2.

9. Co-Immunoprecipitation Assay

For co-immunoprecipitation (Co-IP) experiments, HeLa cells transfected with ERK5WT/MEK5DD or A375 melanoma cells were lysed in Co-IP buffer (50 mM Tris-HCl, pH 7.4, NaCl 150 Mm, 1 mM EDTA, Triton-X-100 1%, with 1 mM Na_3VO_4, 20 mM $Na_4P_2O_7$, 1 mM PMSF, 0.1 U/ml Aprotinin, 1 mM TPKC). Samples (2 mg of proteins) were then incubated with primary antibodies (1 µg of anti-ERK5 (C-7) or 1 µg of anti-KPNB1 in 500 µl final volume) for 2 hours at 4°C and then with 20 µl beads protein A/G-Sepharose beads (sc-2003, Santa Cruz Biotechnology, CA, USA) overnight at 4°C. After several washes with Co-IP buffer, bound proteins were eluted in Laemmli buffer 1X and analyzed by SDS-PAGE.

10. Cell Viability Assay

Cell viability was measured by 3-(4,5-dimethylthiazol-2-yl)-3,5-diphenyltetrazolium bromide (MTT) assay. Cells were seeded in triplicate in 96-well plate in DMEM/10% FBS. After 24 hours, medium was replaced medium containing increasing drug concentrations (0.1; 0.3; 1; 3; 10; 20; 30 µM) and cells further incubated for 72 hours. MTT (0.5 mg/ml) was added during the last 4 hours. Plates were read at 595 nm using a Microplate reader-550 (Bio-Rad, Hercules, CA, USA).

11. Colony Formation Assay

A375, HeLa and Sk-Mel-5 cells were seeded in p60 dishes in DMEM 10% FBS in a number of 500, 2500 and 4000 cells/dish, respectively. After 24 hours, cells were treated with ivermectin, AX15836 or with the combination of the two drugs. Colonies (i.e. more than 50 cells) were counted following crystal violet staining after 7 (for A375 and HeLa cells) or 14 days (for Sk-Mel-5 cells).

12. Apoptosis evaluation and Cell cycle phase distribution analysis

A375 or HeLa cells were seeded in 6-well plate in a number of 150 000 cells/well in DMEM 10%FBS. 24h after seeding, cells have been treated with AX15836 1μM, IVM (5 or 7.5 μM for HeLa cells and 7.5 or 10 μM for A375 cells) or with the combination of the two drugs for 24h. Then, medium was discarded, cells have been washed once in PBS1X, detached with Accutase solution (EuroClone, Paignton, UK) and resuspended in DMEM 10% FBS in flow cytometry tubes. Cells have been centrifugated 5 min at 1200 rpm, media has been removed and cells have been washed once with PBS1X before staining with Annexin V-FITC (Roche Diagnostics, Basel, Switzerland) and PI for 15 min at room temperature protected from light. Flow cytometry was performed using a FACSCanto (Beckton & Dickinson, San Josè, CA, USA). Annexin-V+/PI- cells were considered early apoptotic and annexin-V+/PI+ cells late apoptotic, whereas Annexin-V+ cells defined total apoptosis.

A375 and SSM2c cells upon ERK5 KD were seeded in 6-well plates in a number of 150 000 cells/well and were cultured for 72h. A375 and SSM2c cells were seeded in 6-well plates in a number of 150 000 cells/well and treated after 24h with XMD8-92 for 72h (treatment with H_2O_2 for first three hours was used as positive control). After 72 hours, cells were treated with 10% FBS for 8 hours or left untreated. Cell-cycle phase distribution was then determined by resuspending the cells in 500 μl of a hypotonic solution containing 50 μg/mL propidium iodide, 0.1% w/v trisodium citrate and 0.1% NP40. Cytometric analysis was performed with FACS Canto II (Beckton & Dickinson, San Josè, CA, USA) and analyzed using FlowJo software (Ashland, OR: Becton, Dickinson and Company).

13. Determination of cellular senescence by senescence-associated β-Gal staining

Cells were incubated for 72 hours with the treatment of interest and then fixed (2% formaldehyde, 10 minutes, room temperature). After washing, senescence-associated (SA)

βGal staining solution (X-gal 1 mg/mL, 40 μM citric acid, 5 μM $C_6FeK_4N_6$, 5 μM $C_6N_6FeK_3$, 150 μM NaCl and 2 μM $MgCl_2$; pH 6.1 -SK-Mel-5- or 5.9 -A375 and SSM2c) was added (16 hours, 37°C). Senescent cell quantification was performed by counting SA-βGal-positive (blue) cells in 10 random images/well taken using a brightfield microscope 20X. An average of 800 cells/condition were counted. In other experiments, cell area was evaluated with ImageJ software.

14. Xenografts

A375 and SSM2c melanoma cells transduced with LV-c or LV-shERK5 were resuspended in Matrigel (Corning, www.corning.com)/DMEM and subcutaneously injected (10000 cells/injection) into lateral flanks of adult (8 weeks) female athymic-nude mice (Foxn1 nu/nu) (Harlan Laboratories, Udine, Italy). Number of animals per group was 6 for A375 and SSM2c LV-shERK5 and 7 for SSM2c LV-c. In the second set of experiments, parental A375 cells were subcutaneously injected as above. Mice were randomized in four groups of 9 mice each and treated intraperitoneally (IP) twice a day for 19 days with vehicle (30% 2-hydroxypropyl-β-cyclodextrin), XMD8-92 (25 mg/Kg), Vemurafenib (20 mg/Kg) or a combination of both drugs. In both experiments subcutaneous tumor size was measured three times a week with a caliper. Tumor volumes were calculated using the formula: V=W2 x L x 0.5, where W and L are, respectively, tumor width and length.The experiments were approved by the Italian Ministry of Health (Authorization n. 213/2015- PR) and were in accordance with the Italian guidelines and regulations.

15. Immunohistochemistry and determination of cellular senescence in vivo

Formalin-fixed paraffin-embedded (FFPE) sections from archival xenografts established with shNT or shERK5–2 A375 or SSM2c cells, or with A375 cells from XMD8–92 (25 mg/kg)- or vehicle (2-hidroxypropyl-b-cyclodextrin 30%)-treated mice were used (Tusa *et al.,* 2018). Experiments had been approved by the Italian Ministry of Health (authorization no. 213/2015-PR) and were in accordance with the Italian ethic guidelines and regulations. Sections (3 μm thick) were deparaffinized and stained with Sudan Black Blue (SBB; Bio-Optica) to reveal lipofuscin (28, 29), and counterstained with Nuclear Fast Red (NFR, Bio-Optica). Immunohistochemistry (IHC): After citrate buffer antigen retrieval, staining was performed with the UltraVision LP Detection System HRP Polymer Kit (Thermo Fisher Scientific) following the manufacturer's instructions. Sections were incubated overnight at 4°C

with primary antibodies (Table 1) and (3,30-diaminobenzidine; Thermo Fisher Scientific; DAB) used as a chromogen. Sections were counterstained with hematoxylin.

16. PCNA quantification

A375 and SSM2c ERK5-KD cells were seeded in 6-well plates and incubated in DMEM 10% FBS. After 72h cells were permeabilized with 0.5% Tween, incubated with primary antibody anti-PCNA for 30 min and then with FITC-conjugated secondary antibody for 20 min. Quantification was performed by flow cytometry using a FACSCanto (Beckton & Dickinson, San Josè, CA, USA).

17. Chemokines determination in conditioned media

Fourteen days after lentiviral transduction, medium was replaced with DMEM/10% FBS. Conditioned media (CM) were harvested after 72 hours. Chemokine expression was measured in CM using RayBiotech Quantibody array (RayBiotech) following the manufacturer's instructions. Each antigen was measured in quadruplicate and relative fluorescence intensity determined using ImageJ software. Results were normalized for protein content in cell lysates.

18. Immunofluorescence Analysis

Cells were plated on glass coverslips and incubated for 72 hours in DMEM/2,5%FBS, and fixed with 4% paraformaldehyde (10 minutes, room temperature). Cells were permeabilized (0.2% Triton X-100) and saturated with 10% horse serum in PBS/1% BSA for 45 minutes. Incubation with primary antibody (overnight, 4°C) and with Cy2- or Cy3-labeled secondary antibodies was performed. Cell nuclei were labelled with DAPI (Invitrogen). Images were analyzed with a TCS SP8 scanning confocal microscopy system (Leica Microsystems, Mannheim, Germany) with a Leica Plan Apo 60X immersion oil objective (Sigma-Aldrich, St. Louis, Missouri, USA).

19. Transcriptomic Analysis

Total RNA was isolated using RNeasy Mini Kit (Qiagen), and mRNA expression evaluated with Affymetrix Clariom-S Human Genechip following the manufacturer's instructions. Transcriptome analysis console (TAC) software was used (fold change >1.5/< -1.5 and $P \leq 0.05$) to identify differentially expressed genes (DEG). Most enriched pathways were identified by Meta-analysis of DEG using WebMeV (Multiple Experiment Viewer).

20. Quantitative real-time PCR

Total RNA was isolated using TRIzol (Life Technologies). cDNA synthesis was carried out using ImProm-II Reverse Transcription System, while quantitative PCR (qPCR) was performed using GoTaq qPCR Master Mix (Promega Corporation). Primers used were: IL6, for 5′-AGACAGCCACTCACCTCTTCAG-3′, rev 5′-TTCTGCCAGTGCCTCTTTGCTG-3′; IL8, for 5′-GAGAGTGATTGAGAGTGGACCAC-3′, rev 5′-CACAACCCTCTGCACCCAGTTT-3′. QPCR was performed using CFX96 Touch Real-Time PCR Detection System (Bio-Rad). mRNA expression was normalized to GAPDH and 18S mRNA.

21. Cell viability assay and neutralization experiments

Cells were seeded in 96-well plate in DMEM/10% FBS. After 24 hours, medium was replaced with CM and cells further incubated for 72 hours. MTT was performed. For neutralization experiments, control isotype IgG or neutralizing antibodies were added to CM prior to administration to cells. MTT was performed on A375 cells treated with CM harvested from shNT (white column) or shERK5–2 (dark columns) A375 cells in the presence of 10 mg/mL of the indicated blocking antibodies or control IgG.

22. 3D Spheroid Culture

22.1 Quantification of Spheroid Volume

A375 and HeLa cells were seeded in 96-well plate previously coated with a base coating solution of 1.5% agarose in water, in a number of 1000 cells/well in DMEM 10%FBS. After 72h, photos of time 0 were taken and then spheroids were treated with ivermectin and/or

AX15836 at different concentrations. Photos have been taken after 3, 4 and 5 days of treatment and the volume of the A375 spheroids have been quantified with ImageJ using the formula Volume = $0.5*L*W^2$, L=length (major axis) W=width (minor axis).

22.2 LiveDead assay

HeLa cells were seeded in 96-well plate previously coated with a base coating solution of 1.5% agarose in water, in a number of 1000 cells/well in DMEM 10%FBS. After 72h, spheroids were with ivermectin and/or AX15836 at different concentrations. After 96h, media was removed, and spheroids have been washed once in with PBS1X and stained with Calcein AM (CAS 148504-34-1, ChemCruz Biochemicals, from Santa Cruz, Dalls, Texas, USA) and Propidium Iodide (PI) (Sigma-Aldrich, St. Louis, Missouri, USA) diluted in DMEM without phenol red to a final concentration of 4 µM and 2 µM respectively, for 30 min at 37°C. Images were analyzed with a TCS SP8 scanning confocal microscopy system (Leica Microsystems, Mannheim, Germany) with a Leica Plan Apo 60X immersion oil objective (Sigma-Aldrich, St. Louis, Missouri, USA). Calcein AM is a cell-permeant dye that can be used to determine cell viability in most eukaryotic cells. In live cells, the non-fluorescent calcein AM is converted to green fluorescent calcein, after acetoxymethyl ester hydrolysis by intracellular esterases. Conversely, the DNA-binding agent PI is a cell membrane impermeable dye and only enters dead cells or those with damaged cell membranes. Intracellular PI binds DNA and undergoes an approximate 40-fold enhancement in fluorescence intensity. As a result, live cells will produce a strong green fluorescence resulting from the conversion of Calcein-AM to calcein, while dead cells produce a strong red fluorescence due to the presence of Propidium Iodide.

23. Super-resolution Imaging

HeLa cells seeded on cover glass coated with polylysine were transfected with ERK5-HaloTag-expressing vector using JetPEI PolyPlus in DMEM/10%FBS without Penn/Strep following manufacturer's procedure. After 24h, cells were washed once with Leibovitz medium and then labelled with JaneliaFluor646 (diluted in Leibovitz medium to 0.05 µM final concentration) for 15 min at 37°C. Among available HaloTag-binding chromophores useful for super-resolution technique, we chose JaneliaFluo646 for its prominent features. Indeed, JaneliaFluor646 is a photo-activatable and cell permeant dye (for live cell imaging), with higher brightness and higher photostability compared to others. Cells were washed once and glass were

placed in a microscope chamber and covered with Leibovitz medium for living imaging. Single molecule localization imaging of ERK5-HaloTag-Janelia was performed on an inverted wide-field fluorescence microscope (Nikon ECLIPSE TE300) with 643 nm excitation laser and 405 nm activation laser. Excitation and activation were performed with inclined illumination through a TIRF 60 X objective (Nikon 60 X, oil immersion, NA 1.49 TIRF) to optimize the signal-to-background ratio. Emitted fluorescence was collected through the same objective and imaged on an EMCCD Camera (Andor iXon X3) after an additional 3x magnification. Full field of view is $40 \times 40\mu m^2$, with 80 nm pixel size. A total of 3000 frames was acquired for each cell, with 30 ms exposure time and 400 EMgain. Activation of fluorophores was performed at frames 100, 1000 and 2000 with 200 ms exposure to 405 nm laser light (10 W on the sample). A brightfield (BF) image of each cell was recorded in order to create masks of the nucleus and of the cytoplasm. Masks are created using custom and built-in tools in MATLAB, starting from the nuclear edge contrast visible in BF images. ERK5-HaloTag molecules were localized using ThunderSTORM (Ovesný *et al.,* 2014) plugin for ImageJ with the following parameters: Image filtering: Wavelet filter (B-Spline), order=8, scale=2; Approximate localization: Local maximum, PIT=std (Wave.F1), Connectivity=8; Sub-pixel localization: Radial symmetry, R=3px. A 200 of post-activation and 20 pre-activation frames are omitted which gives a total of 2280 images included in the analysis for each measurement. The ratio r of the densities of detected ERK5 molecules is determined as:

$$r = \frac{N_n/S_n}{N_c/S_c}$$

where N is the number of detected molecules in a masked region (i.e. the nucleus or the cytoplasm), S is the area of the masked region, while indices n and c indicates the nucleus and the cytoplasm respectively.

24. Statistical Analysis

Data represent mean or ± SD values calculated on at least three independent experiments. P values were calculated using Student t test (two groups) or one-way ANOVA (more than two groups). $P < 0.05$ was considered statistically significant.

Protein	Use	Source	Cat. No	Company
ERK5	WB	Rabbit p	#3372	Cell Signaling Technology, Danvers, MA,USA
Cyclin B1	WB	Rabbit m	sc7393	Santa Cruz Biotechnology, Santa Cruz, CA,USA
Importin β1	WB	Rabbit m	#8673	Cell Signaling Technology, Danvers, MA,USA
Fibrillarin	WB	Mouse m	sc374022	Santa Cruz Biotechnology, Santa Cruz, CA,USA
α Tubulin	WB	Mouse m	sc32293	Santa Cruz Biotechnology, Santa Cruz, CA,USA
p21Waf1/Cip1	WB	Rabbit m	#2947	Cell Signaling Technology, Danvers, MA,USA
p21Waf1/Cip1	IHC	Mouse m	#2946	Cell Signaling Technology, Danvers, MA,USA
ERK5	IHC	Mouse m	sc398015	Santa Cruz Biotechnology, Santa Cruz, CA,USA
pRb-S807/811	WB	Rabbit m	#8516	Cell Signaling Technology, Danvers, MA,USA
HSP90	WB	Mouse m	sc13119	Santa Cruz Biotechnology, Santa Cruz, CA,USA
Cyclin A2	WB	Mouse m	#4656	Cell Signaling Technology, Danvers, MA,USA
Cyclin D1	WB	Mouse m	sc8396	Santa Cruz Biotechnology, Santa Cruz, CA,USA
Cyclin E	WB	Rabbit p	sc481	Santa Cruz Biotechnology, Santa Cruz, CA,USA
P14ARF	IHC	Mouse m	#2407	Cell Signaling Technology, Danvers, MA,USA
P14ARF	WB	Rabbit m	#74560	Cell Signaling Technology, Danvers, MA,USA
MacroH2.A1	IF	Rabbit m	#12455	Cell Signaling Technology, Danvers, MA,USA
ERK5 (C-7)	IP	Mouse m	sc398015	Santa Cruz Biotechnology, Santa Cruz, CA,USA
PCNA	FC	Rabbit m	#13110	Cell Signaling Technology, Danvers, MA,USA

Table 2. List of the antibodies used and their application. m = monoclonal, p = polyclonal

RESULTS

1. ERK5 INHIBITION ELICITS CELLULAR SENESCENCE IN MELANOMA

1.1 ERK5 inhibition induces cellular senescence in melanoma cells and xenografts

It has been previously demonstrated by my group that ERK5 inhibition reduces the proliferation of melanoma cells in vitro and the growth of melanoma xenografts in vivo (Tusa et al.2018). To deepen the role of ERK5 in the biology of melanoma, transcriptomic experiments were performed in BRAFV600E A375 and SK-Mel-5 melanoma cells after ERK5 knock-down (KD) with two different shRNAs (Figure 1A). Intriguingly, DEG analysis confirmed the relevant role of EK5 in cell cycle regulation and revealed that cellular senescence was the tenth most impacted pathway (0.0032 degree of enrichment; Figure 1B). Indeed, we found that the expression of several senescence-related genes significantly changed following ERK5 KD (Table 1).

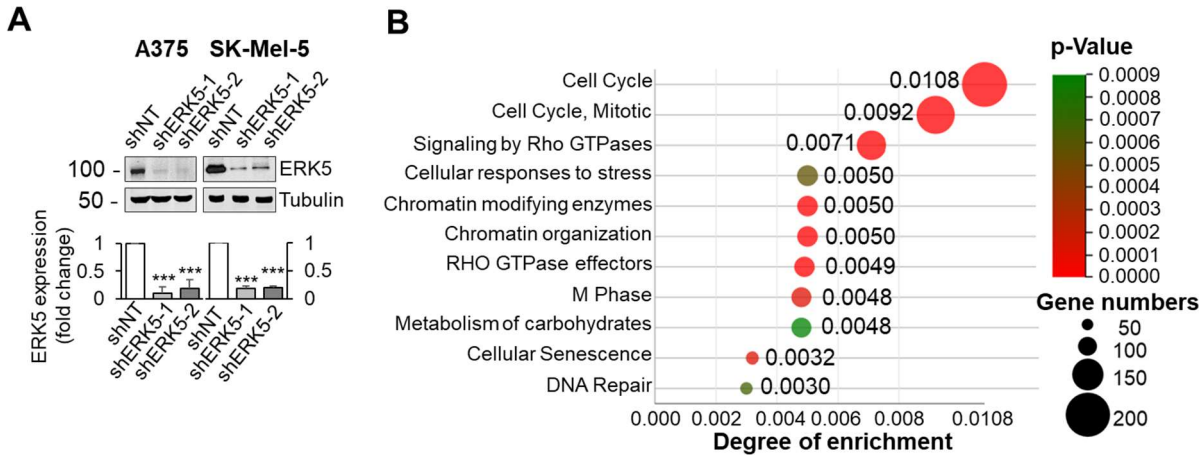

Figure 1. *Senescence is one of the most impacted pathways upon ERK5 KD in A375 and SK-Mel-5 cells*. **A**) Cells were lysed after infection with lentiviral vectors carrying control nontargeting shRNA (shNT) or ERK5-specific shRNA (shERK5-1 and shERK5-2). Western blot was performed with the indicated antibodies. Migration of molecular weight markers is indicated on the left (kDa). The graphs show average densitometric values of ERK5 protein levels normalized for tubulin content from three independent experiments. **B**) WebMeV analysis was performed on transcriptomic data after infection with lentiviral vectors carrying control or ERK5-specific shRNA. Data obtained from the two shRNA targeting ERK5 were averaged (A375, n=4; SK-Mel-5, n=3). Shown are the first eleven most impacted pathways based on degree of enrichment. Size of circles indicate the number of genes that are upregulated or downregulated in each pathway. *, $P < 0.05$; **, $P < 0.01$; ***, $P < 0.001$ (**CO** Alessandro Tubita. Published in: Lombardi Z. Tubita A. Tusa I. et al. Cancer Res. 2022 Feb 1. doi: 10.1158/0008-5472).

	A375		SK-Mel-5	
Gene symbol	**Fold change shNT/shERK5**	**P-value**	**Fold change shNT/shERK5**	**P-value**
HIST1H3B	-2.36	0.0178	-9.57	0.0252
HIST1H3F	-3.41	0.007	-5.96	0.0223
HIST1H4B	-2.61	0.0045	-2.25	0.0094
HIST1H4D	-1.7	0.0106	-4.7	0.0091
HIST1H4E	-2.45	0.0197	-2.35	0.0025
HIST1H4H	-2.85	0.0053	-2.13	0.0279
HIST1H4J	-1.88	0.0271	-2.9	0.0046
HIST1H4K	-1.75	0.0411	-2.9	0.0311
HIST2H3D	-1.8	0.0189	-1.7	0.0318
HIST2H4A	-1.8	0.0023	-9	0.0249
HIST2H4B	-1.88	0.0011	-4.3	0.0369
RBL1	-1.6	0.0389	-2.25	0.0159
LAMA1	-1.55	0.0306	-1.7	0.0194
CDC25A	-4.9	0.0063	-4.2	0.0022
LIN9	-1.6	0.004	-2.1	0.0078
CDKN1B	1.8	0.0136	2.04	0.05
CXCL1	6.7	0.0432	3.8	0.0496
CXCL8	20.3	0.0389	54.57	0.0434
CCL20	2	0.046	9.9	0.012
IGFBP7	7	0.0229	1.3	0.05
TP53	3.5	0.0189	1.6	0.028
RRAS	2.85	0.0000456	2.7	0.05
AKT3	2	0.008	1.96	0.03

Table 1. Senescence and SASP associated genes significantly deregulated in either SK-Mel-5 and A375 melanoma cells upon ERK5 genetic inhibition. Data for shERK5 referred to average results from shERK5-1 and shERK5-2. (**CO** Alessandro Tubita. Published in: Lombardi Z. Tubita A. Tusa I. et al. Cancer Res. 2022 Feb 1. doi: 10.1158/0008-5472).

Based on the above evidence, we investigated whether ERK5 inhibition induces cellular senescence using three melanoma cell lines. Among these we chose two cell lines, A375 and SK-Mel-5, harboring mutated BRAFV600E and one cell line, SSM2c, expressing wt BRAF. In both SK-Mel-5 and A375 ERK5-KD cells revealed a marked increase (20%-30%) of SA-βGal-positive cells, when compared with naive or with control non-targeting shRNA-transduced cells (Figure 2A and B). The same effect was detected in triple wild-type SSM2c cells (Figure 2C). In all three melanoma cell lines, ERK5 genetic inhibition induced an increase of the cell area (Figure 2D), which is a morphological change typical of senescent cells (Munoz-Espín et al.2014).

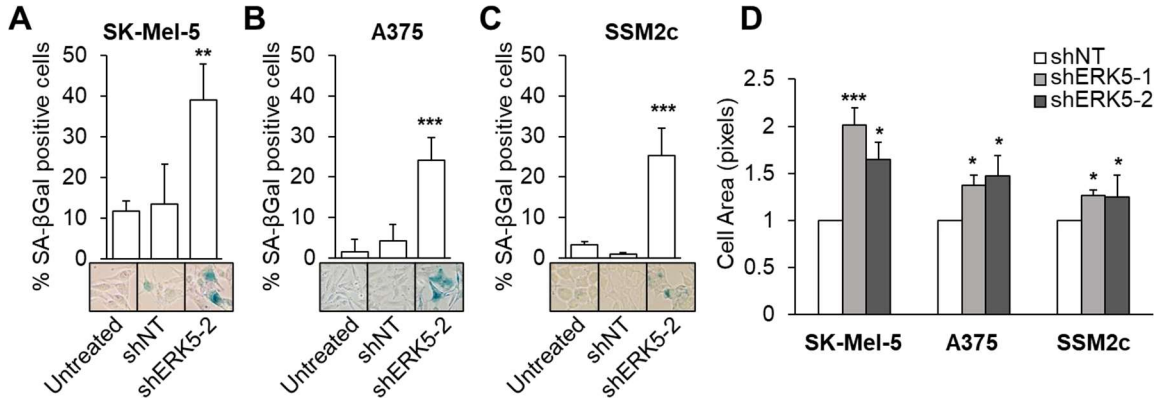

Figure 2. *ERK5 KD increased SA-βGal positivity in melanoma cells*. **A-C)** Untreated cells or cells transduced with lentiviral vectors carrying control (shNT) or ERK5-specific shRNA (shERK5-2) were cultured for 72 hours. The percentage of SA-βGal–positive cells (blue ones) with respect to total number of cells/well was evaluated in three independent experiments. Representative images from each condition are shown. **D)** ERK5 KD induces an increase of melanoma cell area. Cell area was evaluated with ImageJ software. P values refer to differences with respect to shNT; *, $P < 0.05$; **, $P < 0.01$; ***, $P < 0.001$. (**MOD**-My Own Data-Published in: Lombardi Z. Tubita A. Tusa I. et al. Cancer Res. 2022 Feb 1. doi: 10.1158/0008-5472).

In keeping with these results, the ERK5 inhibitors XMD8-92 (Figure 3A-C) and JWG-045, used at concentrations with negligible off-target effects (Tusa *et al.,* 2018), as well as JWG-071, a more specific inhibitor of ERK5 without off target effects on bromodomain-containing proteins (Wang *et al.,* 2018; Williams *et al.,* 2016), were able to elicit a marked cellular senescence (Figure 4A and B). On the other hand, the MEK5 inhibitor BIX02189 did not induce cellular senescence (Figure 4B). Also, ERK5 pharmacologic inhibition, determined an increase of cell area (Figure 3D).

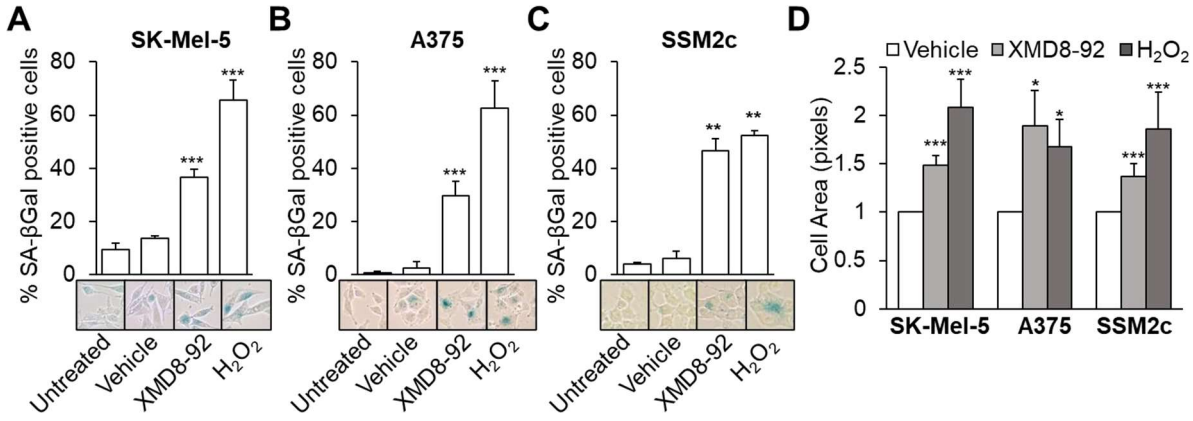

Figure 3. *Pharmacological inhibition of ERK5 induces cellular senescence in melanoma cells.* **A-C**) Cells were left untreated or treated with DMSO (vehicle) or with 5 μM XMD8-92 for 72 hours. Treatment with 300 μM H_2O_2 during the first 2 hours was used as a positive control. The percentage of SA-βGal–positive cells (blue) with respect to the total number of cells/well was evaluated in three independent experiments. Representative images from each condition are shown. P values refer to differences with respect to vehicle-treated samples. **, $P < 0.01$; ***, $P < 0.001$. **D**) The area of the cells quantified in A-C was evaluated with ImageJ software. P values refer to differences with respect to shNT. *, $P < 0.05$; ***, $P < 0.001$. (**MOD**-My Own Data-Published in: Lombardi Z. Tubita A. Tusa I. et al. Cancer Res. 2022 Feb 1. doi: 10.1158/0008-5472).

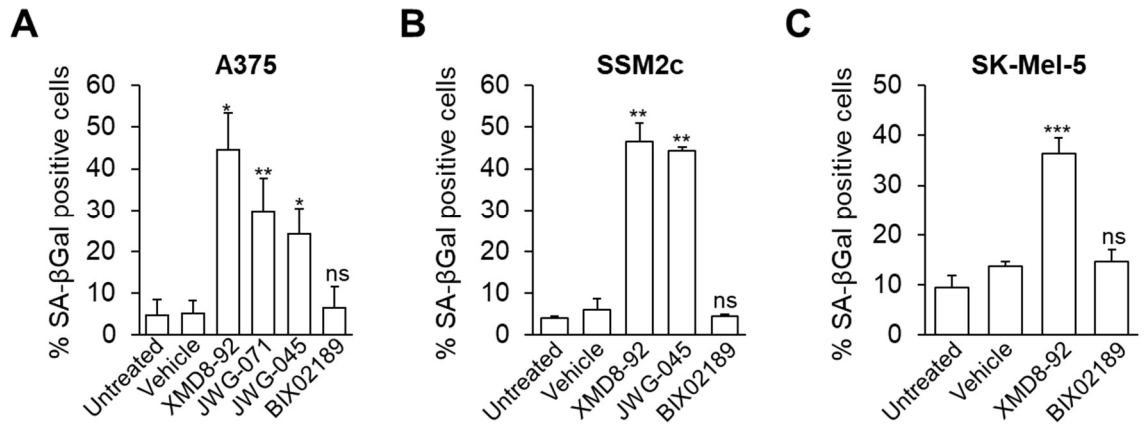

Figure 4. ERK5 pharmacological inhibition induces cellular senescence in melanoma cells. **A)** A375 **(B)** SSM2c **(C)** SK-Mel-5 cells were left untreated or treated with DMSO (Vehicle) or with the indicated drugs (10 μM) for 72 hours DMEM/2.5 % FBS. The percentage of SA-βGal positive cells was then evaluated. Graphs show data from three independent experiments. P values refers to differences with respect to vehicle treated samples. *, $p < 0.05$; **, $p < 0.01$; ***, $p < 0.001$ (**MOD**-My Own Data-Published in: Lombardi Z. Tubita A. Tusa I. et al., Cancer Res. 2022 Feb 1. doi: 10.1158/0008-5472).

Moreover, treatment with XMD8-92 induced the increase of the number of cells containing senescence-associated heterochromatin foci (SAHF) as determined by immunofluorescence experiments staining macroH2A1(Fig. 5A and B), a marker of DNA damage, that are often associated with senescent phenotype. The latter effect was observed also after ERK5 KD in SSM2c cells (Figure 6A). Interestingly, the BRAFV600E inhibitor vemurafenib, but not the MEK1/2 inhibitor trametinib, induced the increase SA-βGal-positive cells similarly to XMD8-92, and in combination with the latter further increased the percentage of senescent cells (Figure 6B).

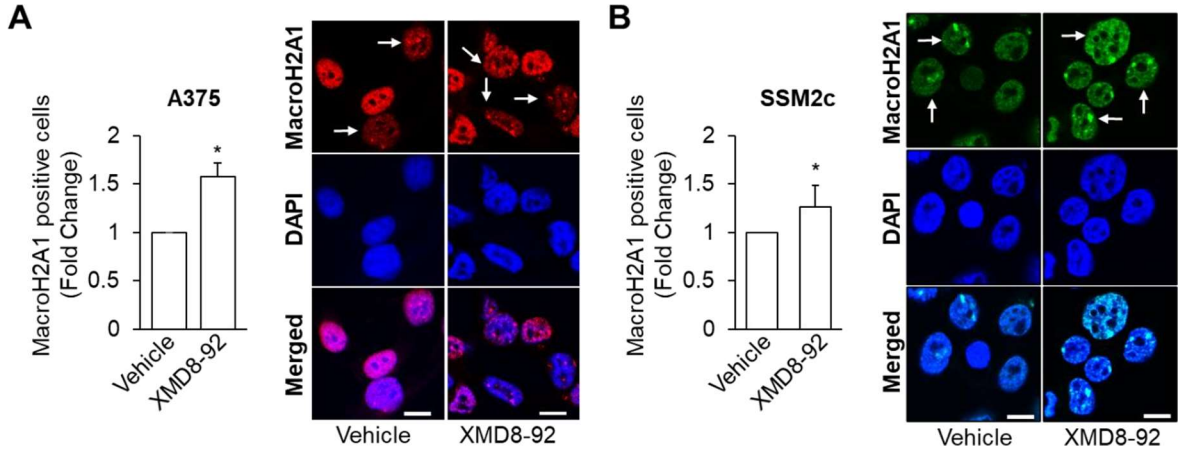

Figure 5. *Pharmacologic inhibition of ERK5 induces an increase in macroH2A1-positive foci formation*. **A-B)** A375 and SSM2c cells were treated with DMSO (vehicle) or with 5 μM XMD8-92 for 72 hours and then stained for macroH2A1. Confocal images were analyzed to quantify macroH2A1-positive cells. P values refer to differences with respect to vehicle-treated cells. *, $P < 0.05$. Scale bar, 10 μm. (**MOD**-My Own Data-Published in: Lombardi Z. Tubita A. Tusa I. et al., Cancer Res. 2022 Feb 1. doi: 10.1158/0008-5472).

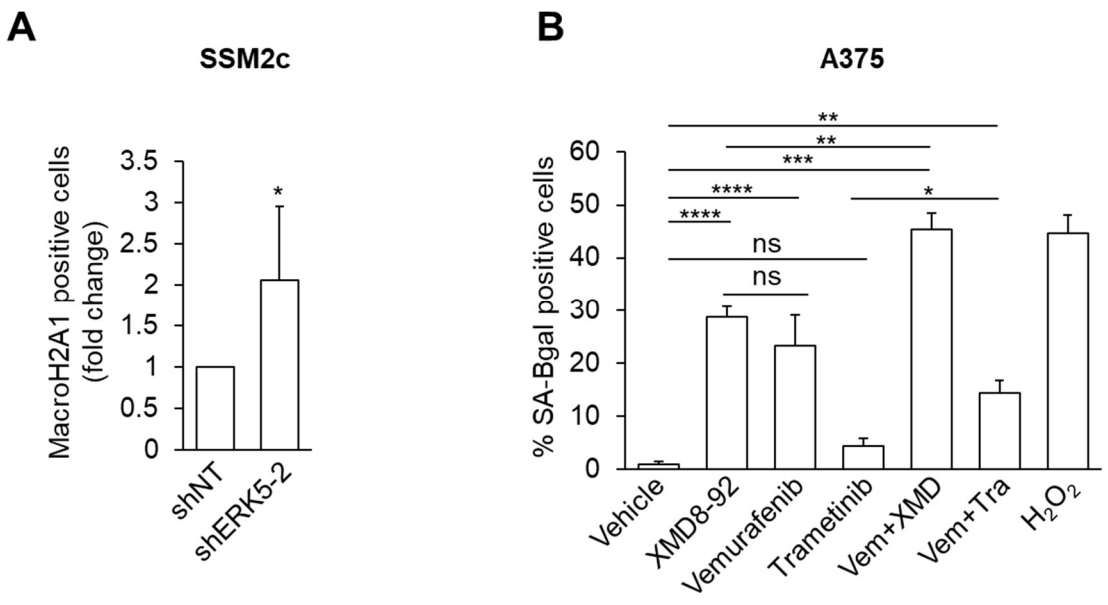

Figure 6. A) SSM2c KD ERK5 cells were cultured for 72 hours and then stained for macroH2A1. Confocal images were analyzed to quantify macroH2A1-positive cells. P values refer to differences with respect to shNT cells. *, P < 0.05. Scale bar, 10 μm. Graphs show data from three independent experiments. P values refers to differences with respect to vehicle treated samples: *, $p < 0.05$. F **B)** A375 cells were treated with DMSO (Vehicle) or with XMD8-92 (5 μM, XMD), Vemurafenib (0.5 μM, Vem), Trametinib (30 nM, Tra) or the combinations of the indicated drugs, for 72 hours in DMEM/2.5 % FBS. Treatment with 300 nM H2O2 during the first 2 hours was used as a positive control. The percentage of SA-βGal positive cells was then evaluated. Graphs show data from three independent experiments. P values refers to differences with respect to vehicle treated samples. *, $p < 0.05$; **, $p < 0.01$; ***, $p < 0.001$; ****, $p < 0.0001$ as determined by one-way ANOVA. (**MOD**-My Own Data-Published in: Lombardi Z. Tubita A. Tusa I. et al., Cancer Res. 2022 Feb 1. doi: 10.1158/0008-5472).

The occurrence of cellular senescence in vivo was then investigated performing lipofuscin staining on archival xenografts of A375 and SSM2c cells transduced with shNT- or shERK5-encoding lentiviral vectors (Tusa *et al.,* 2018). The amount of lipofuscin and the percentage of lipofuscin-stained area were markedly higher in A375 and SSM2c ERK5-KD xenografts than in the control ones (Figure 7A and B). These results are in keeping with in vivo experiments that had previously demonstrated that ERK5 KD in A374 and SSM2c xenografts drastically reduced tumor growth (Figure 7D; Tusa *et al.,* 2018). Similarly, systemic administration of XMD8-92, which induced a marked reduction of tumor growth (Figure 7F; Tusa *et al.,* 2018), determined a robust increase of lipofuscin in A375 xenografts with respect to vehicle-treated mice (Figure 7C).

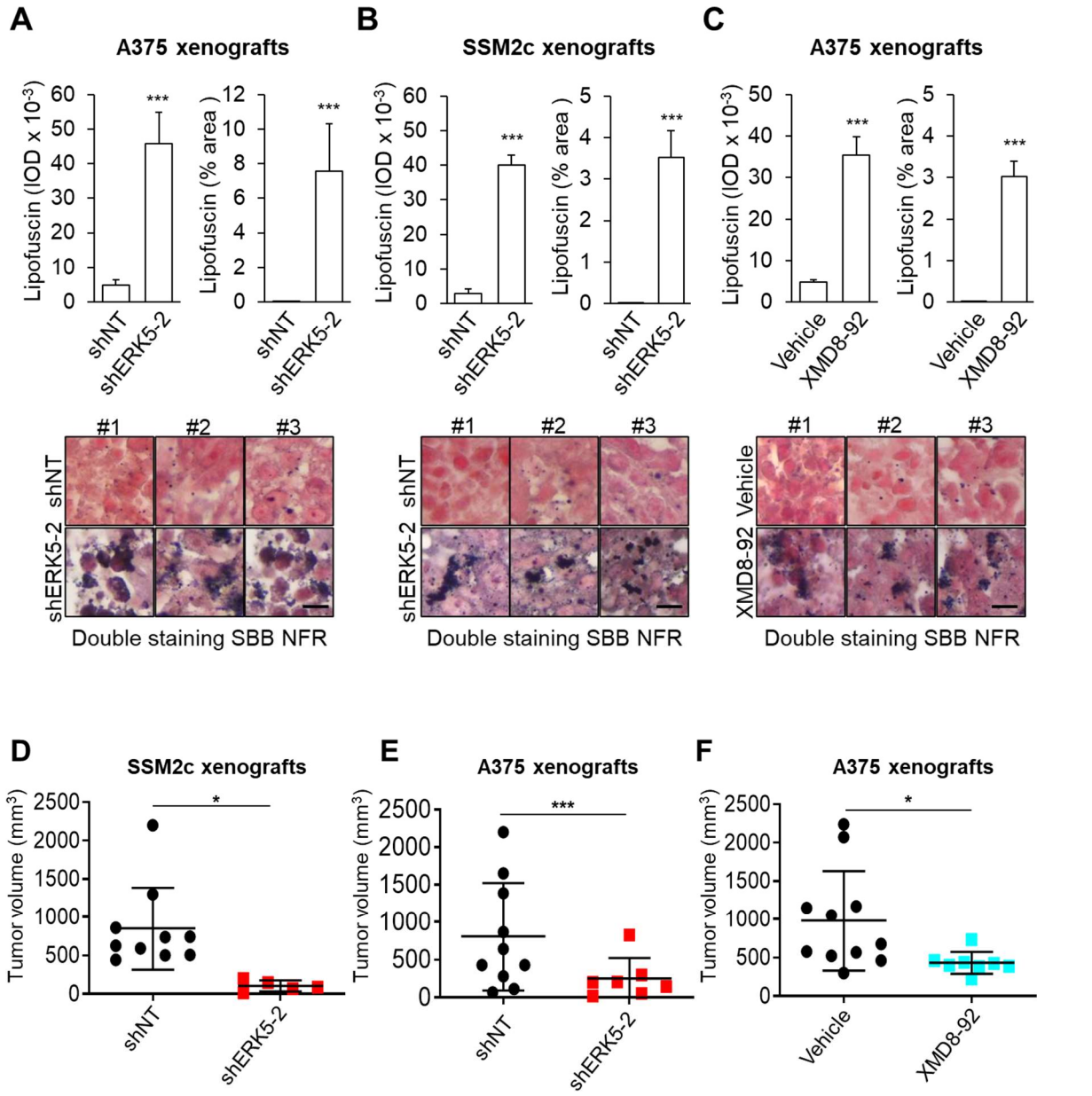

Figure 7. *Genetic inhibition of ERK5 induces senescence in human melanoma xenografts*. **A-C)** FFPE sections from A375 **(A)** and SSM2c **(B)** shNT and shERK5-2 xenografts or A375 xenografts obtained from mice treated with vehicle or XMD8-92 **(C)** were stained with Sudan Black B (SBB) to evaluate lipofuscin content and Nuclear Fast Red (NFR). Integrated optical density (IOD; left graphs) or percentage (%) of area of positively stained tissues (right graphs) was used to quantify the amount of lipofuscin. The integrated optical density and percent area was calculated from six different x40 magnified fields from three xenografts. Representative images are shown. Scale bar, 40 μm. ***, P < 0.001. **D, E)** In vivo tumor growth after subcutaneous injection of 1 × 104 SSM2c (A) or A375 (B) cells transduced with shNT or shERK5-2 lentiviruses. Mice were sacrificed after 47 or 34 days, respectively. Subcutaneous tumor volumes were measured before sacrifice. **F**) In vivo tumor growth of A375 cells subcutaneously injected (1 × 104). Mice were treated at tumor appearance with XMD8-92 (25 mg/kg). After 19 days of treatment mice were sacrificed. Subcutaneous tumor volumes were measured before sacrifice. **D-F)** Data shown are mean ± SEM. *p < 0.05; ***p < 0.001 as determined by Student's t-test. (**CO** Ignazia Tusa, Published in: Lombardi Z. Tubita A. Tusa I. et al. Cancer Res. 2022Feb 1. doi: 10.1158/0008-5472).

1.2 ERK5 inhibition impairs cell-cycle progression and affects cell cycle regulators in melanoma cells

Cellular senescence is a permanent state of cell cycle arrest, so that we evaluated the effects of ERK5 inhibition on cell-cycle progression. Our data revealed that ERK5 genetic inhibition induced an increase of cells in G0-G1 phase in A375 cells and an increase of cells in G2-M phase in SSM2c cells (Figure 8A and B). This increase is robust when taking into consideration that 20% to 30% of the population undergoes senescence upon ERK5 KD (Fig. 2A-C). Furthermore, ERK5 KD determined a reduction of PCNA protein, in keeping with a reduced proliferation (Figure 8C and D).

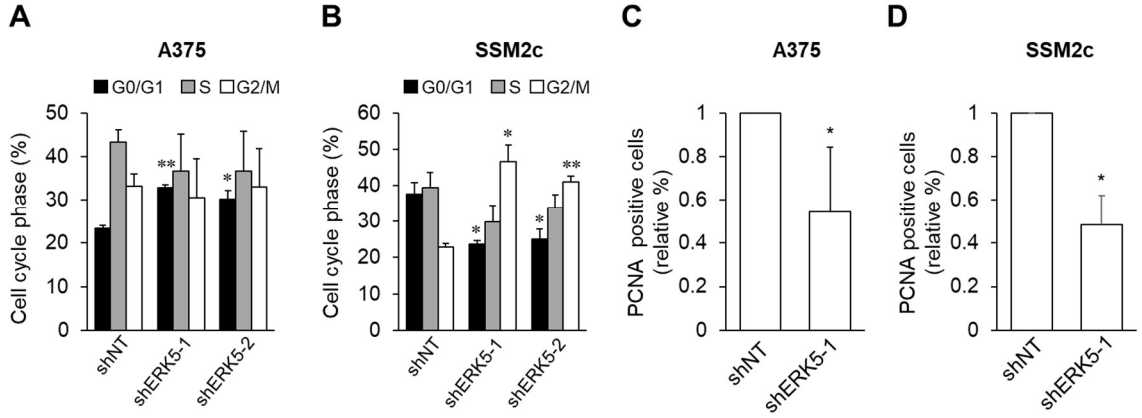

Figure 8. *Effects of ERK5 genetic inhibition on cell-cycle progression and PCNA expression*. **A-B**) Cells were transduced with lentiviral vectors carrying control (shNT) or ERK5-specific shRNA (shERK5-1 or shERK5-2) and were cultured for 72 hours. Cell-cycle phase distribution was then determined in three independent experiments. P values refer to differences with respect to shNT cells. *, $P < 0.05$; **, $P < 0.01$. (**CO** Ignazia Tusa, Published in: Lombardi Z. Tubita A. Tusa I. et al. Cancer Res. 2022 Feb 1. doi: 10.1158/0008-5472). **C-D)** A375 and SSM2c were transduced with lentiviral vectors carrying control (shNT) or ERK5-specific shRNA (shERK5-1) and stained for PCNA. PCNA positive cells were quantified by Flow Cytometry analysis. (**MOD**, My Own Data, Published in: Lombardi Z. Tubita A. Tusa I. et al., Cancer Res. 2022 Feb 1. doi: 10.1158/0008-5472).

Moreover, exposure to mitogens (i.e., 10% FBS), that increased the percentage of vehicle-treated cells in S phase, did not affect cell-cycle phase distribution in XMD8-92-treated cells (Figure 9A and B). In keeping with ERK5-KD cell results, ERK5 pharmacologic inhibition with XMD8-92 determined the block of cell-cycle progression with a significant increase of cells in G0-G1 or G2-M phase in A375 and SSM2c cells, respectively, (Figure 9A and B). Finally, 72 hours treatment with XMD8-92 zeroed A375 and SSM2c colony forming ability, proving evidence of their irreversible inability to proliferate (Figure 9C and D).

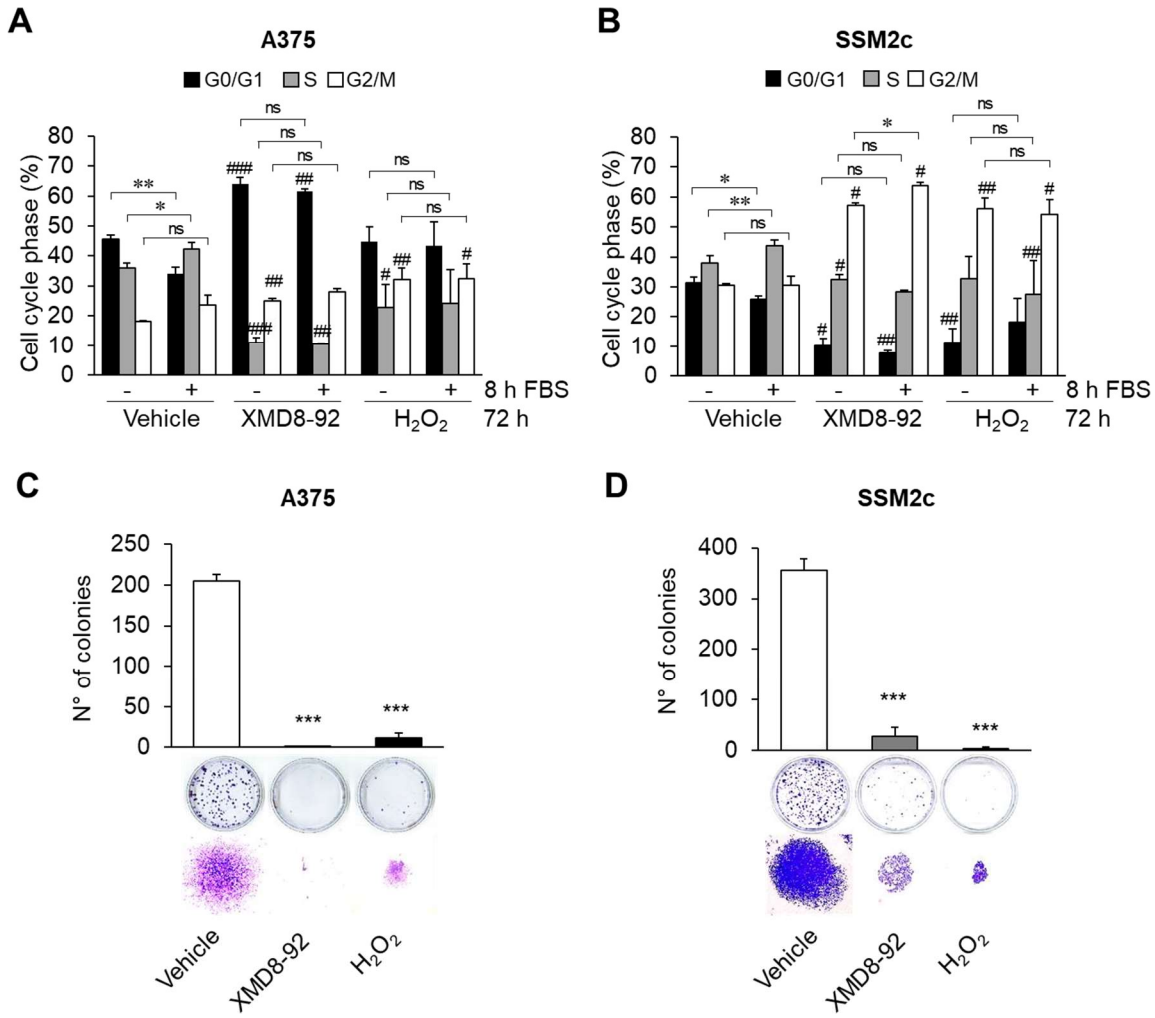

Figure 9. *Effects of ERK5 pharmacologic inhibition on cell-cycle progression and colony formation ability* **A-B)** Cells were treated with vehicle or 5 μM XMD8-92 for 72 hours. Treatment with 300 μM H_2O_2 during the first 2 hours was used as a positive control. After 72 hours, cells were treated with 10% FBS for 8 hours or left untreated. Cell-cycle phase distribution was then determined in three independent experiments. #, $P < 0.05$; ##, $P < 0.01$; ###, $P < 0.001$ refer to differences with vehicle-treated samples; *, $P < 0.05$; **, $P < 0.01$ (**CO** Ignazia Tusa, Published in: Lombardi Z. Tubita A. Tusa I. et al., Cancer Res. 2022 Feb 1. doi: 10.1158/0008-5472). **C-D)** Cells were treated with vehicle or 5 μM XMD8-92 for 72 hours. Treatment with 300 μM H_2O_2 during the first 2 hours was used as a positive control. After 72 hours, colony-forming assay was performed. P values refer to differences with respect to vehicle-treated cells. ***, $P < 0.001$. ns, nonsignificant. (**MOD**, My Own Data, Published in: Lombardi Z. Tubita A. Tusa I. et al., Cancer Res. 2022 Feb 1. doi: 10.1158/0008-5472).

1.3 The cyclin-dependent kinase inhibitor p21 mediates cellular senescence induced by ERK5 inhibition

Western Blot evaluation of cell-cycle regulators involved in cellular senescence showed that ERK5 KD determined a reduction of RB phosphorylation and an increase of the cyclin-dependent kinase inhibitor (CDKi) p21 protein level in A375 and SSM2c cells (Figure 10A), both representing the most used markers of cellular senescence. Moreover, A375 and SSM2c showed the reduced expression of cyclin E, D1, and A2 following ERK5 KD (Figure 10A), in keeping with the reduction of cell proliferation. Intriguingly, the expression of the CDKi p14 protein is increased after genetic (Figure 10A and B) or pharmacologic (Figure 10C and D) ERK5 inhibition. The increased protein levels of p21 (Figure 11A and B) and of p14 (Figure 11C and D) upon ERK5 KD were confirmed also in vivo in IHC analysis using archival A375 and SSM2c xenografts. Of note, the increase in the percentage of p14 positive cells in ERK5-KD A375 xenografts, although significant, was relatively low (Figure 11C), and, accordingly, the increased amount of p14 protein was appreciable in nuclear extracts only (Figure 10A-C).

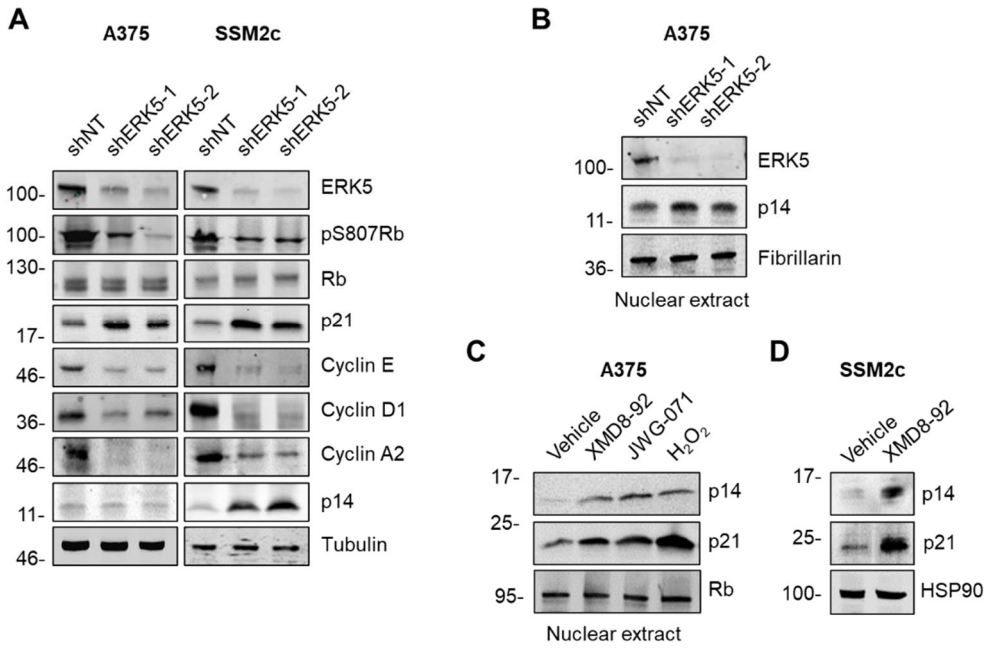

Figure 10. *Effects of ERK5 inhibition on signaling molecules involved in cell cycle and senescence*. **A)** Cells transduced with control nontargeting shRNA (shNT) or ERK5-specific shRNAs (shERK5-1 and shERK5-2) were lysed, and Western blotting was performed with the indicated antibodies. Images are representative of three independent experiments showing similar results. Migration of molecular weight markers is indicated on the left (kDa) **B)** Cells transduced with control nontargeting shRNA (shNT) or ERK5-specific shRNAs (shERK5-1 and shERK5-2) were lysed, and Western blotting was performed on nuclear extracts with the indicated antibodies. Images are representative of three independent experiments showing similar results. Migration of molecular weight markers is indicated on the left (kDa). **C)** Cells were treated with DMSO (vehicle) or with the indicated drugs (5 μM) for 72 hours. Treatment with 300 μM H_2O_2 during the first 2 hours was used as a positive control. **D)** Cells were treated with DMSO (vehicle) or with XMD8-92 (5 μM) for 72 hours. Cells were lysed, and Western blotting was performed with the indicated antibodies. Images are representative of three independent experiments showing similar results. Migration of molecular weight markers is indicated on the left (kDa). (**MOD**, My Own Data).

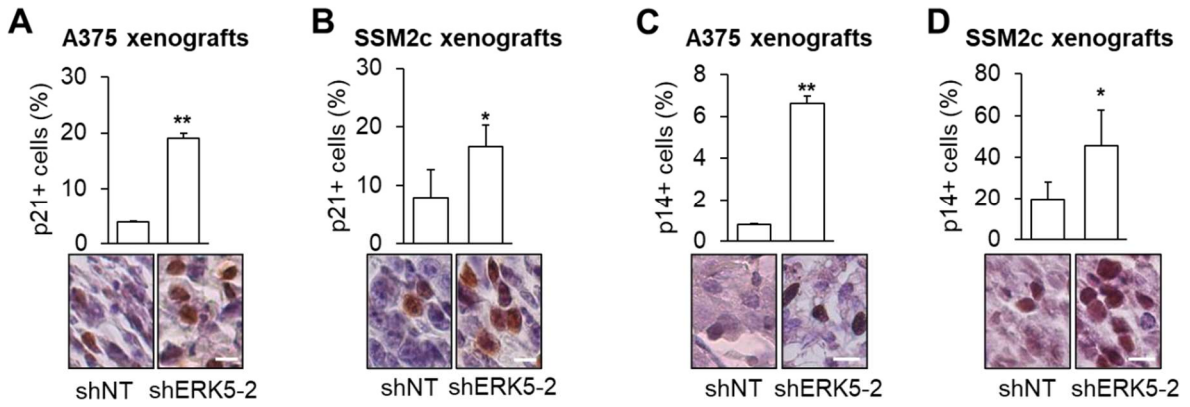

Figure 11. A-D) IHC detection of p21 (**A-B**) or p14 (C-**D**) proteins in shNT- or shERK5-2 xenografts. Hematoxylin counterstaining was performed. Bar plots of percentage (%) of p21 (**E-F**)-or p14 (**G-H**)-positive cells are shown. The percentage of positive cells was calculated from six different 40 magnified fields from three shNT and three shERK5-2 tumors. Representative photographs are shown (original magnification, x40). Scale bar, 40 μm (**CO** Ignazia Tusa, Published in: Lombardi Z. Tubita A. Tusa I. et al., Cancer Res. 2022 Feb 1. doi: 10.1158/0008-5472).

Consistently, we observed an increase of p21 and a decrease of PCNA positive A375 cells after treatment with XMD8-92 in vivo (Figure 12A and B). With regard to additional cell cycle regulators affected by ERK5 KD, we also found an increase of p27 and p53 protein levels (Figure 12C), and the reduction of RBL-1 mRNA (Figure 13A and B), the latter in keeping with the transcriptomic analysis (Table 1).

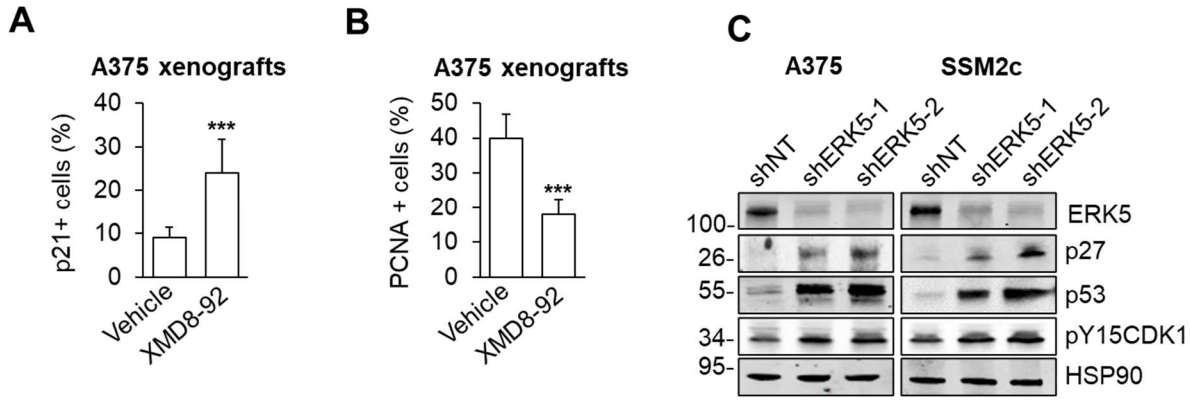

Figure 12. *ERK5 genetic and pharmacological inhibition affects cell-cycle regulators expression.* **A-B)** IHC detection of p21 (**A)** or PCNA (**B**) proteins in Vehicle- or XMD8-92- xenografts. Hematoxylin counterstaining was performed. Bar plots of percentage (%) of p21 or PCNA positive cells are shown. The percentage of positive cells was calculated from six different 40 magnified fields from three vehicle and three XMD8-92- tumors. **C)** A375 or SSM2c cells transduced with control nontargeting shRNA (shNT) or ERK5-specific shRNAs (shERK5–1 and shERK5-2) were lysed, and Western blotting was performed with the indicated antibodies. Images are representative of three independent experiments showing similar results. Migration of molecular weight markers is indicated on the left (kDa). (**CO** Ignazia Tusa and Alessandro Tubita, Published in: Lombardi Z. Tubita A. Tusa I. et al., Cancer Res. 2022 Feb 1. doi: 10.1158/0008-5472).

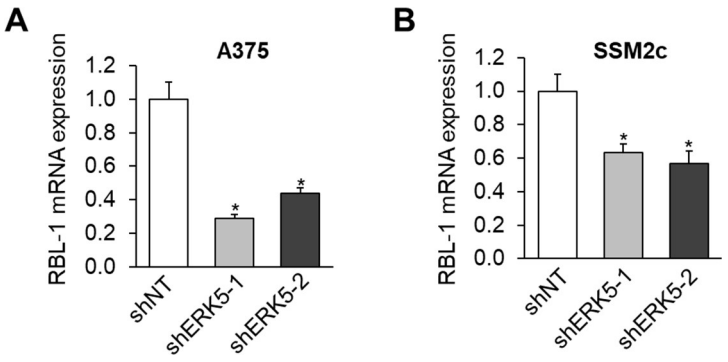

Figure 13. A-B) RBL-1 mRNA levels were determined by qPCR in shNT- or shERK5- A375 **(A)** or SSM2c **(B)** cells. **(CO** Ignazia Tusa, Published in: Lombardi Z. Tubita A. Tusa I. et al., Cancer Res. 2022 Feb 1. doi: 10.1158/0008-5472).

Among the cell-cycle regulators whose expression is markedly deregulated upon ERK5 inhibition, we focused on p21 to deepen the mechanism of ERK5 KD-associated senescence. Of note, p53 was found increased in the transcriptomic data (and confirmed at the protein level), and p21 is the effector of the majority of p53-induced biological effects including cellular senescence. Genetic inhibition of p21 using two different shRNAs (Figure 14A) halved the percentage of A375 cells undergoing cellular senescence following treatment with XMD8-92 or H_2O_2 (Figure 14B), revealing a key role of p21 in ERK5- dependent cellular senescence.

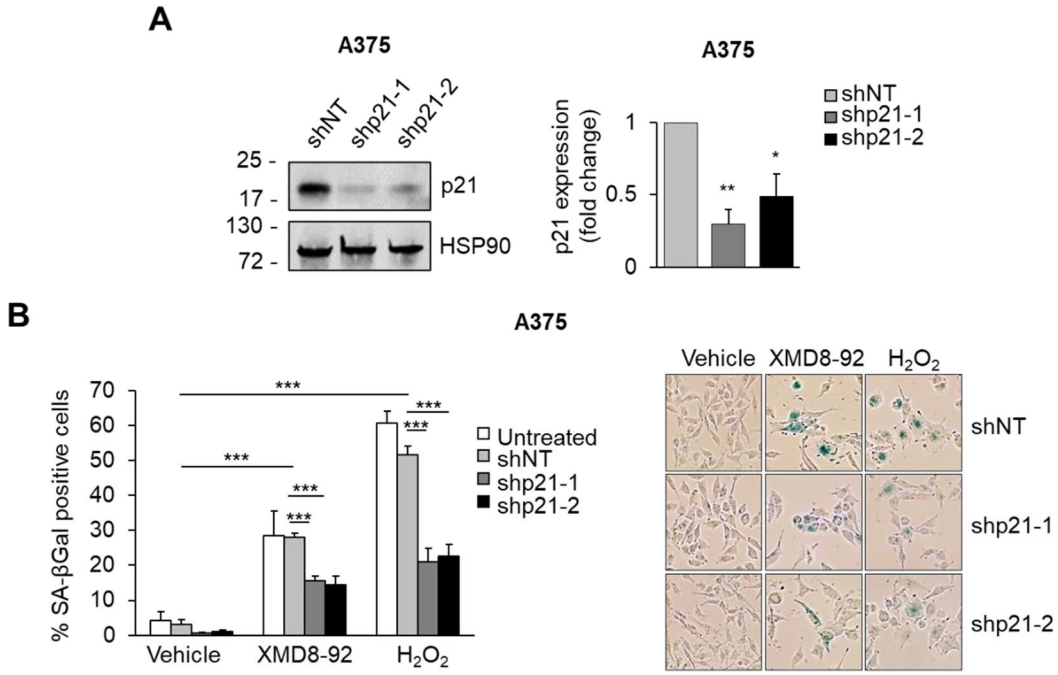

Figure 14. *Genetic inhibition of p21 prevents cellular senescence induced by ERK5 inhibition in A375 cells*. **A)** Cells transduced with control nontargeting shRNA (shNT) or p21- shRNA (shp21-1 and shp21-2) were lysed, and Western blotting was performed with the indicated antibodies. **B)** Untreated A375 or A375 infected with lentiviral vectors carrying shNT, shp21-1, or shp21-2 was treated with DMSO (vehicle) or with XMD8-92 5 μM for 72 hours. Treatment with 300 μM H_2O_2 during the first 2 hours was used as a positive control. The percentage of SA-βGal-positive cells with respect to the total number of cells/well was evaluated in three independent experiments. Representative images from each condition are shown (**MOD,** My Own Data, Published in: Lombardi Z. Tubita A. Tusa I. et al., Cancer Res. 2022 Feb 1. doi: 10.1158/0008-5472).

The observed reduction of the percentage of cells undergoing senescence upon p21 KD was robust, taking into consideration that XMD8-92 induced a slight but significant increase of p21 protein level in p21 KD cells (Figure 15A; compare lanes 5 and 6 vs. 2 and 3, respectively). In this respect, the lack of effect of BIX02189 on cellular senescence (Figure 4) is in keeping with the previously reported ineffectiveness of this compound in increasing p21 protein level (Tusa *et al.,* 2018), while XMD8-92 induced a dose dependent increase of cellular senescence and p21 protein (Figure 15B and C). The above data indicate that cellular senescence induced by ERK5 inhibition in melanoma cells relies, at least in part, on p21.

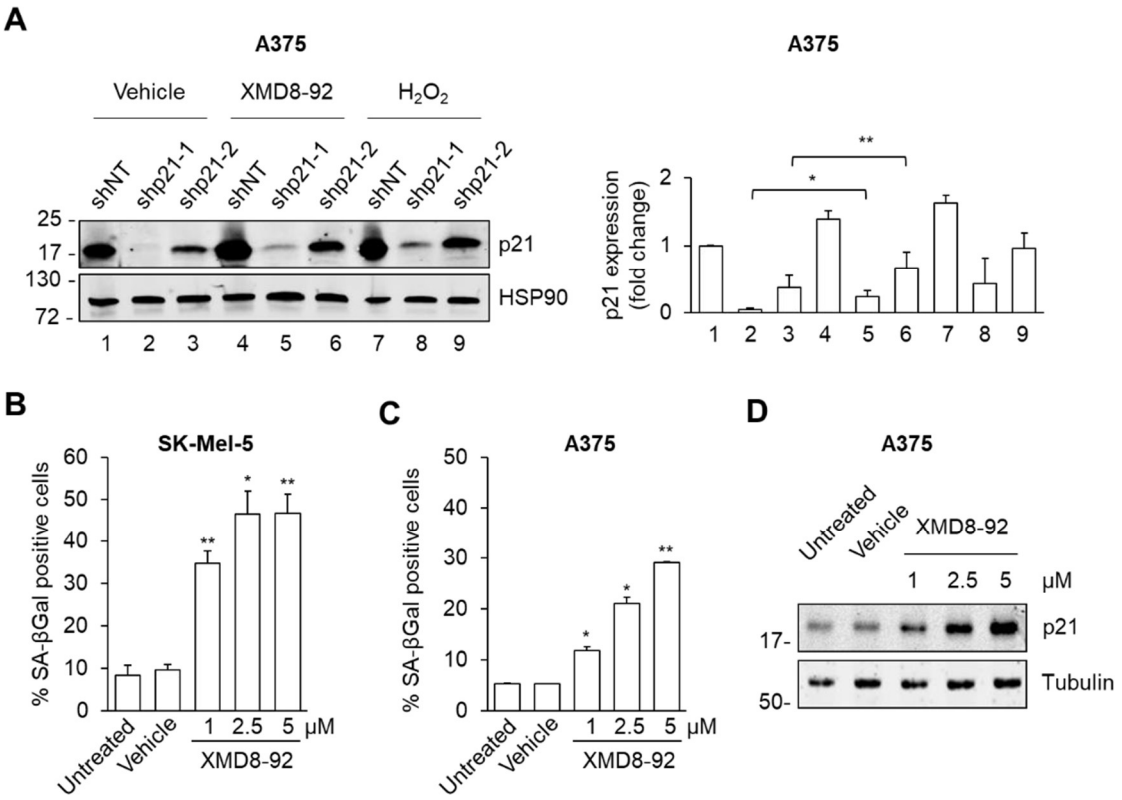

Figure 15. *XMD8-92 induces cellular senescence and p21 expression in melanoma cells in a dose-dependent manner*. **A)** A375 cells infected with lentiviral vectors carrying shNT, shp21-1 or shp21-2 were treated with DMSO (vehicle) or 5 μM XMD8-92 for 72 hours and H_2O_2 (300 μM for 2 hours) and then lysed. p21 expression was evaluated by Western blotting. Blots are representative of three independent experiments showing similar results. The graph shows average densitometric values of p21 protein normalized for HSP90 content. **B-C)** A375 and Sk-Mel-5 cells were treated with DMSO (vehicle) or with increasing concentrations of XMD8-92 for 72 hours. The percentage of SA-βGal-positive cells with respect to the total number of cells/well was evaluated in three independent experiments. **D)** A375 cells treated with vehicle or with increasing concentrations of XMD8-92 for 72h were lysed, and Western blotting was performed with the indicated antibodies. Images are representative of three independent experiments showing similar results. Migration of molecular weight markers is indicated on the left (kDa). *, $P < 0.05$; **, $P < 0.01$; ***, $P < 0.001$. (**MOD**, Published in: Lombardi Z. Tubita A. Tusa I. et al., Cancer Res. 2022 Feb 1. doi: 10.1158/0008-5472).

1.4 ERK5 inhibition induces the senescence-associated secretory phenotype

One of the key features of senescent cells is the senescence-associated secretory phenotype (SASP). Transcriptomic data showed that SASP and SASP-related genes (Table 1) were significantly modulated upon ERK5 KD. Among the latter, transcriptomic analysis indicated that CXCL1/GROalpha and CXCL8/IL8, two of the most prominent SASP products, and CCL20/MIP3alpha mRNA were significantly upregulated in both A375 and SK-Mel-5 ERK5-KD cells (Figure 16A). IL6, another key component of the SASP, was not altered upon ERK5 KD (Figure 16A). QPCR experiments confirmed that lack of increase of IL6 mRNA in the same experimental settings in which CXCL8 mRNA was significantly increased in A375, SK-Mel-5, and SSM2c ERK5-KD cells (Figure 16B). Importantly, protein array performed using CM (Figure 16C) confirmed that CXCL1, CXCL8, and CCL20 protein levels were significantly increased in the supernatant of ERK5-KD A375 cells.

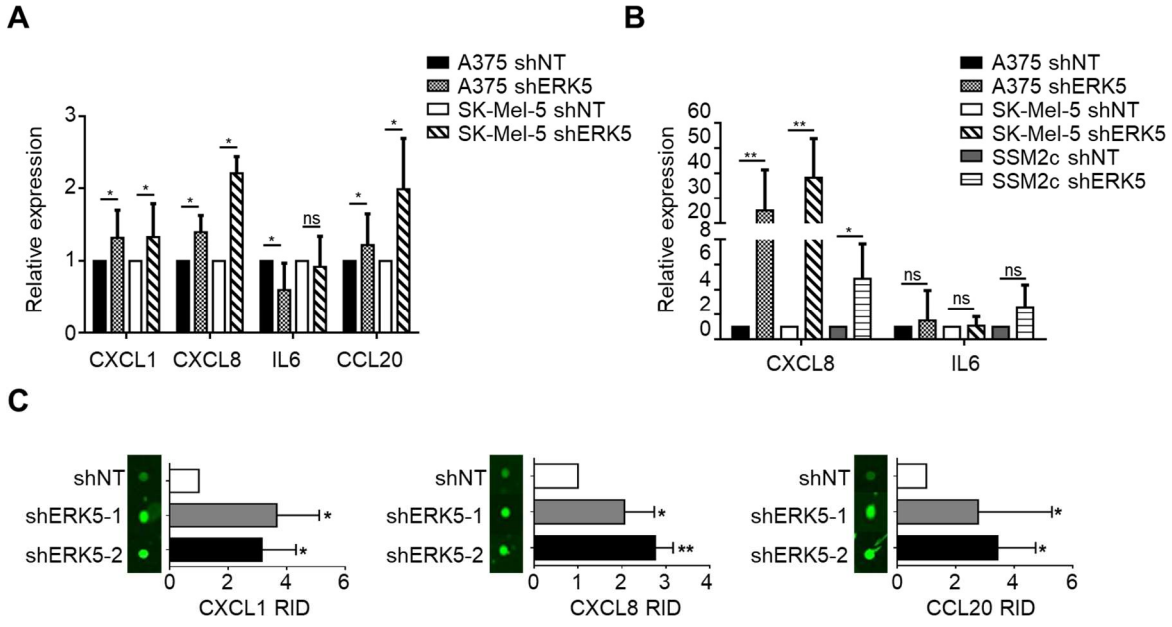

Figure 16. *ERK5 KD increases SASP soluble factors*. **A**) mRNA expression profiles were determined using TAC software. Data shown for shERK5 are mean (±SD) of pulled data from shERK5-1 and shERK5-2 (A375, n =4; SK-Mel-5, n=3). P < 0.05 as determined using one-way ANOVA. **B)** CXCL8 and IL6 mRNA levels determined by qPCR in ERK5 KD cells. Data shown for shERK5 are mean (±SD) of pulled data from shERK5-1 and shERK5-2 (A375, n=6; SK-Mel-5, n=6). **C)** Chemokines expression in CM from ERK5-KD (shERK5-1 and shERK5-2) A375 cells was analyzed using Quantibody Human Array (#QAA-CUST-SW; RayBiotech). Each antigen was measured in quadruplicate from three independent experiments and the relative fluorescence intensity (RID) was determined using ImageJ software (NIH). The obtained results were normalized for protein content in cell lysates. Data shown are mean ± SD. Representative fluorescent dots are shown. (**CO** Alessandro Tubita, Published in: Lombardi Z. Tubita A. Tusa I. et al., Cancer Res. 2022 Feb 1. doi: 10.1158/0008-5472).

Interestingly, publicly available datasets from the cBioPortal for Cancer Genomics (Cerami *et al.,*2012; Gao *et al.,* 2013) confirmed the coexpression of the above-mentioned SASP products in patients with melanoma (Figure 17A and B). Indeed, the amount of CXCL1/GROalpha mRNA showed a robust positive correlation with that of CXCL8 (0.58 Spearman correlation; P=6.68e–41), and with that of CCL20 (0.49 Spearman correlation; P=1.34e–27; Skin Cutaneous Melanoma TCGA, PanCancer Atlas; Figure 17A). The positive correlation between the mRNA levels of CXCL1/GROalpha and of CXCL8 was confirmed (0.35 Spearman correlation; P=0.028) in another data set (Metastatic Melanoma, DFCI, Science 201; Figure 17B). SASP products may elicit either pro- or antiproliferative effects on tumor cells (Evangelou *et al.,* 2017).

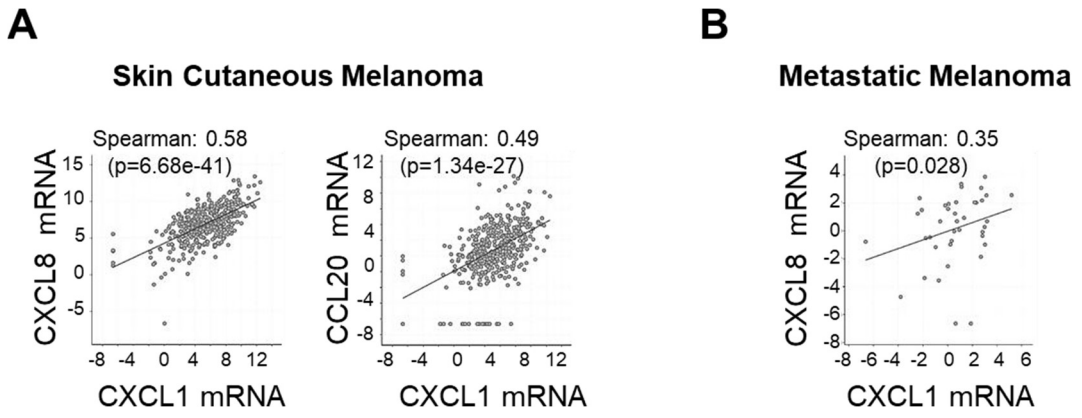

Figure 17. *ERK5 KD increases SASP soluble factors.* **A-B)** Data from Skin Cutaneous Melanoma TCGA, PanCancer Atlas and Metastatic Melanoma, DFCI, Science 201.

To discriminate between these possible opposite outcomes, we tested CM from A375 and SK-Mel-5 cells and found that CM recovered from ERK5-KD cells markedly reduced the viability of either A375 or SK-MEL-5 cells with respect to CM from shNT cells (Figure 18A). The proof that CXCL1, CXCL8, and CCL20 are among the SASP products responsible for the reduced proliferation was obtained using neutralizing antibodies (Figure 18B). Indeed, each blocking antibody was able to partially rescue melanoma cell proliferation.

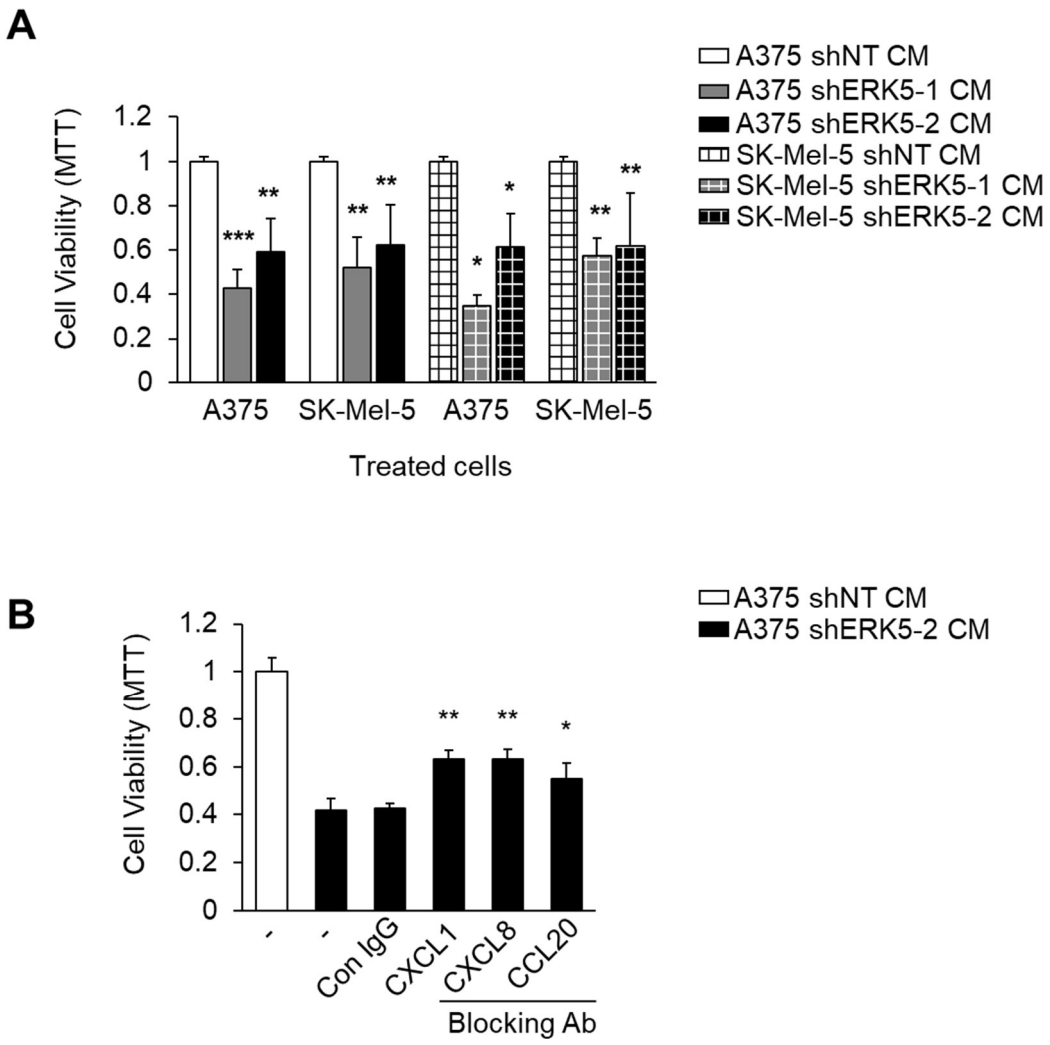

Figure 18. A) MTT was performed in A375 or SK-Mel-5 cells treated with CM harvested from A375 or SK-Mel-5 cells 14 days posttransduction with shNT or shERK5 (shERK5-1 or shERK5-2) lentiviral vectors. Data shown are mean ± SD from three independent experiments. **B)** MTT was performed on A375 cells treated with CM harvested from shNT (white column) or shERK5-2 (dark columns) A375 cells in the presence of 10 mg/mL of the indicated blocking antibodies or control IgG. Data shown are mean ± SD from three independent experiments. *, $P < 0.05$; **, $P < 0.01$; ***, $P < 0.001$ as determined by Student t test. ns, nonsignificant. (**CO** Alessandro Tubita, Published in: Lombardi Z. Tubita A. Tusa I. et al., Cancer Res. 2022 Feb 1. doi: 10.1158/0008-5472).

2. ERK5 NUCLEAR SHUTTLING

2.1 α/β1 importin mediates ERK5 nuclear shuttling

The presence of a classical NLS (Figure 1) in ERK5 sequence (Yan *et al.,* 2001) and the work of Flores and colleagues that hypothesized that ERK5 goes into the nucleus through α/β importin (Flores *at al.,* 2019) prompted us to investigate on the involvement of α/β1 importin in ERK5 nuclear translocation.

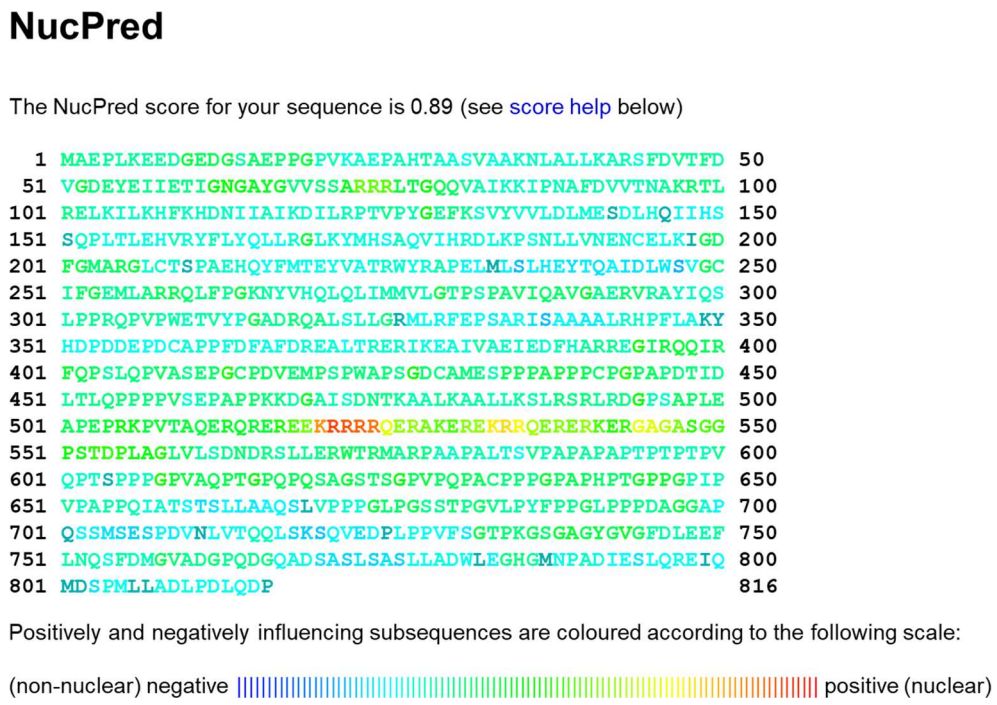

Figure 1. Predicted NLS in the ERK5 sequence. Created with https://nucpred.bioinfo.se/cgi-bin/single.cgi.

To this end, we knocked down (KD) Importin beta-1 (gene name *KPNB1*), by using two different siRNA, in HEK293T cells in which ERK5 nuclear translocation is achieved by overexpressing ERK5 together with the constitutively active form of its activator MEK5 (MEK5DD). Western blot analysis showed that the amount of ERK5 in the nucleus, but not in total cell lysates, of siKPNB1-treated cells was reduced by 50 % with respect to that of cells treated with a non-targeting control siRNA (siNT) (Figure 2A). Similarly, *KPNB1* KD was able to halve the amount of endogenous ERK5 in the nuclear fraction in BRAFV600E A375

melanoma cells, with respect to control ones (Figure 2B). In the same experimental conditions, the overall amount of ERK5 in whole cell lysates did not change after *KPNB1* knock down.

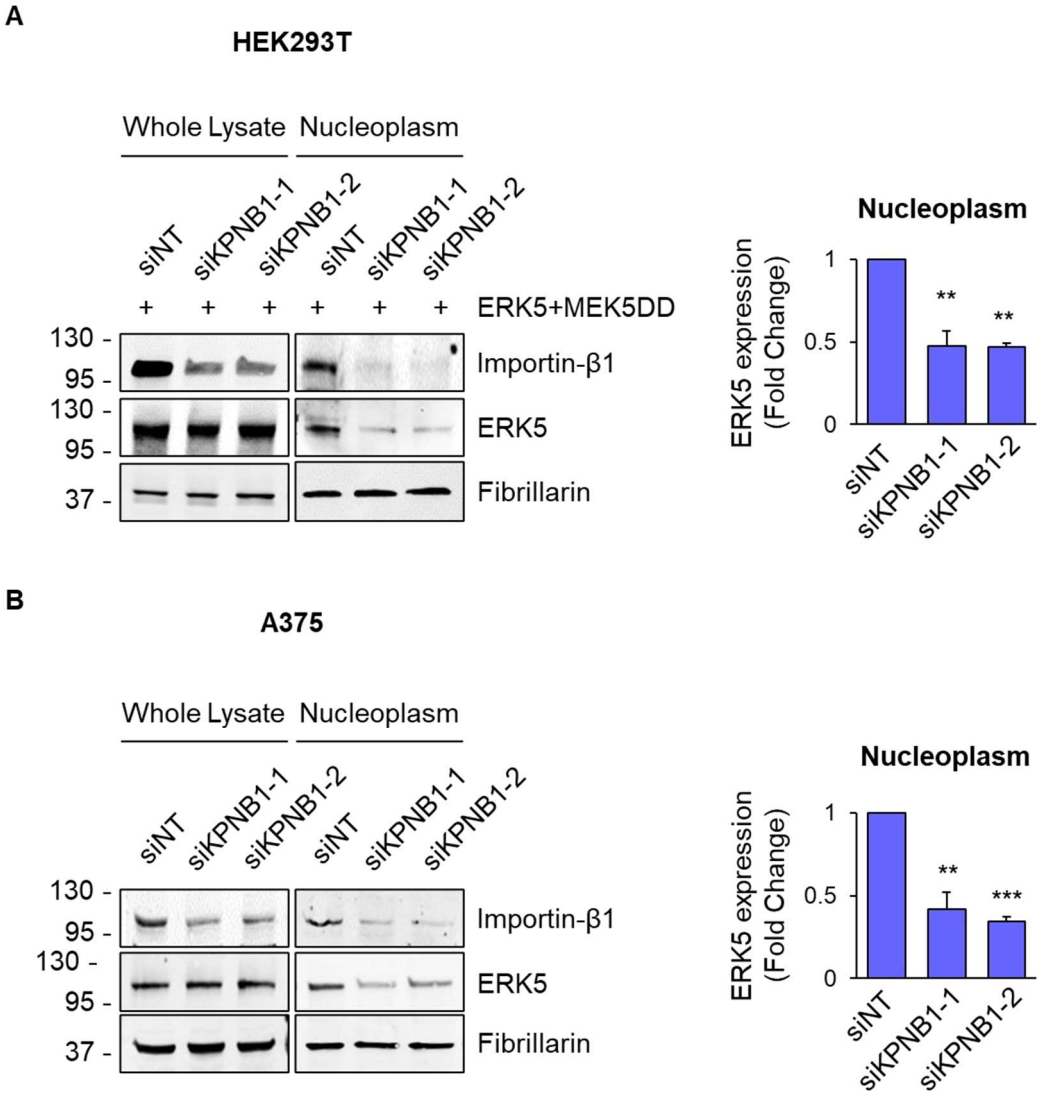

Figure 2. *KPNB1 KD reduces the amount of nuclear ERK5.* HEK293T ERK5WT+/MEK5DD+ (**A**) or A375 (**B**) cells transfected with two siRNA targeting *KPNB1* or with non-targeting control siRNA were lysed and Western Blot was performed on whole cell lysates or nuclear extracts with the indicated antibodies. Migration of molecular weight markers is indicated on the left (kDa). The graph show average densitometric values of nuclear ERK5 protein levels normalized for fibrillarin content from three independent experiments. P values refer to differences with respect to siNT control cells. **, $P < 0.01$; ***, $P < 0.001$. (**MOD**, My Own Data).

Cell fractionating lysis was performed 72h after transfection with siRNA anti-KPNB1, resulting the best time to achieve a good silencing efficacy, as obtained upon *KPNB1* KD in A375 cells lysed 24, 48 or 72h after transfection with siRNA anti-KPNB1 (Figure 3).

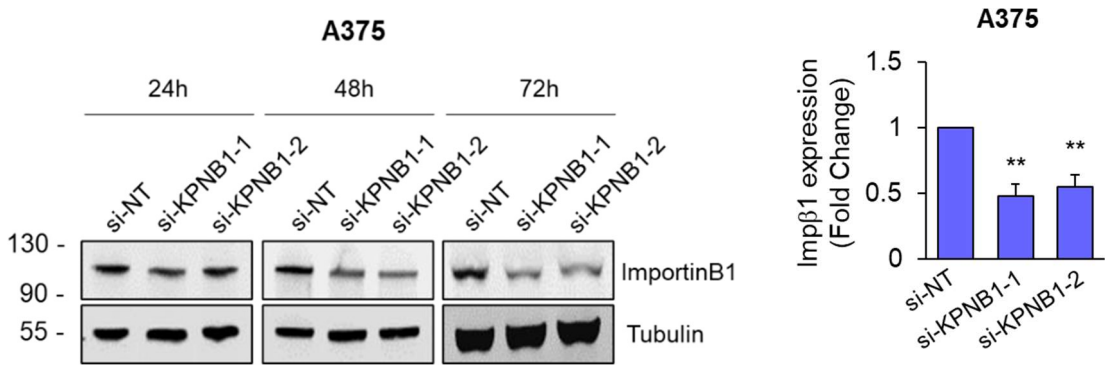

Figure 3. *KPNB1 silencing efficacy.* A375 cells transfected with two siRNA targeting *KPNB1* or with non-targeting siRNA were lysed after 24, 48 or 72h and Western Blot was performed with the indicated antibodies. Migration of molecular weight markers is indicated on the left (kDa). The graph shows average densitometric values of *KPNB1* protein levels normalized for tubulin content 72h after siRNA transfection. P values refer to differences with respect to siNT control cells. **, $P < 0.01$. (**MOD**, My Own Data).

In order to identify pharmacological treatments able to prevent ERK5 nuclear translocation and to confirm the involvement of the α/β1 importin complexes (since it has been reported that importin β1 requires α subunit to mediate cNLS-cargo nuclear import), we performed pharmacological inhibition of α/β1 importin using ivermectin (IVM). Ivermectin is a potent inhibitor of IMPα/β1-dependent transport, with no effect on proteins containing NLSs recognized by alternative nuclear import pathways (Wagstaff *et al.,* 2011). Treatment with ivermectin reduced the amount of ERK5 in the nucleus in a dose dependent manner, with a measurable and statistically significant effect starting at 5 μM, in both ERK5/MEK5DD-overexpressing HEK293T cells and A375 cells (Figure 4A and 4B). The kinetics of the reduction of nuclear ERK5 was similar to that of CyclinB1, a known target of α/β1 importin and used as a positive control. In the same experimental conditions, the overall amount of ERK5 in whole cell lysates did not change after ivermectin treatment.

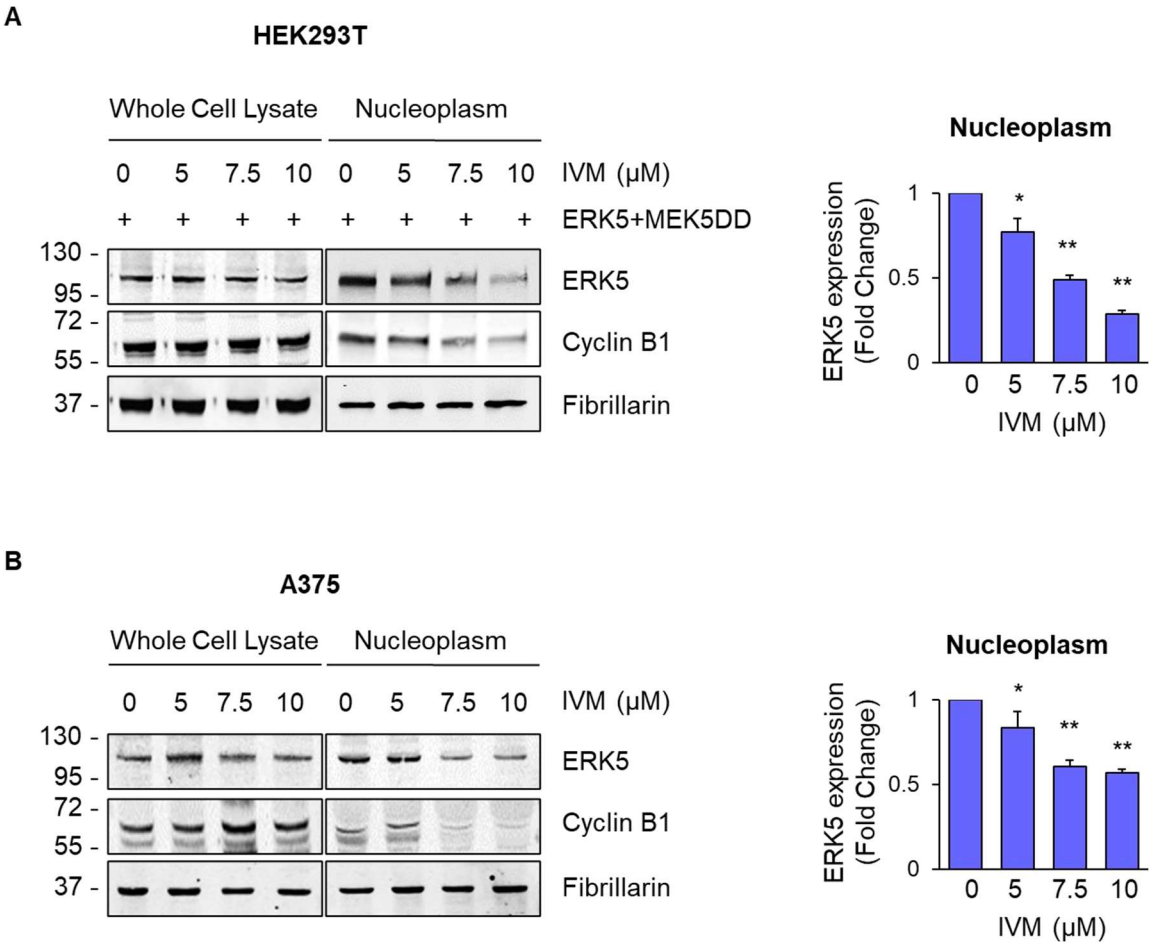

Figure 4. *IVM reduces ERK5 nuclear amounts in a dose dependent manner, without affecting the total amount of ERK5 within the cell.* HEK293T ERK5WT+/MEK5DD+ (**A**) and A375 (**B**) cells treated for 24h with increased concentration of IVM were lysed and Western Blot was performed on whole cell lysates or nuclear extracts with the indicated antibodies Migration of molecular weight markers is indicated on the left (kDa). The graphs show average densitometric values of nuclear ERK5 protein levels normalized for fibrillarin content from three independent experiments. Cyclin B1, a known target of α/β1 importin, has been used as a positive control. P values refer to differences with respect to vehicle-treated cells. *, $P < 0.05$; **, $P < 0.01$. (**MOD**, My Own Data).

We previously showed that oncogenic BRAF enhances ERK5 nuclear localization, including that in the chromatin-bound fraction, thus increasing its transcriptional transactivator activity (Tusa et al., 2018). Interestingly, more recent experiments showed that treatment with ivermectin reduced the amount of ERK5 linked to chromatin in a dose-dependent manner, in both ERK5/MEK5DD-overexpressing HEK293T cells and A375 cells (Figure 5).

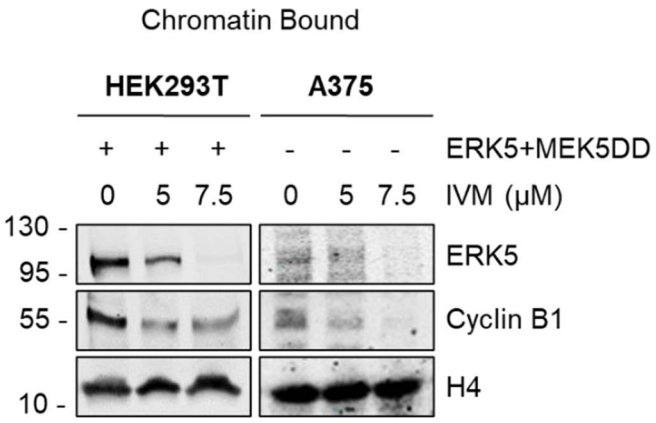

Figure 5. *Ivermectin reduces ERK5 amount in the chromatin-bound fraction.* HEK293T overexpressing ERK5WT and MEK5DD and A375 cells were treated with the indicated doses of IVM for 24h. Cells were lysed and Western Blot was performed chromatin-bound extracts with the indicated antibodies. Cyclin B1, a known target of α/β importin, has been used as a positive control. Migration of molecular weight markers is indicated on the left (kDa). (**MOD**, My Own Data).

2.2 Single molecule analysis confirmed the involvement of α/β1 importin in ERK5 nuclear shuttling by super resolution microscopy

To study ERK5 shuttling in more depth, we developed a method to localize single ERK5 molecules using super-resolution microscopy. To this end, we made a vector for the expression of wt ERK5 linked to the HaloTag (Figure 6A). The accuracy of the cloning strategy was confirmed by agarose electrophoretic gel, in which ERK5 sequence and HaloTag sequence were detected at the expected size, upon enzymatic digestion (Figure 6B). We then overexpressed ERK5-HaloTag in HEK293T cells, and ERK5-Halo was clearly detected in WB at a higher MW compared to ERK5 WT (Figure 6C).

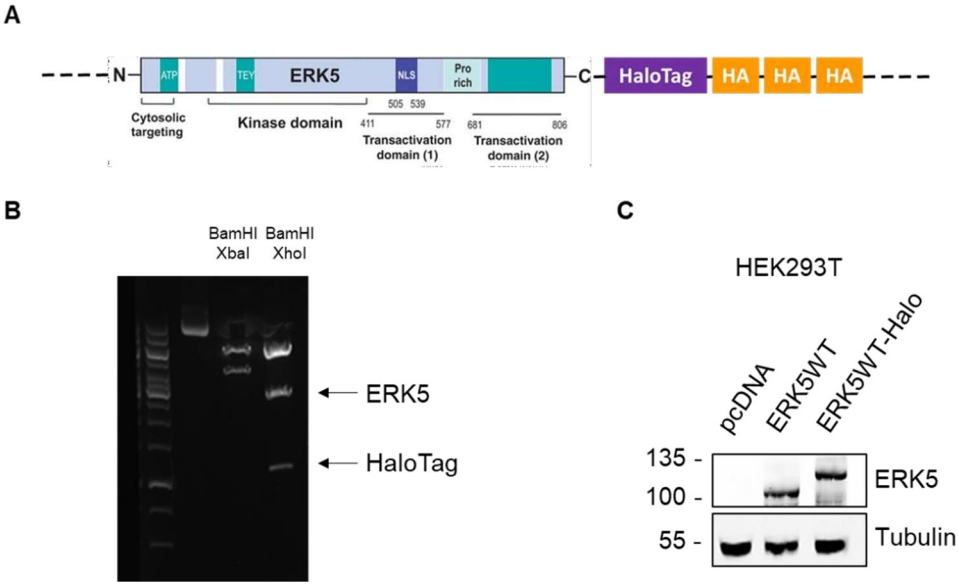

Figure 6. *JaneliaFluor646 selectively binds ERK5-HaloTag molecules.* **A)** Schematic representation of ERK5-HaloTag. **B)** pCDNA3.1 ERK5-HaloTag-3xHA cloned vector was digested with the indicated restriction enzymes and agarose electrophoretic gel was performed. ERK5 sequence and HaloTag sequence were detected with the expected size. **C)** HEK293T cells transfected with ERK5-HaloTag or with ERKWT vector were lysed and Western Blot was performed with indicated antibodies. ERK5-HaloTag is detectable with an anti-ERK5 antibody at a higher molecular weight compared to ERKWT. Migration of molecular weight markers is indicated on the left (kDa).

The HaloTag present in the ERK5-HaloTag molecules could be selectively bound by the photo-activatable and cell permeable fluorescent dye JaneliaFluor646 (schematic representation in Figure 7A) useful for the detection technique. In fact, fluorescent signals were collected by confocal microscopy in HeLa cells transfected with ERK5-HaloTag, whereas no signal was collected in empty vector transfected cells (Figure 7B). HeLa cell line, indeed, is more suitable for further super resolution microscopy analysis due to a higher adhesion capacity and a more enlarged morphology with respect to HEK293T cells.

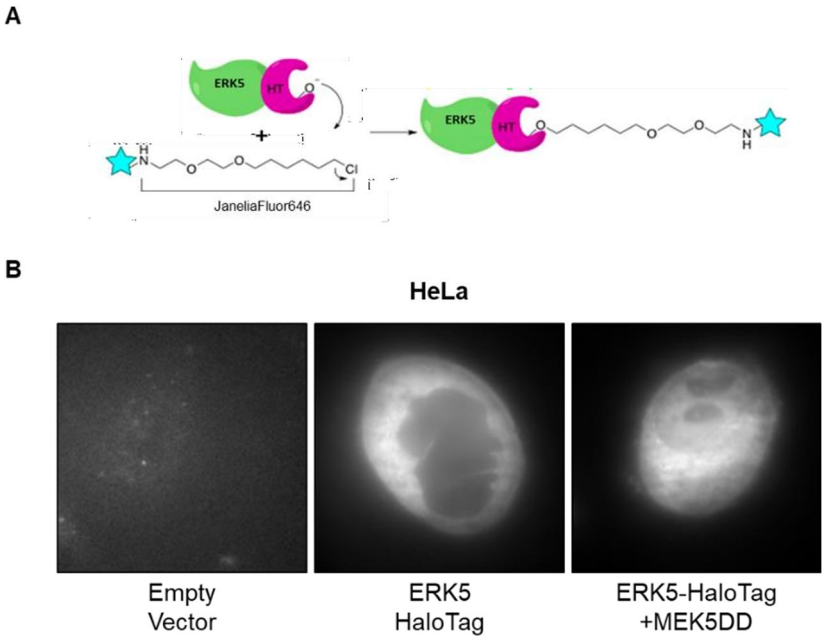

Figure 7. A) Schematic representation of the JaneliaFluor646 structure binding the HaloTag. **B)** Confocal imaging of HeLa cells transfected with ERK5-HaloTag, ERK5-HaloTag+MEK5DD or with a control empty vector and labelled with JaneliaFluor646. The signal is absent in empty vector transfected cells. (**MOD**, My Own Data).

Cell fractionation experiments showed that ivermectin was able to robustly reduce ERK5 nuclear amount also in HeLa cells transfected with ERK5-HaloTag vector with respect to untreated cells (Figure 8).

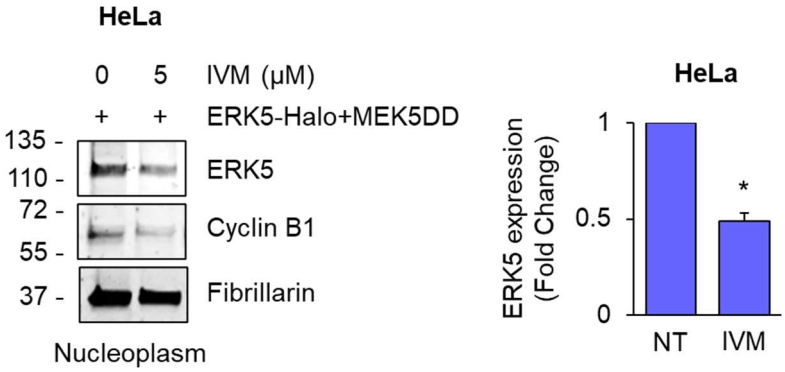

Figure 8. *Ivermectin reduces ERK5-HaloTag nuclear amount*. HeLa cell transfected with ERK5-HaloTag and MEK5DD vectors and treated with 5 μM IVM or with vehicle (DMSO) for 24h were lysed and Western Blot was performed on nuclear extracts with the indicated antibodies. The graphs show average densitometric values of nuclear ERK5 protein levels normalized for fibrillarin content from three independent experiments. Cyclin B1, a known target of α/β1 importin, has been used as a positive control. Migration of molecular weight markers is indicated on the left (kDa). P values refer to differences with respect to vehicle-treated cells. *, $P < 0.05$. (**MOD**, My Own Data).

To further confirm the effect of ivermectin on ERK5 nuclear translocation, we moved to super resolution microscopy that allowed to localize single ERK5 molecules in a living cell. The quantification of ERK5 spatial density (i.e. the number of ERK5 nuclear particles normalized for the nuclear area or the number of ERK5 cytoplasmic particles normalized for the cytoplasm area) shows an increase in the ERK5 nucleus/cytoplasmic density ratio in HeLa cells transfected with ERK5-Halotag and MEK5DD with respect to those transfected with ERK5-HaloTag alone. In line with the previous results obtained in Western Blot experiments, treatment with ivermectin was able to markedly reduce the nucleus/cytoplasmic ratio of ERK5 instances in HeLa ERK5-HaloTag+/MEK5DD+ cells (Figure 9).

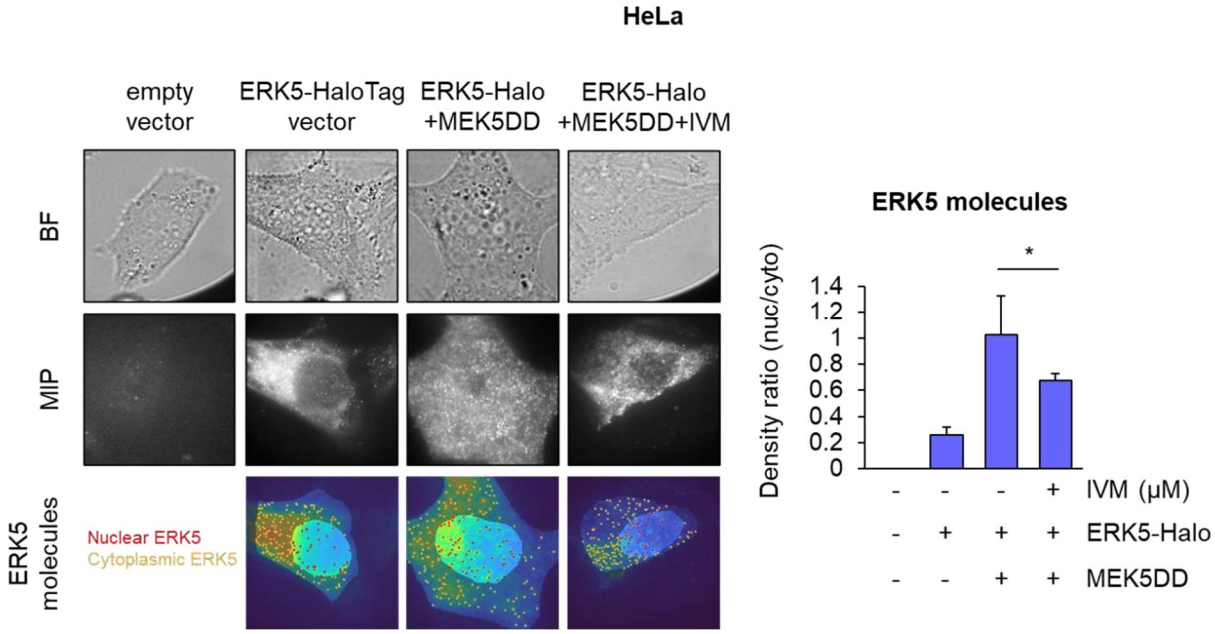

Figure 9. *Ivermectin treatment inhibits ERK5 single molecules nuclear translocation in super resolution analysis*. Bright-field images (BF, first row), maximum intensity projection images of super-resolution videos (MIP, second row) and single frames of super-resolution videos overlapped with cytoplasmic and nuclear masks (third row) of HeLa cells transfected with an empty vector (first column), ERK5-HaloTag (second column) or ERK5-HaloTag+MEK5DD (third column). Cells were left untreated (first-third columns) or treated with 5 μM IVM for 24h. All samples were labelled with JaneliaFluor646. The graph on the right represents the nucleus/cytoplasmic ratio of ERK5 single molecules detected in the super-resolution videos in each sample condition. Number of cells/samples = 20. P values refer to differences with respect to ERK5-HaloTag+MEK5DD Hela vehicle-treated cells. *, $P < 0.05$. (**MOD**, My Own Data, **CO** European Laboratory of Non-Linear Spectroscopy, LENS).

The nuclear region was determined based on the bright field image of the cells to create masks for super resolution videos and quantify the number of localized ERK5 in the two distinct areas (i.e. nucleus and cytoplasm) (Figure 10).

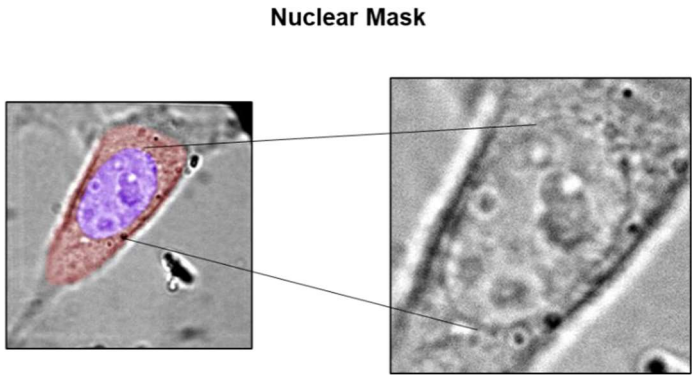

Figure 10. Visualization of nuclear masks drawn from the nuclear edges that are visible in bright-field images of HeLa cells. (**MOD**, My Own Data, **CO** Anatolii Kashuck, LENS).

2.3 ERK5 co-immunoprecipitates with importin-β1

To prove the interaction between ERK5 and α/β1 importin, we overexpressed ERK5WT and MEK5DD to boost ERK5 nuclear shuttling, and immunoprecipitated importin β1 in the lysates of HeLa cells. Using an ERK5 antibody in WB we were able to reveal the presence of ERK5 in the importin β1 immunoprecipitates (Figure 11A). The same interaction was obtained upon immunoprecipitation of ERK5 and subsequent immunoblotting with an anti-importin β1 antibody (Figure 11B). The occurrence of the interaction (i.e. co-immunoprecipitation) between endogenous (i.e not overexpressed) ERK5 and β1 importin was also detected in the A375 melanoma cell line (Figure 11C and 11D).

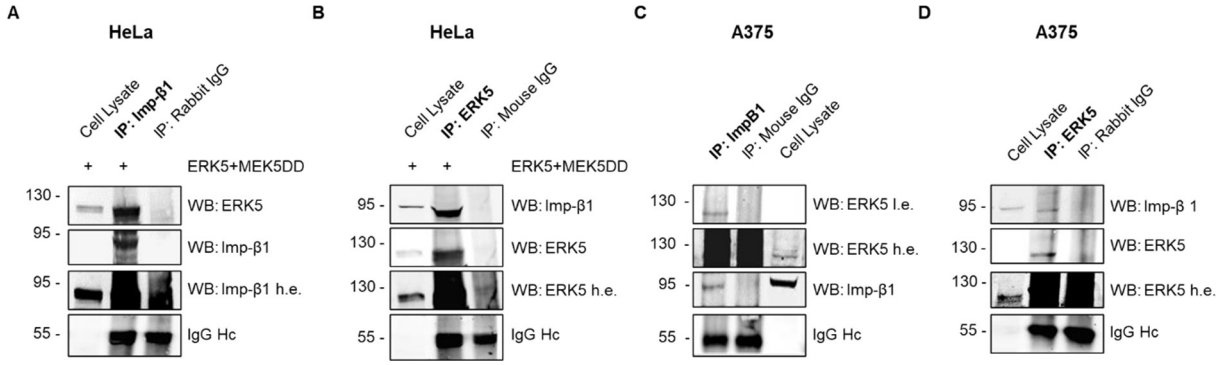

Figure 11. *ERK5 co-immunoprecipitates with importin-β1.* Hela ERK5WT+/MEK5DD+ **(A-B)** and A375 cells **(C-D)** were lysed and *KPNB1* **(A-C)** or ERK5 **(B-D)** were immunoprecipitated with specific antibodies. Western Blot was performed with the indicated antibodies. Migration of molecular weight markers is indicated on the left (kDa). **l.e**. means low exposure, **h.e.** means high exposure. (**MOD**, My Own Data).

2.4 AX15836 reduces melanoma cell proliferation only in combination with ivermectin

MTT assay results showed that the ERK5 inhibitor AX15836 has no effect on the viability of A375 (Figure 12A) and SK-Mel-5 melanoma cells (Figure 12B), nor on that of HeLa cervical cancer cells (Figure 12C), in accordance with previous data obtained in other cell lines (Lin *et al.,* 2016).

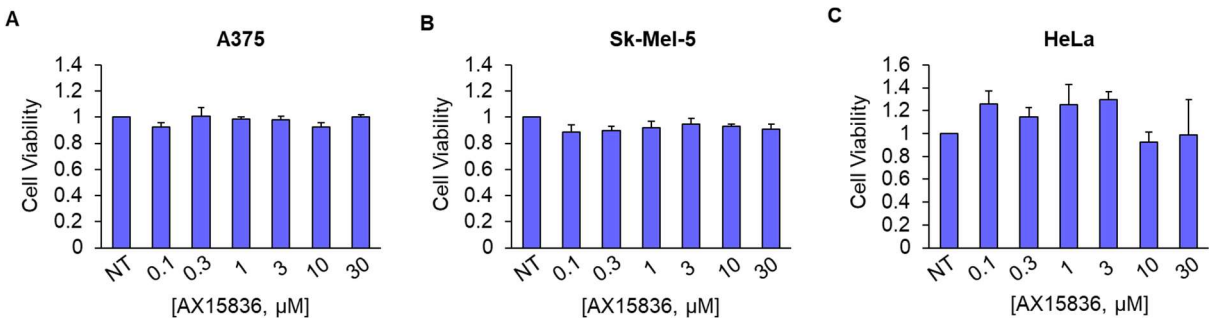

Figure 12. *AX15836 does not affect cancer cell proliferation.* A375 **(A)**, Sk-Mel-5 **(B)** and HeLa cells **(C)** were treated with increasing concentrations of AX15836 and MTT assays was performed after 72h. (**MOD**, My Own Data).

In this respect, the lack of effect of a number of ERK5 kinase inhibitors, including AX15836, has been ascribed to an increased ERK5 nuclear translocation and activation of the C-terminal TAD upon treatment (Lochhead et al. 2020). We confirmed this paradoxical effect by showing that AX15836 increases the amount of endogenous ERK5 in the nuclear fraction of HeLa cells, in a dose dependent manner. The same effect was obtained in A375 melanoma cells using 5 μM AX15836 (Figure 13A). Notably, Western Blot analysis revealed that ivermectin reverted the increase of ERK5 in the nucleus after AX15836 treatment in A375 cells (Figure 13B).

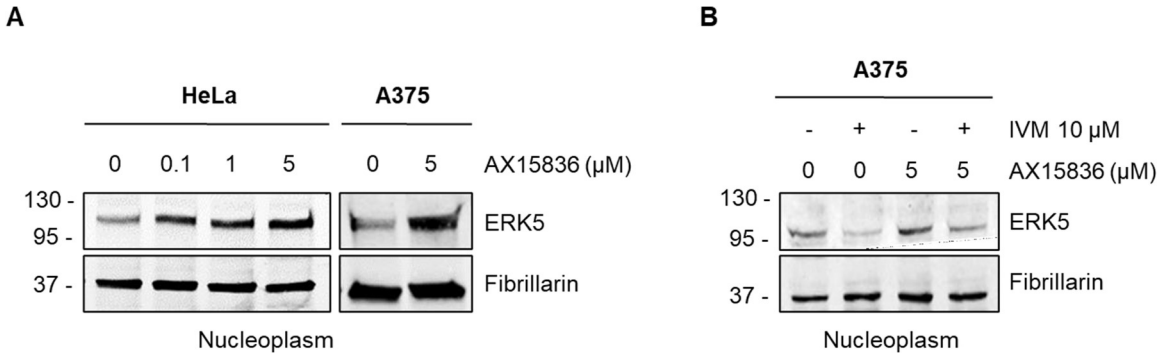

Figure 13. *AX15836 increases ERK5 nuclear translocation and ivermectin reverted this paradoxical effect.* **(A)** HeLa and A375 cells treated with the indicated concentration of AX15836 for 30min were lysed and Western Blot was performed on nuclear extracts with the indicated antibodies. **B)** A375 cells treated with IVM 10 μM for 24h, AX15836 5 μM for 30min or with the combination of the two drugs were lysed and Western Blot was performed on nuclear extracts with the indicated antibodies. Migration of molecular weight markers is indicated on the left (kDa). (**MOD**, My Own Data).

In view of the possible exploitation of AX15836 as an anticancer drug on the basis of its ability to effectively and specifically inhibit ERK5 kinase activity, we tested the combination of AX15836 and ivermectin on cell viability. MTT assays showed that AX15836 reduced

melanoma and cervical cancer cell proliferation only in combination with ivermectin. In particular, 1 µM AX15836, ineffective when used alone, reduced melanoma and cervical cancer cell viability only when used in combination with 7.5 µM and 10 µM ivermectin (Figure 14A and 14B). Of note, in A375 melanoma cells the combination of the two drugs reduced by 75% cell viability and the higher dose of ivermectin used (10 µM) showed a limited effect (i.e. reduction by 15%). Conversely, HeLa cell line is more sensitive to ivermectin alone that affects cell viability by 40% and 60% (used at 7.5 µM and 10 µM), but the combination with AX15836 further enhanced this effect.

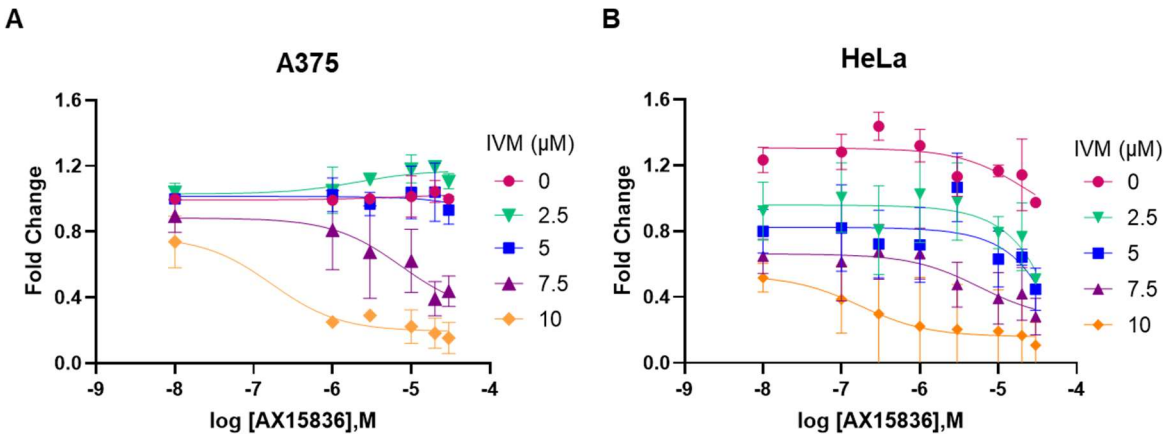

Figure 14. *AX15836 inhibits cancer cell proliferation only in combination with ivermectin*. A375 **(A)** and Hela **(B)** cells were treated with increasing concentrations of AX15836 and with the indicated doses of ivermectin for 72h and MTT assay was performed. Graphs have been created with GraphPad software. P values refer to differences with respect to vehicle-treated cells. *, $P < 0.05$; **, $P < 0.01$. § indicate synergistic effect (bliss test < 0). (**MOD**, My Own Data).

Based on these results, we performed 2D clonogenic assay using those concentrations of AX15836 and ivermectin that showed the best effect in reducing cancer cell proliferation in each cell line. Colony formation ability experiments performed with A375 cells showed that treatment with 10 µM ivermectin or 1 µM AX15836 did not affect the number of colonies formed with respect to vehicle-treated cells. In contrast, the combination of ivermectin and AX15836 halved the number of colonies formed by A375 cells, providing a synergist effect (Figure 15A). The existence of a synergistic effect was also obtained in HeLa cells. In these cells, ivermectin 5 µM alone reduced the colony formation ability by 25%, and on combination with AX15836 1 µM, IVM reduces by 75% the number of colonies providing a synergist effect (Figure 15B). The same synergistic effects were observed in Sk-Mel-5 melanoma cells (Figure 15C and D).

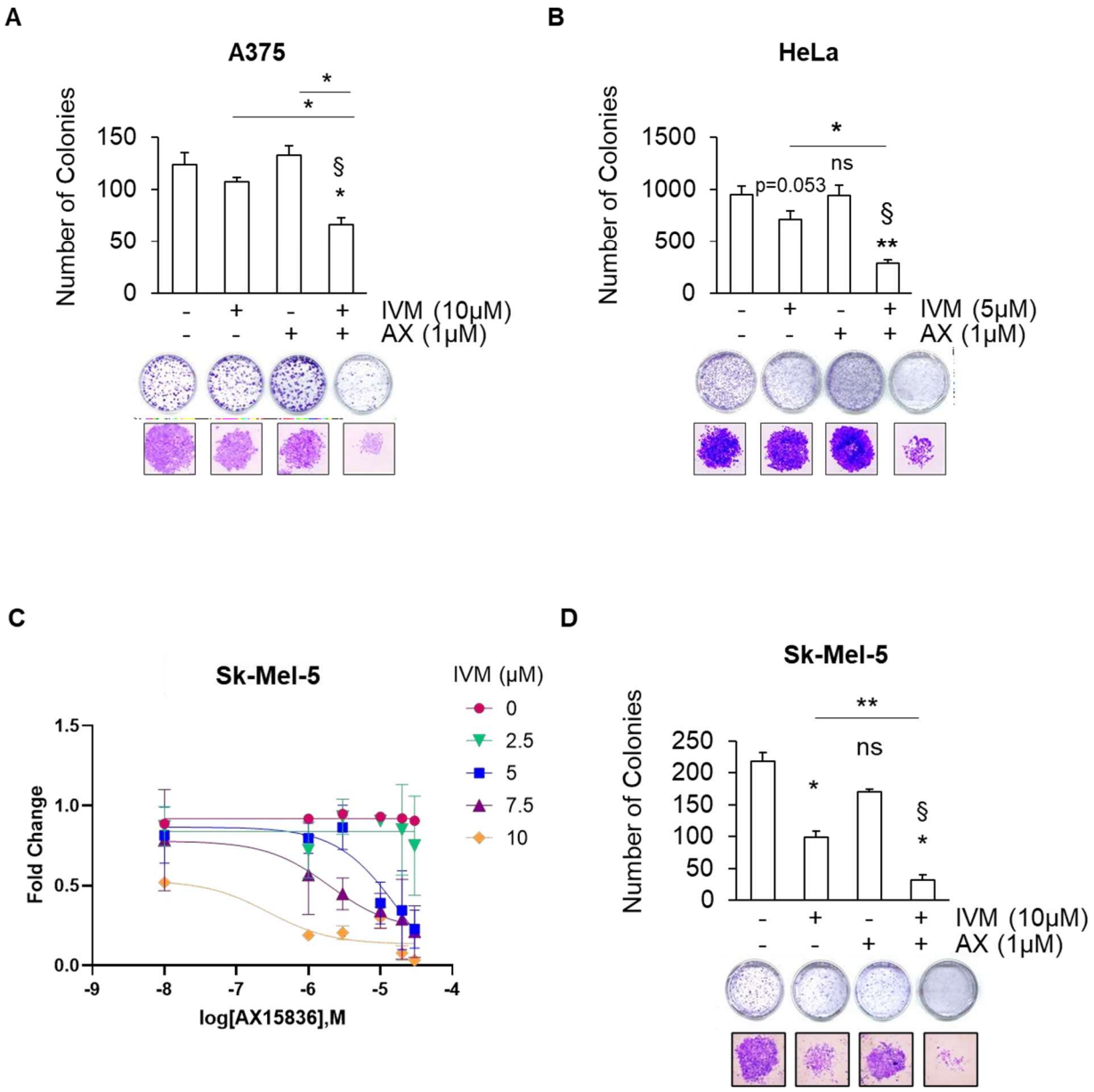

Figure 15. *AX15836 inhibits cancer cell proliferation only in combination with ivermectin*. Colony forming assay was performed with A375 **(A)**, Hela **(B)** and Sk-Mel-5 **(D)** treated with 10 µM (C and F) or 5 µM (D) ivermectin, 1µM AX15836 or with the combination of both. **(C)** Sk-Mel-5 cells were treated with increasing concentrations of AX15836 and with the indicated doses of ivermectin for 72h and MTT assay was performed. Graphs have been created with GraphPad software. P values refer to differences with respect to vehicle-treated cells. *, $P < 0.05$; **, $P < 0.01$. § indicate synergistic effect (bliss test < 0). (**MOD**, My Own Data).

We then evaluated the effect of the combination of AX15836 and IVM on the apoptosis of cancer cells. Our data shows that 1 µM AX15836 has no effect in inducing apoptosis in A375 or HeLa cells. The high dose of ivermectin (10 µM for A375 and 7.5 µM for HeLa cells) induces approximately 15% of apoptosis in A375 cells and a negligible effect (not significative) in HeLa cell line. Interestingly, in A375 cells the combination of the two drugs induced an increase of apoptotic cells by 25% and 35% with 7.5 or 10 µM ivermectin, respectively (Figure 16A). Similar results were obtained in HeLa cells. Indeed, in these cells, AX15836 increased by 50% or 60% the apoptotic cell population, when used in combination with 5 or 7.5 µM ivermectin respectively (Figure 16B).

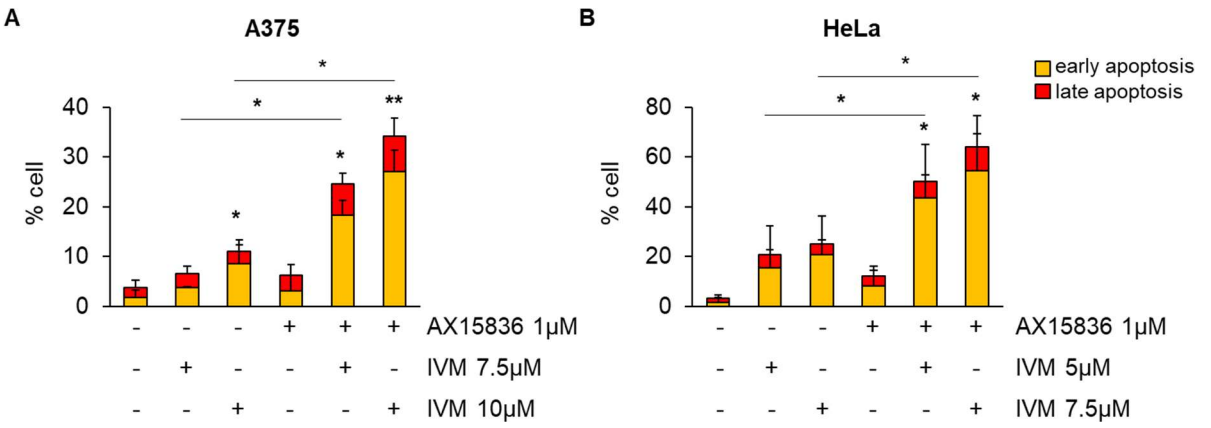

Figure 16. *AX15836 induces apoptosis in cancer cells only in combination with ivermectin.* **A)** A375 cells were treated with vehicle (DMSO) or treated with 1 µM AX15836, 7.5 or 10 µM ivermectin or with the combination of them for 24h. The percentage of apoptotic cells was evaluated through Flow Cytometry following Annexin-PI staining. P values refer to differences with respect to untreated cells. *, $P < 0.05$; **, $P < 0.01$. **B)** HeLa cells were left untreated or treated with 1 µM AX15836, 5 or 7.5 µM ivermectin or with the combination of them for 24h. The percentage of apoptotic cells was evaluated through Flow Cytometry following Annexin-PI staining. P values refer to differences with respect to untreated cells. *, $P < 0.05$; **, $P < 0.01$. (**MOD**, My Own Data).

We then used A375 and HeLa spheroids to move to a 3D cancer model of in vitro tumor growth. Interestingly, treatment with AX15836 alone did not affect spheroid volume after 5 days, whereas in combination with ivermectin halved A375 and HeLa spheroid volumes (Figure 17A and B). Of note, ivermectin showed a negligible effect on A375 spheroid volume and the result of the combination of the two drugs was significant also compared to ivermectin alone. Conversely, the detected reduction of the HeLa spheroid volume obtained with the combination of the two drugs compared to ivermectin alone is not significant.

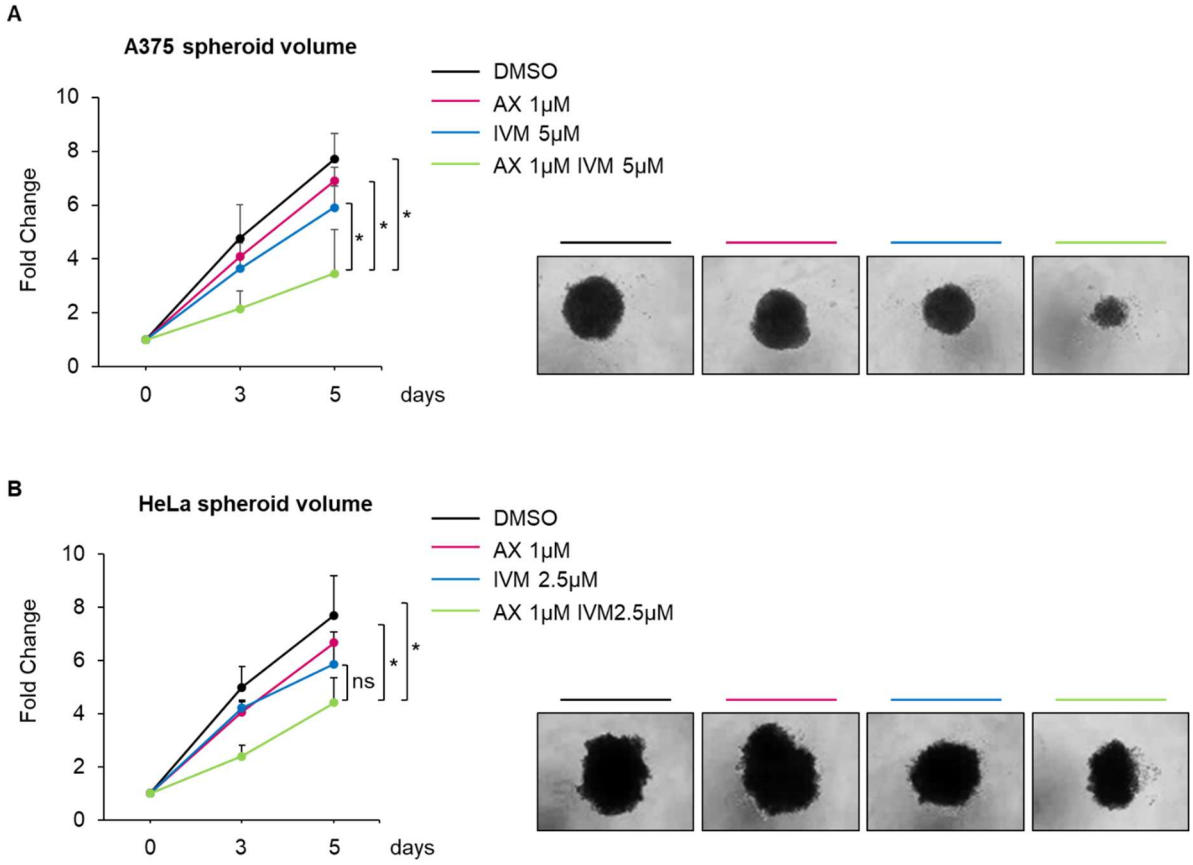

Figure 17. *AX15836 affects spheroid volume and necrosis only in combination with ivermectin.* **A)** A375 spheroids were treated with Vehicle, 1 μM AX15836, 5 μM ivermectin or with the combination of the two drugs. **B)** HeLa spheroids were treated with Vehicle, 1 μM AX15836, 2.5 μM ivermectin or with the combination of the two drugs. Graphs show the quantification of spheroid volume at different time points (0, 3 and 5 days) normalized for the time point 0. Representative images of spheroids taken at day 5 are shown. P values refer to differences with respect to vehicle- treated spheroids. *, $P < 0.05$. (**MOD**, My Own Data, **CO** Alessio Menconi).

In addition, the quantification of necrotic cells in A375 spheroids with the LiveDead assay, showed that the combination of AX15836 1 μM with ivermectin 5 μM determined a robust increase of the percentage of Propidium Iodide (PI)-positive cells with respect to vehicle treated-spheroids. In the same experiments, each drug alone did not show any effect (Figure 18A). The same result was obtained also in HeLa spheroids, using AX15836 1 μM and ivermectin 2.5 μM (Figure 18B).

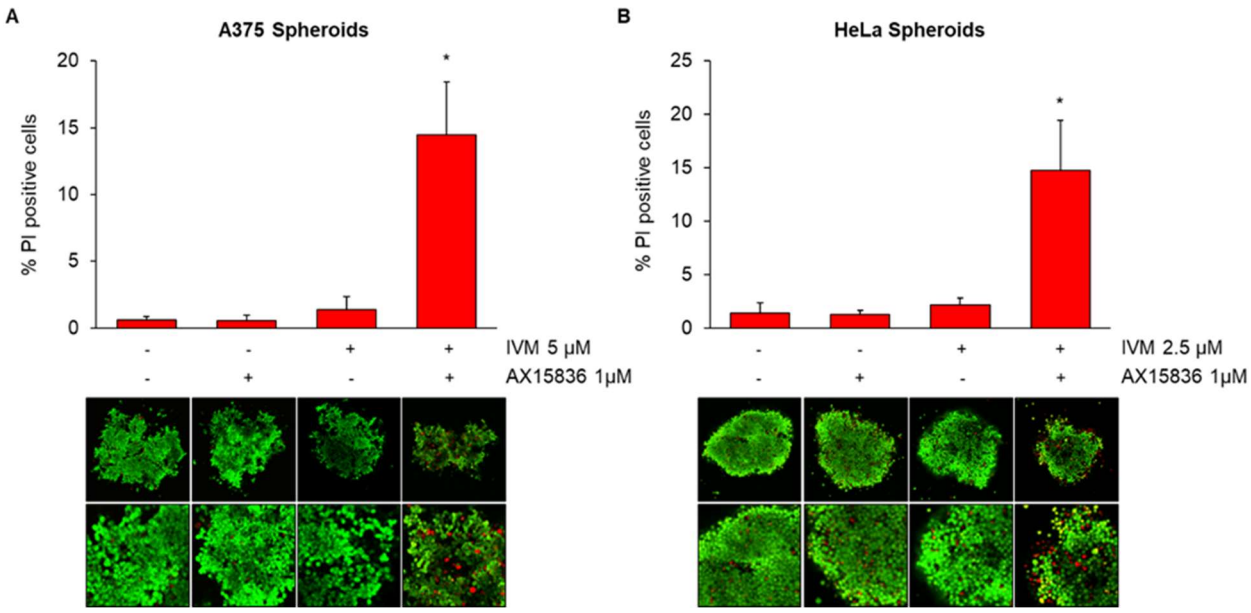

Figure 18. Quantification of the percentage of PI positive cells in A375 (**A**) and HeLa (**B**) spheroids stained with calceinAM and PI after treatment with vehicle, IVM (5 µM for A375, 2.5 µM for HeLa), AX15836 1µM or with the combination of the two drugs for 96h. Representative images of the experiments used for quantification, obtained with confocal analysis. P values refer to differences with respect to vehicle-treated spheroids. *, $P < 0.05$. (**MOD**, My Own Data, **CO** Alessio Menconi).

Finally, to demonstrate that the effects of the combination between ivermectin and AX15836 in reducing cancer cell proliferation relies, at least in part, on ERK5, we used ERK5 KO HUH-7 cells. We used this hepatocellular carcinoma cell line, in which ERK5 plays a relevant role in supporting cell proliferation (Rovida *et al.,* 2015), because of their availability as ERK5 KO cells in the lab. MTT assay showed that combined treatment with 5 µM ivermectin and 1 µM AX15836 induced a reduction by 35% in cell viability of HUH-7 WT cells, whereas it was ineffective in HUH-7 ERK5 KO cells (Figure 18A and B).

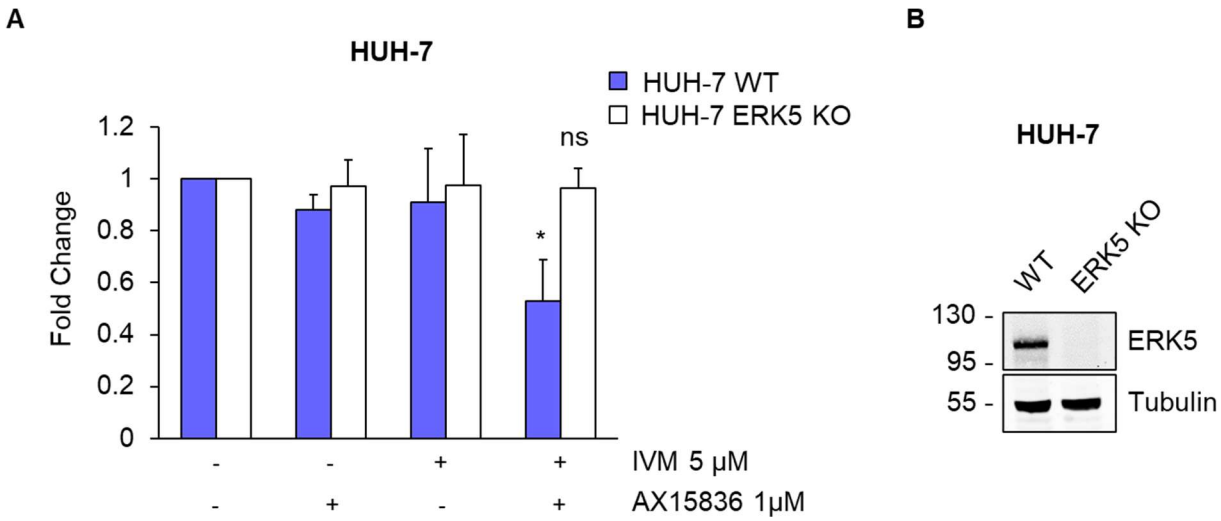

Figure 18. *The synergistic effect of AX15836 and ivermectin is at least in part ERK5-related.* **A)** HUH-7 WT and HUH-7 ERK5 KO cells were treated with AX15836 1 µM and/or with ivermectin 5 µM for 72h and MTT assay was performed. P values refer to differences with respect to untreated cells. *, $P < 0.05$. **B)** HUH-7 WT and HUH-7 ERK5 KO were lysates and western blot was performed with the indicated antibodies. Migration of molecular weight markers is indicated on the left (kDa). (**MOD**, My Own Data).

DISCUSSION

Malignant melanoma is one of the most aggressive type of cancer and its incidence is increasing worldwide. In the last few years, targeted therapies, like BRAF- and MEK1/2-targeting drugs, and immunotherapy have improved the survival of patients with metastatic melanoma. However, available treatments are still unsatisfactory, especially due to the development of resistance in patient with oncogenic mutations that are eligible for molecularly-tailored therapies, or to the lack of responsiveness to immunotherapy (Samatar *et al.,*2014). Thus, the identification of new therapeutic targets is urgently needed.

In this study, we provide compelling evidence that ERK5 possess a prominent role in cellular senescence in human melanoma. Indeed, in BRAF-mutated and wild-type melanoma cells and xenografts, ERK5 inhibition induced considerable cellular senescence and production of several soluble mediators involved in the SASP. We demonstrated that, mechanistically, ERK5-dependent senescence is mediated by the CDKi p21. Cellular senescence is considered a powerful suppressive mechanism of tumorigenesis, and therapies inducing senescence, besides promoting a stable cell growth arrest, may stimulate the activation of the antitumor immune response. Therefore, the identification of key signals involved in cellular senescence and of prosenescent molecules represent a valid contribution to the development of novel antitumor treatment (Acosta *et al.,* 2012; Nardella *et al.,* 2011).

In particularly, in this work different approaches have been exploited to evaluate the induction of cellular senescence following ERK5 inhibition. We started from the fact that senescence emerged, in transcriptomic experiments, as one of the tenth most impacted pathways upon ERK5 KD in BRAFV600E-mutated melanoma cells. Aside from cellular senescence, ERK5 inhibition significantly impacted oxidative stress induced senescence and the SASP. In this respect, ERK5 had been previously reported to be activated in colorectal adenocarcinoma cells undergoing methotrexate-induced senescence (Dabrowska *et al.,* 2011). Our results showed that ERK5 genetic and pharmacological inhibition induced a marked increase of SA-βGal positivity in melanoma cells expressing wild-type or oncogenic BRAF, as well as of cellular area and of SAHF, all of them being typical features of senescent cells. Moreover, ERK5 KD altered the expression of a number of genes known to regulate cell cycle and cellular senescence, including CDC25a, RBL-1, p27, and p53.

The occurrence of cellular senescence upon ERK5 inhibition was also demonstrated *in vivo*. Indeed, in A375 and SSM2c xenografts, ERK5 KD determined a robust increase of

lipofuscin, an indicator of cellular senescence *in vivo* (Georgakopoulou *et al.,* 2013). More importantly in view of a possible translation to the clinics, similar effects were observed in melanoma xenografts of XMD8-92-treated mice. Furthermore, ERK5-KD cells underwent an accumulation in G0-G1 or G2-M phase, depending on the cell line, and cells treated with XMD8-92 showed reduced ability to respond to mitogens, and did not form colonies upon replating, supporting the occurrence of a block of cell-cycle progression, an event invariably linked to cellular senescence (Munoz-Espín *et al.,* 2014). Consistently, ERK5 inhibition determined a reduction of RB phosphorylation and cyclin protein levels, as well as an increase of p21 protein. This CDKi was identified as a prominent actor of ERK5-dependent cellular senescence. Indeed, ERK5 pharmacologic inhibition supports the increase of p21 protein levels, whereas p21 genetic inhibition reverted the prosenescence effect obtained upon XMD8-92 treatment. While the involvement of p21 in ERK5-mediated biological effects has been largely reported (Yang *et al.,* 2010; Perez-Madrigal *et al.,* 2012), the role of p21 in ERK5-mediated cellular senescence represents a novel finding.

Cellular senescence may be characterized by the SASP, which consists of the secretion of several soluble factors in the surrounding microenvironment. SASP can have pro- as well as anti-tumorigenic effects, thus making senescence a double-edged sword with respect to cancer onset and development (Coppè *et al.,* 2010; Wang *et al.,* 2020). In this work, several SASP-related chemokines, including CXCL1, CXCL8, and CCL20, are found to be markedly increased in conditioned media (CM) of ERK5-KD cells undergoing cellular senescence. Our findings provide evidence that the viability of melanoma cells is strongly reduced following treatment with these CM, and that the treatment with neutralizing antibodies for each of the above chemokines rescued the proliferation of melanoma cells. In this respect, despite it has been reported in literature that CXCL8, CXCL1 and CCL20 possess growth-promoting functions (Green *et al*., 2020; Samaniego *et al*., 2020) that appear in contrast with the antiproliferative effects elicited by CM from ERK5-KD cells, it has been demonstrated that senescent cells may activate a self-amplifying secretory network in which CXCR2-binding chemokines (i.e., CXCL1 and CXCL8) reinforce growth arrest (Acosta *et al.,* 2008). As regard the link between ERK5 inhibition and SASP occurrence, multiple different nuclear and cytoplasmic factors have been shown to trigger SASP, including chromatin remodeling and SAHF formation. In this respect, it should be underlined that ERK5 KD determined a robust remodeling of the mRNA levels of a number of histone variants, as well as SAHF increase. However, the molecular mechanism linking ERK5 KD to chemokine regulation remains to be investigated.

Another relevant finding of our study is the identification of prosenescent drugs that may be exploited for cancer treatment. Indeed, we found that the ERK5 inhibitors XMD8-92, JWG-045, and JWG-071 promote cellular senescence in melanoma cells. The fact that XMD8-92, extensively showed to reduce tumor growth *in vitro* and *in vivo* (Stecca, Rovida 2019), has off-target effects (Lin *et al.,* 2016) does not reduce the possibility to exploit this small-molecule inhibitor as a prosenescent drug. Interestingly, the ability of XMD8-92 in inducing senescence was increased when used in combination with vemurafenib, that we found able to induce senescence in melanoma cells, in keeping with a previous report (Haferkamp *et al.,* 2017). Thus, combination treatments directed to BRAF and ERK5 supports prosenescent features, reducing tumor growth more efficiently than the single treatments (Tusa *et al,* 2018). These effects are in line with the well-established fact that, either chemo and radio, as well as targeted therapies engage a senescence response as part of the outcome (Nardella *et al.,* 2013). However, if this combination is more effective in preventing resistance mechanisms with respect to BRAF/MEK inhibitors alone remains to be investigated.

As mentioned above, in spite of remarkable advances in the diagnosis and treatment of melanoma, there is an urgent need to identify novel molecular targets to counteract melanoma progression. The prominent role of ERK5 in supporting melanoma cell proliferation (Tusa *et al.,* 2018) is strictly linked to its localization into the nucleus (Gomez *et al.,* 2016), where ERK5 acts as a transcriptional transactivator for pro-proliferative genes. ERK5 translocation from the cytoplasm to the nucleus is a very complex process in which many events are involved, among the others, the phosphorylation by its activator MEK5. However, the mechanisms involved in this process are still poorly characterized, and in particular how ERK5 enters the nucleus remained to be clarified. Based on the presence of a classical NLS and on the high molecular weight of this protein, it has been postulated that ERK5 shuttles into the nucleus through α/β importin (Flores *et al.,* 2019), although evidence has not yet been provided. The present study indicates that genetic inhibition of importin β1 prevents ERK5 nuclear translocation, demonstrating the involvement of this importin in this nuclear-import process. The impairment of ERK5 nuclear translocation using the α/β1 importin inhibitor ivermectin, an anti-parasite FDA approved drug (Wagstaff *et al.,* 2011), proved the need of α/β1 importin complexes in ERK5 nuclear translocation process. Indeed, the nuclear carrier importin β1 requests importin α subunit to bind cargo proteins harboring cNLS (Christie *et al.,* 2016). Importantly, these functional data were accompanied by the observation that ivermectin zeroed the amount of ERK5 bound to chromatin. This effect is of great importance taking into consideration that it is the nuclear subpopulation of ERK5 that is relevant for the support of cell proliferation, relying

on ERK5 activity as a transactivator. Additional experiments should be directed to evaluate whether ivermectin affects ERK5 regulated genes such as MEF2, KLF4 and KLF2 or cJUN, with a particular attention to those involved in cell proliferation. The identification of the efficacy of ivermectin in preventing ERK5 translocation to the nucleus paves the way to a possible use of this drug to inhibit ERK5 function as coactivator of pro-proliferative factors.

These above results were nicely complemented by another approach relying on super-resolution microscopy. Indeed, besides optimizing a STORM technology (Gardini *et al*., 2015) to perform single molecule imaging of ERK5, we were able to quantify ERK5 particles within the different cellular compartment (cytoplasm or nucleus) with nanometer accuracy, exploiting available ThunderSTORM plugin (Kashchuk *et al.,* 2022). The reduction of ERK5 molecules in the nucleus upon ivermectin treatment, provides further evidence that α/β1 importin complexes are involved in ERK5 nuclear shuttling. It should be emphasized that the optimized technique could be useful for future studies to better characterize several aspects of ERK5 functions within the nucleus. Indeed, STORM imaging might be useful to dissect the dynamic interaction between two biological partners at single-molecule level, as reported for the transcription factor cAMP response element-binding protein (CREB) and its target sequence cAMP-response element (CRE) (Sugo *et al.*, 2014) or for glucocorticoid receptor and its cofactors (Paakinaho *et al.*, 2017). Thus, super-resolution analysis could further help the investigation of ERK5 transcriptional transactivator activity, and of its dynamic interactions with transcription factors or with chromatin. Finally, single-molecule superresolution imaging allowed the study of the dimerization and multimerization of the protein kinase RAF providing critical insight into the biological regulation of RAF signaling and oncogenesis (Nan *et al.,* 2013). Indeed, conventional biochemical and imaging approaches have provided important insights into biological processes, but do not easily give direct information about nanometer-scale structures such as protein dimerization or multimer formation. Thus, single molecule imaging in living cells could help future study in the characterization of ERK5, or of other MAPKs, multimer formation to further study their biological outcomes.

It has been recently reported that AX15836, a small molecule ERK5 inhibitor that effectively reduces ERK5 kinase activity, induces paradoxical activation of ERK5 by supporting its nuclear translocation and its transcriptional transactivation activity (Lockhead *et al.,*2020). Accordingly, while ERK5 knock down and other MEK5 or ERK5 inhibitors have been reported to reduce melanoma growth *in vitro* and *in vivo* (Tusa *et al.,* 2018), this study provides evidence that AX15836 is ineffective in reducing melanoma and endometrial cancer

cell proliferation. Additionally, similarly to what previously demonstrated in HeLa cells (Lockhead *et al.,*2020), we showed here that AX15836 induced the increase of ERK5 nuclear translocation also in A375 melanoma cell line. More importantly, we identified ivermectin as a valid approach to counteract AX15836 paradoxical effect. Indeed, ivermectin unmask the ability of AX15836 to reduce cancer cell viability and colony formation ability, as well as to increase apoptosis. Of note, ivermectin alone, induces, at certain dosage, a reduction in cancer cell proliferation and an increase in the percentage of apoptotic cells. This is expected taking into consideration that importin β1 is overexpressed in several cancers and it is involved in the nuclear translocation of factors activating pro-proliferative genes (van der Watt PJ *et al.,* 2015; Yang *et al.,* 2015; Lu *et al.,* 2016) and that ivermectin inhibits ERK5 nuclear translocation that occurs also without AX15836 paradoxical activation, especially in cancer cells with hyperactivated MEK5-ERK5 pathway. Spheroids culture have been used as a 3D-model for in vitro tumor growth and our data suggest that AX15836 and low doses of ivermectin do not affect spheroid volume, while they are able to reduce cancer cell proliferation when used in combination.

We also provide evidence that the existence of a synergistic effect between AX15836 and ivermectin is to be considered ERK5-related. Indeed, in HUH-7 ERK KO cells, the combination of ivermectin and AX15836 does not induce significant variation in cell viability compared to HUH-7 parental cells. The latter result suggest that the effects observed using ivermectin and AX15836 in reducing cancer cell proliferation are not due to the overall ivermectin ability of inhibiting the nuclear translocation of factors involved in proliferative events, but to its ability to prevent AX15836-dependent ERK5 nuclear shuttling and subsequent paradoxical activity. Overall, these results suggest that targeting ERK5 nuclear translocation could provide a valid additional approach *per se* or in combination with ERK5 kinase inhibitors to counteract melanoma growth. More in general, this strategy could be used in combination with other established targeted therapies to fight against those tumors in which ERK5 plays a relevant role in cancer onset and progression.

REFERENCES

Acosta JC, Gil J. Senescence: a new weapon for cancer therapy. Trends Cell Biol. 2012 Apr;22(4):211-9. doi: 10.1016/j.tcb.2011.11.006. Epub 2012 Jan 13. PMID: 22245068.

Acosta JC, O'Loghlen A, Banito A, Guijarro MV, Augert A, Raguz S, et al. Chemokine signaling via the CXCR2 receptor reinforces senescence. Cell 2008; 133:1006–18.

Adam SA, Lobl TJ, Mitchell MA, Gerace L. Identification of specific binding proteins for a nuclear location sequence. Nature. 1989 Jan 19;337(6204):276-9. doi: 10.1038/337276a0. PMID: 2911368.

Al-Ejeh F, Simpson PT, Sanus JM, Klein K, Kalimutho M, Shi W, Miranda M, Kutasovic J, Raghavendra A, Madore J, Reid L, Krause L, Chenevix-Trench G, Lakhani SR, Khanna KK. Meta-analysis of the global gene expression profile of triple-negative breast cancer identifies genes for the prognostication and treatment of aggressive breast cancer. Oncogenesis. 2014 Apr 21;3(4):e100. doi: 10.1038/oncsis.2014.14. Erratum in: Oncogenesis. 2014 Oct 27;3:e124. PMID: 24752235; PMCID: PMC4007196.

Alnabulsi A, Agouni A, Mitra S, Garcia-Murillas I, Carpenter B, Bird S, Murray GI. Cellular apoptosis susceptibility (chromosome segregation 1-like, CSE1L) gene is a key regulator of apoptosis, migration and invasion in colorectal cancer. J Pathol 2012; 228:471–481

Álvarez-Fernández S, Ortiz-Ruiz MJ, Parrott T, Zaknoen S, Ocio EM, San Miguel J, Burrows FJ, Esparís-Ogando A, Pandiella A. Potent antimyeloma activity of a novel ERK5/CDK inhibitor. Clin Cancer Res. 2013 May 15;19(10):2677-87. doi: 10.1158/1078-0432.CCR-12-2118. Epub 2013 Mar 26. PMID: 23532886.

Anerillas C, Abdelmohsen K, Gorospe M. Regulation of senescence traits by MAPKs. APMIS, 115: 1161-1176. https://doi.org/10.1111/j.1600-0463.2007.apm_855.xml.x

Arias-González, L.; Moreno-Gimeno, I.; del Campo, A.R.; Serrano-Oviedo, L.; Valero, M.L.; Esparís-Ogando, A.; de la Cruz-Morcillo, M.Á.; Melgar-Rojas, P.; García-Cano, J.; Cimas, F.J.; et al. ERK5/BMK1 is a novel target of the tumor suppressor VHL: Implication in clear cell renal carcinoma

Ayanlaja AA, Ji G, Wang J, Gao Y, Cheng B, Kanwore K, Zhang L, Xiong Y, Kambey PA, Gao D. Doublecortin undergo nucleocytoplasmic transport via the RanGTPase signaling to promote glioma progression. Cell Commun Signal. 2020 Feb 12;18(1):24. doi: 10.1186/s12964-019-0485-5. PMID: 32050972; PMCID: PMC7017634.

Balint, K., et al., Activation of Notch1 signaling is required for beta-cateninmediated human primary melanoma progression. J Clin Invest, 2005. 115(11): p. 3166-76.

Bavik C, Coleman I, Dean JP, Knudsen B, Plymate S, Nelson PS. The gene expression program of prostate fibroblast senescence modulates neoplastic epithelial cell proliferation

Behrens P, Brinkmann U, Fogt F, Wernert N, Wellmann A. Implication of the

proliferation and apoptosis associated CSE1L/CAS gene for breast cancer development. Anticancer Res 2001; 21:2413–2417

Buschbeck M, Ullrich A. The unique C-terminal tail of the mitogen-activated protein kinase ERK5 regulates its activation and nuclear shuttling. J Biol Chem. 2005 Jan 28;280(4):2659-67. doi: 10.1074/jbc.M412599200. Epub 2004 Nov 17. PMID: 15548525.

Calcinotto A, Kohli J, Zagato E, Pellegrini L, Demaria M, Alimonti A. Cellular Senescence: Aging, Cancer, and Injury. Physiol Rev. 2019 Apr 1;99(2):1047-1078. doi: 10.1152/physrev.00020.2018. PMID: 30648461.

Caly L, Druce JD, Catton MG, Jans DA, Wagstaff KM. The FDA-approved drug ivermectin inhibits the replication of SARS-CoV-2 in vitro. Antiviral Res. 2020 Jun; 178:104787. doi: 10.1016/j.antiviral.2020.104787. Epub 2020 Apr 3. PMID: 32251768; PMCID: PMC7129059.

Cargnello M, Roux PP. Activation and function of the MAPKs and their substrates, the MAPK-activated protein kinases. Microbiol Mol Biol Rev. 2011 Mar;75(1):50-83. doi: 10.1128/MMBR.00031-10. Erratum in: Microbiol Mol Biol Rev. 2012 Jun.
Cell Mol Life Sci, 2013. 70(21): p. 4055-65.

Chapman, P.B., et al., Improved survival with vemurafenib in melanoma with BRAF V600E mutation. N Engl J Med, 2011. 364(26): p. 2507-16.

Choi S, Yamashita E, Yasuhara N, Song J, Son SY, Won YH, Hong HR, Shin YS, Sekimoto T, Park IY, Yoneda Y, Lee SJ. Structural basis for the selective nuclear import of the C2H2 zinc-finger protein Snail by importin β. Acta Crystallogr D Biol Crystallogr. 2014 Apr;70(Pt 4):1050-60. doi: 10.1107/S1399004714000972. Epub 2014 Mar 19. PMID:

Christie M, Chang CW, Róna G, Smith KM, Stewart AG, Takeda AA, Fontes MR, Stewart M, Vértessy BG, Forwood JK, Kobe B. Structural Biology and Regulation of Protein Import into the Nucleus. J Mol Biol. 2016 May 22;428(10 Pt A):2060-90. doi: 10.1016/j.jmb.2015.10.023. Epub 2015 Oct 30. PMID: 26523678.

Cingolani G, Bednenko J, Gillespie MT, Gerace L. Molecular basis for the recognition of a nonclassical nuclear localization signal by importin beta. Mol Cell. 2002 Dec;10(6):1345-53. doi: 10.1016/s1097-2765(02)00727-x. PMID: 12504010.

Cingolani G, Petosa C, Weis K, Müller CW. Structure of importin-beta bound to the IBB domain of importin-alpha. Nature. 1999 May 20;399(6733):221-9. doi: 10.1038/20367. PMID: 10353244.

Clark WH Jr, Elder DE, Guerry D 4th, Epstein MN, Greene MH, Van Horn M. A study of tumor progression: the precursor lesions of superficial spreading and nodular melanoma.

Conti E, Kuriyan J. Crystallographic analysis of the specific yet versatile recognition of distinct nuclear localization signals by karyopherin alpha. Structure. 2000 Mar 15;8(3):329-38. doi: 10.1016/s0969-2126(00)00107-6. PMID: 10745017.

Coppè JP, Desprez PY, Krtolica A, Campisi J. The senescence-associated secretory phenotype: the dark side of tumor suppression. Annu Rev Pathol 2010; 5:99–118.

Coppé JP, Kauser K, Campisi J, Beauséjour CM. Secretion of vascular endothelial growth factor by primary human fibroblasts at senescence. J Biol Chem. 2006 Oct 6;281(40):29568-74. doi: 10.1074/jbc.M603307200. Epub 2006 Jul 31. PMID: 16880208.

Coppé JP, Patil CK, Rodier F, Sun Y, Muñoz DP, Goldstein J, Nelson PS, Desprez PY, Campisi J. Senescence-associated secretory phenotypes reveal cell-nonautonomous functions of oncogenic RAS and the p53 tumor suppressor. PLoS Biol. 2008 Dec 2;6(12):2853-68. doi: 10.1371/journal.pbio.0060301. PMID: 19053174; PMCID: PMC2592359.

Corcoran RB, Settleman J, Engelman JA. Potential therapeutic strategies to overcome acquired resistance to BRAF or MEK inhibitors in BRAF mutant cancers. Oncotarget. 2011 Apr;2(4):336-46. doi: 10.18632/oncotarget.262. PMID: 21505228; PMCID: PMC3248170.

Cosgarea, I., et al., Update on the clinical use of kinase inhibitors in melanoma. J Dtsch Dermatol Ges, 2017. 15(9): p. 887-893.

Coulombe, P.; Meloche, S. Atypical mitogen-activated protein kinases: structure, regulation and functions. Biochim. Biophys. Acta. 2007, 1773, 1376–1387, doi: 10.1016/j.bbamcr.2006.11.001.

Dabrowska M, Skoneczny M, Rode W. Functional gene expression profile underlying methotrexate-induced senescence in human colon cancer cells. Tumour Biol 2011; 32:965–76.

D'Adda di Fagagna F. Living on a break: cellular senescence as a DNA-damage response. Nat Rev Cancer. 2008 Jul;8(7):512-22. doi: 10.1038/nrc2440. PMID: 18574463.

Dahl, C. and Guldberg, P. (2007), The genome and epigenome of malignant melanoma. APMIS. 2007 Oct;115(10):1161-76. doi: 10.1111/j.1600-0463.2007.apm_855.xml.x. PMID: 18042149.

Das Thakur M, Salangsang F, Landman AS, Sellers WR, Pryer NK, Levesque MP, Dummer R, McMahon M, Stuart DD. Modelling vemurafenib resistance in melanoma reveals a strategy to forestall drug resistance. Nature. 2013 Feb 14;494(7436):251-5. doi: 10.1038/nature11814. Epub 2013 Jan 9. PMID: 23302800; PMCID: PMC3930354.

Davis LE, Shalin SC, Tackett AJ. Current state of melanoma diagnosis and treatment. Cancer Biol Ther. 2019;20(11):1366-1379. doi: 10.1080/15384047.2019.1640032. Epub 2019 Aug 1. PMID: 31366280; PMCID: PMC6804807.

Delord JP, Robert C, Nyakas M, McArthur GA, Kudchakar R, Mahipal A, Yamada Y, Sullivan R, Arance A, Kefford RF, Carlino MS, Hidalgo M, Gomez-Roca C, Michel D, Seroutou A, Aslanis V, Caponigro G, Stuart DD, Moutouh-de Parseval L, Demuth T, Dummer R. Phase I Dose-Escalation and -Expansion Study of the BRAF Inhibitor Encorafenib (LGX818) in Metastatic BRAF-Mutant Melanoma. Clin Cancer Res. 2017 Sep 15;23(18):5339-5348. doi: 10.1158/1078-0432.CCR-16-2923. Epub 2017 Jun 13. PMID: 28611198.

Deng F, Xu Q, Long J, Xie H. Suppressing ROS-TFE3-dependent autophagy enhances ivermectin-induced apoptosis in human melanoma cells. J Cell Biochem. 2018 Sep 6. doi: 10.1002/jcb.27490. Epub ahead of print. PMID: 30187952.

Di Micco R, Sulli G, Dobreva M, Liontos M, Botrugno OA, Gargiulo G, dal Zuffo R, Matti V, d'Ario G, Montani E, Mercurio C, Hahn WC, Gorgoulis V, Minucci S, d'Adda di Fagagna F. Interplay between oncogene-induced DNA damage response and heterochromatin in senescence and cancer. Nat Cell Biol. 2011 Mar;13(3):292-302. doi: 10.1038/ncb2170. Epub 2011 Feb 20. PMID: 21336312; PMCID: PMC3918344.

Diaz-Rodriguez, E.; Pandiella, A. Multisite phosphorylation of Erk5 in mitosis. J. Cell Sci. 2010, 123, 3146–3156.

Drew, B.A., M.E. Burow, and B.S. Beckman, MEK5/ERK5 pathway: the first fifteen years. Biochim Biophys Acta, 2012. 1825(1): p. 37-48.

Ellerhorst JA, Greene VR, Ekmekcioglu S, Warneke CL, Johnson MM, Cooke CP, Wang LE, Prieto VG, Gershenwald JE, Wei Q, Grimm EA. Clinical correlates of NRAS and BRAF mutations in primary human melanoma. Clin Cancer Res. 2011 Jan 15;17(2):229-35. doi: 10.1158/1078-0432.CCR-10-2276. Epub 2010 Oct 25. Erratum in: Clin Cancer Res. 2011 Mar 15.

Erazo T, Espinosa-Gil S, Diéguez-Martínez N, Gómez N, Lizcano JM. SUMOylation Is Required for ERK5 Nuclear Translocation and ERK5-Mediated Cancer Cell Proliferation. Int J Mol Sci. 2020 Mar 23;21(6):2203. doi: 10.3390/ijms21062203. PMID: 32209980; PMCID: PMC7139592.

Erazo T, Moreno A, Ruiz-Babot G, Rodríguez-Asiain A, Morrice NA, Espadamala J, Bayascas JR, Gómez N, Lizcano JM. Canonical and kinase activity-independent mechanisms for extracellular signal-regulated kinase 5 (ERK5) nuclear translocation require dissociation of Hsp90 from the ERK5-Cdc37 complex. Mol Cell Biol. 2013 Apr;33(8):1671-86. doi: 10.1128/MCB.01246-12. Epub 2013 Feb 19. PMID: 23428871; PMCID: PMC3624243.

Ewald JA, Desotelle JA, Wilding G, Jarrard DF. Therapy-induced senescence in cancer. J Natl Cancer Inst. 2010 Oct 20;102(20):1536-46. doi: 10.1093/jnci/djq364. Epub 2010 Sep 21. PMID: 20858887; PMCID: PMC2957429.

Fang D, Nguyen TK, Leishear K, Finko R, Kulp AN, Hotz S, Van Belle PA, Xu X, Elder DE, Herlyn M. A tumorigenic subpopulation with stem cell properties in melanomas. Cancer Res. 2005 Oct 15;65(20):9328-37. doi: 10.1158/0008-5472.CAN-05-1343. PMID: 16230395.

Filipp FV, Birlea S, Bosenberg MW, Brash D, Cassidy PB, Chen S, D'Orazio JA, Fujita M, Goh BK, Herlyn M, Indra AK, Larue L, Leachman SA, Le Poole C, Liu-Smith F, Manga P,

Flores K, Yadav SS, Katz AA, Seger R. The Nuclear Translocation of Mitogen-Activated Protein Kinases: Molecular Mechanisms and Use as Novel Therapeutic Target. Neuroendocrinology. 2019;108(2):121-131. doi: 10.1159/000494085. Epub 2018 Sep 27.

Formstecher Etienne, Joe W. Ramos, Mireille Fauquet, David A. Calderwood, Jyh-Cheng Hsieh, Brigitte Canton, Xuan-Thao Nguyen, Jean-Vianney Barnier, Jacques Camonis, Mark H. Ginsberg, Hervé Chneiweiss, PEA-15 Mediates Cytoplasmic Sequestration of ERK

MAP Kinase, Developmental Cell, Volume 1, Issue 2, 2001, Pages 239-250.

García-Borrón JC, Sánchez-Laorden BL, Jiménez-Cervantes C. Melanocortin-1 receptor structure and functional regulation. Pigment Cell Res. 2005 Dec;18(6):393-410. doi: 10.1111/j.1600-0749.2005. 00278. x PMID: 16280005.

Gardini L, Woody MS, Kashchuk AV, Goldman YE, Ostap EM, Capitanio M. High-Speed Optical Traps Address Dynamics of Processive and Non-Processive Molecular Motors. Methods Mol Biol. 2022; 2478:513-557. doi: 10.1007/978-1-0716-2229-2_19. PMID: 36063333.

Georgakopoulou EA, Tsimaratou K, Evangelou K, Fernandez Marcos PJ, Zoumpourlis V, Trougakos IP, et al. Specific lipofuscin staining as a novel biomarker to detect replicative and stress-induced senescence. A method applicable in cryo-preserved and archival tissues. Aging 2013.
Geroscience 2020; 42:397–408.

Gomez, N., T. Erazo, and J.M. Lizcano, ERK5 and Cell Proliferation: Nuclear Localization Is What Matters. Front Cell Dev Biol, 2016. 4: p. 105.

Green D, Eyre H, Singh A, Taylor JT, Chu J, Jeys L, et al. Targeting the MAPK7/MMP9 axis for metastasis in primary bone cancer. Oncogene 2020; 39:5553–69.

Grichnik, J.M., et al., Melanoma, a tumor based on a mutant stem cell? J Invest Dermatol, 2006. 126(1): p. 142-53.

Guo, W., Wang, H. & Li, C. Signal pathways of melanoma and targeted therapy. Sig Transduct Target Ther 6, 424 (2021). https://doi.org/10.1038/s41392-021-00827-6

Ha S, Choi J, Min NY, Lee KH, Ham SW. Inhibition of Importin β1 With a 2-Aminothiazole Derivative Resulted in G2/M Cell-cycle Arrest and Apoptosis. Anticancer Res. 2017 May;37(5):2373-2379. doi: 10.21873/anticanres.11575. PMID: 28476803.

Haass, N.K., Smalley, K.S.M., Li, L. and Herlyn, M. (2005), Adhesion, migration and communication in melanocytes and melanoma. Pigment Cell Research, 18: 150-159. https://doi.org/10.1111/j.1600-0749.2005.00235.x

Haferkamp S, Borst A, Adam C, Becker TM, Motschenbacher S, Windhovel S, et al.

Han Y, Liu Y, Gui Y, Cai Z. Inducing cell proliferation inhibition and apoptosis via silencing Dicer, Drosha, and Exportin 5 in urothelial carcinoma of the bladder. J Surg Oncol 2013; 107:201–205.

Hanahan D, Weinberg RA. Hallmarks of cancer: the next generation. Cell. 2011 Mar 4;144(5):646-74. doi: 10.1016/j.cell.2011.02.013. PMID: 21376230.

Hashimoto H, Messerli SM, Sudo T, Maruta H. Ivermectin inactivates the kinase PAK1 and blocks the PAK1-dependent growth of human ovarian cancer and NF2 tumor cell lines. Drug Discov Ther. 2009 Dec;3(6):243-6. PMID: 22495656.

Hayashi M, Kim SW, Imanaka-Yoshida K, Yoshida T, Abel ED, Eliceiri B, Yang Y, Ulevitch RJ, Lee JD. Targeted deletion of BMK1/ERK5 in adult mice perturbs vascular integrity and leads to endothelial failure. J Clin Invest. 2004 Apr;113(8):1138-48. doi: 10.1172/JCI19890. PMID: 15085193; PMCID: PMC385403.

Hendrix, M.J., et al., Vasculogenic mimicry and tumour-cell plasticity: lessons from melanoma. Nat Rev Cancer, 2003. 3(6): p. 411-21.

Hintersteiner M, Ambrus G, Bednenko J, Schmied M, Knox AJ, Meisner NC, Gstach H, Seifert JM, Singer EL, Gerace L, Auer M. Identification of a small molecule inhibitor of importin β mediated nuclear import by confocal on-bead screening of tagged one-bead one-compound libraries. ACS Chem Biol. 2010 Oct 15;5(10):967-79. doi: 10.1021/cb100094k. PMID: 20677820; PMCID: PMC2956136.

Hofmann UB, Westphal JR, Van Muijen GN, Ruiter DJ. Matrix metalloproteinases in human melanoma. J Invest Dermatol. 2000 Sep;115(3):337-44.

Honda, T.; Obara, Y.; Yamauchi, A.; Couvillon, A.D.; Mason, J.J.; Ishii, K.; Nakahata, Hooten N, Evans MK. Techniques to Induce and Quantify Cellular Senescence. J Vis Exp. 2017 May 1;(123):55533. doi: 10.3791/55533. PMID: 28518126; PMCID: PMC5565152.

Hsu M, Andl T, Li G, Meinkoth JL, Herlyn M. Cadherin repertoire determines partner-specific gap junctional communication during melanoma progression. J Cell Sci. 2000 May;113 (Pt 9):1535-42. doi: 10.1242/jcs.113.9.1535. PMID: 10751145.

Huang, F.W., et al., Highly recurrent TERT promoter mutations in human melanoma. Hum Pathol. 1984 Dec;15(12):1147-65. doi: 10.1016/s0046-8177(84)80310-x. PMID: 6500548.

Ishikawa, I., & Iwasa, M. (2020). Toxicological effect of ivermectin on the survival, reproduction, and feeding activity of four species of dung beetles (Coleoptera: Scarabaeidae and Geotrupidae) in Japan. Bulletin of Entomological Research, 110(1), 106-114. doi:10.1017/S0007485319000385.

Jha, S., et al., Dissecting Therapeutic Resistance to ERK Inhibition. Mol Cancer Ther, 2016. 15(4): p. 548-59.

Jiang L, Sun YJ, Song XH, Sun YY, Yang WY, Li J, Wu YJ. Ivermectin inhibits tumor metastasis by regulating the Wnt/β-catenin/integrin β1/FAK signaling pathway. Am J Cancer Res. 2022 Oct 15;12(10):4502-4519. PMID: 36381328; PMCID: PMC9641399.

Juarez M, Schcolnik-Cabrera A, Dominguez-Gomez G, Chavez-Blanco A, Diaz-Chavez J, Duenas-Gonzalez A. Antitumor effects of ivermectin at clinically feasible concentrations support its clinical development as a repositioned cancer drug. Cancer Chemother Pharmacol. 2020 Jun;85(6):1153-1163. doi: 10.1007/s00280-020-04041-z. Epub 2020 May 30. PMID: 32474842.

Kashchuk, A. V., Perederiy, O., Caldini, C., Gardini, L., Pavone, F. S., Negriyko, A. M., & Capitanio, M. (2022). Particle Localization Using Local Gradients and Its Application to Nanometer Stabilization of a Microscope. ACS Nano.

Kato, Y., et al., BMK1/ERK5 regulates serum-induced early gene expression through transcription factor MEF2C. EMBO J, 1997. 16(23): p. 7054-66.

Keung EZ, Gershenwald JE. The eighth edition American Joint Committee on Cancer (AJCC) melanoma staging system: implications for melanoma treatment and care. Expert Rev Anticancer Ther. 2018 Aug;18(8):775-784. doi: 10.1080/14737140.2018.1489246. PMID: 29923435; PMCID: PMC7652033

Kim, E.K.; Choi, E.J. Pathological roles of MAPK signaling pathways in human diseases. Biochim. Biophys. Acta 2010, 1802, 396–405, doi: 10.1016/j.bbadis. 2009.12.009.

Kim, S.C.; Hahn, J.S.; Min, Y.H.; Yoo, N.C.; Ko, Y.W.; Lee, W.J. Constitutive activation of extracellular signal-regulated kinase in human acute leukemias: combined role of activation of MEK, hyperexpression of extracellular signal-regulated kinase, and downregulation of a phosphatase, PAC1. Blood 1999, 93, 3893–3899.

Kimura M, Imamoto N. Biological significance of the importin-β family-dependent nucleocytoplasmic transport pathways. Traffic. 2014 Jul;15(7):727-48. doi: 10.1111/tra.12174. Epub 2014 May 23. PMID: 24766099.

Kobe, Gleichmann, Horne, Jennings, Scotney, Teh, Turn up the HEAT, Structure, Volume 7, Issue 5, 1999, Pages R91-R97.

Kodama M, Kodama T, Newberg JY, Katayama H, Kobayashi M, Hanash SM, Yoshihara K, Wei Z, Tien JC, Rangel R, Hashimoto K, Mabuchi S, Sawada K, Kimura T, Copeland NG, Jenkins NA. In vivo loss-of-function screens identify KPNB1 as a new druggable oncogene in epithelial ovarian cancer. Proc Natl Acad Sci U S A. 2017 Aug 29;114(35):E7301-E7310. doi: 10.1073/pnas.1705441114. Epub 2017 Aug 15. PMID:

Kosyna FK, Depping R. Controlling the Gatekeeper: Therapeutic Targeting of Nuclear Transport. Cells. 2018 Nov 21;7(11):221. doi: 10.3390/cells7110221. PMID: 30469340; PMCID: PMC6262578.

Krauthammer, M., et al., Exome sequencing identifies recurrent mutations in NF1and RASopathy genes in sun-exposed melanomas. Nat Genet, 2015. 47(9): p.996-1002.

Kuilman, Michaloglou, Vredeveld, Douma, van Doorn, Desmet, Aarden, Mooi, Peeper, Oncogene-Induced Senescence Relayed by an Interleukin-Dependent Inflammatory Network, Cell, Volume 133, Issue 6, 2008, Pages 1019-1031, ISSN 0092-8674.

Larue, L. and A. Bellacosa, Epithelial-mesenchymal transition in development and cancer: role of phosphatidylinositol 3' kinase/AKT pathways. Oncogene, 2005. 24(50): p. 7443-

Lee SJ, Sekimoto T, Yamashita E, Nagoshi E, Nakagawa A, Imamoto N, Yoshimura M, Sakai H, Chong KT, Tsukihara T, Yoneda Y. The structure of importin-beta bound to SREBP-2: nuclear import of a transcription factor. Science. 2003 Nov 28;302(5650):1571-5. doi: 10.1126/science.1088372. PMID: 14645851.

Lee, J.D., R.J. Ulevitch, and J. Han, Primary structure of BMK1: a new mammalian map kinase. Biochem Biophys Res Commun, 1995. 213(2): p. 715-24.

Liang XT, Pan K, Chen MS, Li JJ, Wang H, Zhao JJ, Sun JC, Chen YB, Ma HQ, Wang QJ, Xia JC. Decreased expression of XPO4 is associated with poor prognosis in hepatocellular carcinoma. J Gastroenterol Hepatol 2011; 26:544–549.

Lin EC, Amantea CM, Nomanbhoy TK, Weissig H, Ishiyama J, Hu Y, Sidique S, Li B, Kozarich JW, Rosenblum JS. ERK5 kinase activity is dispensable for cellular immune response and proliferation. Proc Natl Acad Sci U S A. 2016 Oct 18;113(42):11865-11870. doi: 10.1073/pnas.1609019113. Epub 2016 Sep 27. PMID: 27679845; PMCID: PMC5081620.

Liu F, Zhang H, Song H. Upregulation of MEK5 by Stat3 promotes breast cancer cell invasion and metastasis. Oncol Rep. 2017 Jan;37(1):83-90. doi: 10.3892/or.2016.5256. Epub 2016 Nov 18. PMID: 27878304.

Lochhead PA, Gilley R, Cook SJ. ERK5 and its role in tumour development. Biochem Soc Trans. 2012 Feb;40(1):251-6. doi: 10.1042/BST20110663. PMID: 22260700.

Lochhead, P.A., Tucker, J.A., Tatum, N.J. et al. Paradoxical activation of the protein kinase-transcription factor ERK5 by ERK5 kinase inhibitors. Nat Commun 11, 1383 (2020). https://doi.org/10.1038/s41467-020-15031-3

Lorenzato A, Biolatti M, Delogu G, Capobianco G, Farace C, Dessole S, Cossu A, Tanda F, Madeddu R, Olivero M, Di Renzo MF. AKT activation drives the nuclear localization of CSE1L and a pro-oncogenic transcriptional activation in ovarian cancer cells. Exp Cell Res 2013; 319:2627–2636

Lu T, Bao Z, Wang Y, Yang L, Lu B, Yan K, Wang S, Wei H, Zhang Z, Cui G. Karyopherinβ1 regulates proliferation of human glioma cells via Wnt/β-catenin pathway. Biochem Biophys Res Commun. 2016 Sep 23;478(3):1189-97. doi: 10.1016/j.bbrc.2016.08.093. Epub 2016 Aug 24. PMID: 27568288.

Lu, J., Wu, T., Zhang, B. et al. Types of nuclear localization signals and mechanisms of protein import into the nucleus. Cell Commun Signal 19, 60 (2021). https://doi.org/10.1186/s12964-021-00741-y

Maik-Rachline G, Hacohen-Lev-Ran A, Seger R. Nuclear ERK: Mechanism of Translocation, Substrates, and Role in Cancer. Int J Mol Sci. 2019 Mar 8;20(5):1194. doi: 10.3390/ijms20051194. PMID: 30857244; PMCID: PMC6429060.

Manzano JL, Layos L, Bugés C, de Los Llanos Gil M, Vila L, Martínez-Balibrea E, Martínez-Cardús A. Resistant mechanisms to BRAF inhibitors in melanoma. Ann Transl Med. 2016 Jun;4(12):237. doi: 10.21037/atm.2016.06.07. PMID: 27429963; PMCID: PMC4930524.

Marfori M, Lonhienne TG, Forwood JK, Kobe B. Structural basis of high-affinity nuclear localization signal interactions with importin-α. Traffic. 2012 Apr;13(4):532-48. doi: 10.1111/j.1600-0854.2012.01329 Epub 2012 Feb 7. PMID: 22248489.

Markovic SN, Erickson LA, Rao RD, Weenig RH, Pockaj BA, Bardia A, Vachon CM, Schild SE, McWilliams RR, Hand JL, Laman SD, Kottschade LA, Maples WJ, Pittelkow MR, Pulido JS, Cameron JD, Creagan ET; Melanoma Study Group of the Mayo Clinic Cancer

Center. Malignant melanoma in the 21st century, part 1: epidemiology, risk factors, screening, prevention, and diagnosis. Mayo Clin Proc. 2007 Mar;82(3):364-80. doi: 10.4065/82.3.364. PMID: 17352373.

Michaloglou C, Vredeveld LC, Soengas MS, Denoyelle C, Kuilman T, van der Horst CM, Majoor DM, Shay JW, Mooi WJ, Peeper DS. BRAFE600-associated senescence-like cell cycle arrest of human naevi. Nature. 2005 Aug 4;436(7051):720-4. doi: 10.1038/nature03890. PMID: 16079850.

Miller SA, Coelho SG, Zmudzka BZ, Bushar HF, Yamaguchi Y, Hearing VJ, Beer JZ. Dynamics of pigmentation induction by repeated ultraviolet exposures: dose, dose interval and ultraviolet spectrum dependence. Br J Dermatol. 2008 Sep;159(4):921-30. doi: 10.1111/j.1365-2133.2008.08708 Epub 2008 Jul 4.

Monti M, Celli J, Missale F, Cersosimo F, Russo M, Belloni E, Di Matteo A, Lonardi S, Vermi W, Ghigna C, Giurisato E. Clinical Significance and Regulation of ERK5 Expression and Function in Cancer. Cancers (Basel). 2022 Jan 11;14(2):348. doi: 10.3390/cancers14020348. PMID: 35053510; PMCID: PMC8773716.

Montoliu L, Norris DA, Shellman Y, Smalley KSM, Spritz RA, Sturm RA, Swetter SM, Terzian T, Wakamatsu K, Weber JS, Box NF. Frontiers in pigment cell and melanoma research. Pigment Cell Melanoma Res. 2018 Nov;31(6):728-735. doi: 10.1111/pcmr.12728. Epub 2018 Oct 3.

Monzani, E., et al., Melanoma contains CD133 and ABCG2 positive cells with enhanced tumourigenic potential. Eur J Cancer, 2007. 43(5): p. 935-46.

Morimoto H, Kondoh K, Nishimoto S, Terasawa K, Nishida E. Activation of a C-terminal transcriptional activation domain of ERK5 by autophosphorylation. J Biol Chem. 2007 Dec 7;282(49):35449-56. doi: 10.1074/jbc.M704079200. Epub 2007 Oct 10. PMID: 17928297.

Morris, E.J., et al., Discovery of a novel ERK inhibitor with activity in models of acquired resistance to BRAF and MEK inhibitors. Cancer Discov, 2013. 3(7): p. 742-50.

Munoz-Espín D, SerranoM. Cellular senescence: from physiology to pathology. Nat Rev Mol Cell Biol 2014; 15:482–96.
N. Phosphorylation of ERK5 on Thr732 is associated with ERK5 nuclear localization and ERK5-dependent transcription. PLoS ONE 2015, 10, e0117914.

Nambara S, Masuda T, Nishio M, Kuramitsu S, Tobo T, Ogawa Y, Hu Q, Iguchi T, Kuroda Y, Ito S, Eguchi H, Sugimachi K, Saeki H, Oki E, Maehara Y, Suzuki A, Mimori K. Antitumor effects of the antiparasitic agent ivermectin via inhibition of Yes-associated protein

Nan X, Collisson EA, Lewis S, Huang J, Tamgüney TM, Liphardt JT, McCormick F, Gray JW, Chu S. Single-molecule superresolution imaging allows quantitative analysis of RAF multimer formation and signaling. Proc Natl Acad Sci U S A. 2013 Nov 12;110(46):18519-24. doi: 10.1073/pnas.1318188110. Epub 2013 Oct 24. PMID: 24158481; PMCID: PMC3831949.

Nardella C, Clohessy JG, Alimonti A, Pandolfi PP. Pro-senescence therapy for cancer treatment. Nat Rev Cancer 2011; 11:503–11.

Narita M, Nũnez S, Heard E, Narita M, Lin AW, Hearn SA, Spector DL, Hannon GJ, Lowe SW. Rb-mediated heterochromatin formation and silencing of E2F target genes during cellular senescence. Cell. 2003 Jun 13;113(6):703-16. doi: 10.1016/s0092-8674(03)00401-x. PMID: 12809602.

Nazarian R, Shi H, Wang Q, Kong X, Koya RC, Lee H, Chen Z, Lee MK, Attar N, Sazegar H, Chodon T, Nelson SF, McArthur G, Sosman JA, Ribas A, Lo RS. Melanomas acquire resistance to B-RAF(V600E) inhibition by RTK or N-RAS upregulation. Nature. 2010 Dec 16;468(7326):973-7. doi: 10.1038/nature09626. Epub 2010 Nov 24. PMID: 21107323; PMCID: PMC3143360.

Nelson, A.A. and H. Tsao, Melanoma and genetics. Clin Dermatol, 2009. 27(1): p. 46-

Nithianandarajah-Jones GN, Wilm B, Goldring CE, Müller J, Cross MJ. ERK5: structure, regulation and function. Cell Signal. 2012 Nov;24(11):2187-96. doi: 10.1016/j.cellsig.2012.07.007. Epub 2012 Jul 16. PMID: 22800864.

Noske A, Weichert W, Niesporek S, Roske A, Buckendahl AC, Koch I, Sehouli J, Dietel M, Denkert C. Expression of the nuclear export protein chromosomal region maintenance/exportin 1/Xpo1 is a prognostic factor in human ovarian cancer. Cancer 2008; 112:1733–1743

Nunes M, Duarte D, Vale N, Ricardo S. Pitavastatin and Ivermectin Enhance the Efficacy of Paclitaxel in Chemoresistant High-Grade Serous Carcinoma. Cancers (Basel). 2022 Sep 7;14(18):4357. doi: 10.3390/cancers14184357. PMID: 36139522; PMCID: PMC9496819.

Ortiz-Ruiz MJ, Álvarez-Fernández S, Parrott T, Zaknoen S, Burrows FJ, Ocaña A, Pandiella A, Esparís-Ogando A. Therapeutic potential of ERK5 targeting in triple negative breast cancer. Oncotarget. 2014 Nov 30;5(22):11308-18. doi: 10.18632/oncotarget.2324. PMID: 25350956; PMCID: PMC4294347.

Ovesný M.; Křížek, P.; Borkovec, J.; Švindrych, Z.; Hagen, G. M. ThunderSTORM: a comprehensive ImageJ Plug-In for PALM and STORM Data Analysis and Super-Resolution Imaging. Bioinformatics 2014, 30, 2389–2390

Paakinaho, V., Presman, D., Ball, D. et al. Single-molecule analysis of steroid receptor and cofactor action in living cells. Nat Commun 8, 15896 (2017). https://doi.org/10.1038/ncomms15896

Patel H, Yacoub N, Mishra R, White A, Long Y, Alanazi S, Garrett JT. Current Advances in the Treatment of BRAF-Mutant Melanoma. Cancers (Basel). 2020 Feb 19;12(2):482. doi: 10.3390/cancers12020482. PMID: 32092958; PMCID: PMC7072236.

Peiro G, Diebold J, Lohrs U. CAS (cellular apoptosis susceptibility) gene expression in ovarian carcinoma: correlation with 20q13.2 copy number and cyclin D1, p53, and Rb protein expression. Am J Clin Pathol 2002; 118:922–929

Pereira, D.M.; Simões, A.E.; Gomes, S.E.; Castro, R.E.; Carvalho, T.; Rodrigues, C.M.; Borralho, P.M. MEK5/ERK5 signaling inhibition increases colon cancer cell sensitivity to 5-

fluorouracil through a p53-dependent mechanism. Oncotarget 2016, 7, 34322–34340

Perez-Madrigal D, Finegan KG, Paramo B, Tournier C. The extracellularregulated protein kinase 5 (ERK5) promotes cell proliferation through the downregulation of inhibitors of cyclin dependent protein kinases (CDKs). Cell Signal 2012

Pi X, Yan C, Berk BC. Big mitogen-activated protein kinase (BMK1)/ERK5 protects endothelial cells from apoptosis. Circ Res. 2004 Feb 20;94(3):362-9. doi: 10.1161/01.RES.0000112406.27800.6F. Epub 2003 Dec 11. PMID: 14670836.
PMID: 30261516.

Ramsay, A.K., et al., ERK5 signalling in prostate cancer promotes an invasive phenotype. Br J Cancer, 2011. 104(4): p. 664-72.

Rastrelli M, Tropea S, Rossi CR, Alaibac M. Melanoma: epidemiology, risk factors, pathogenesis, diagnosis and classification. In Vivo. 2014 Nov-Dec;28(6):1005-11. PMID: 25398793.

Regad, T., Molecular and cellular pathogenesis of melanoma initiation and progression. Cell Mol Life Sci. 2013 Nov;70(21):4055-65. doi: 10.1007/s00018-013-1324-2. Epub 2013 Mar 27. PMID: 23532409.

Rothhammer, T., et al., Functional implication of BMP4 expression on angiogenesis in malignant melanoma. Oncogene, 2007. 26(28): p. 4158-70.

Rovida, E., et al., ERK5/BMK1 is indispensable for optimal colony-stimulating factor 1 (CSF-1)-induced proliferation in macrophages in a Src-dependent fashion. J Immunol, 2008. 180(6): p.4166-72.

Rovida, E., et al., The mitogen-activated protein kinase ERK5 regulates the development and growth of hepatocellular carcinoma. Gut, 2015. 64(9): p. 1454-65.

Rovida, E., Navari, N., Caligiuri, A., Dello, S. P., and Marra, F. (2008). ERK5 differentially regulates PDGF-induced proliferation and migration of hepatic stellate cells. J. Hepatol. 48, 107–115. doi: 10.1016/j.jhep.2007.08.010
S. CDK5 functions as a tumor promoter in human colorectal cancer via modulating the ERK5-AP-1 axis. Cell Death Dis. 2016 Oct 13;7(10):e2415. doi: 10.1038/cddis.2016.333. PMID: 27735944; PMCID: PMC5133995.

Samaniego R, Guti_errez-Gonz_alez A, Guti_errez-Seijo A, Sanchez-Gregorio S, García-Gimenez J, Mercader E, et al. CCL20 expression by tumor-associated macrophages predicts progression of human primary cutaneous melanoma. Cancer Immunol Res 2018; 6:267–75.

Samatar AA, Poulikakos PI. Targeting RAS-ERK signalling in cancer: promises and challenges. Nat Rev Drug Discov. 2014 Dec;13(12):928-42. doi: 10.1038/nrd4281. PMID: 25435214.

Savoia, P.; Fava, P.; Casoni, F.; Cremona, O. Targeting the ERK Signaling Pathway in Melanoma. Int. J. Mol. Sci. 2019, 20, 1483. https://doi.org/10.3390/ijms20061483.

Sawhney RS, Liu W, Brattain MG. A novel role of ERK5 in integrin-mediated cell adhesion and motility in cancer cells via Fak signaling. J Cell Physiol. 2009 Apr;219(1):152-61. doi: 10.1002/jcp.21662. PMID: 19089993; PMCID: PMC7064882.

Schadendorf D, van Akkooi ACJ, Berking C, Griewank KG, Gutzmer R, Hauschild A, Stang A, Roesch A, Ugurel S. Melanoma. Lancet. 2018 Sep 15;392(10151):971- 984. doi: 10.1016/S0140-6736(18)31559-9. Erratum in: Lancet. 2019 Feb 23;393(10173):746. PMID: Science, 2013. 339(6122): p. 957-9.

Shain, A.H., Yeh, I., Kovalyshyn, I. et al. (2015). The Genetic Evolution of Melanoma from Precursor Lesions. N. Engl. J. Med 373, 1926– 1936.

Shao, Y., Akmentin, W., Toledo-Aral, J. J., Rosenbaum, J., Valdez, G., Cabot, J. B., et al. (2002). Pincher, a pinocytic chaperone for nerve growth factor/TrkA signaling endosomes. J. Cell Biol. 157, 679–691. doi: 10.1083/jcb.200201063.

Shen A, Wang Y, Zhao Y, Zou L, Sun L, Cheng C. Expression of CRM1 in human gliomas and its significance in p27 expression and clinical prognosis. Neurosurgery 2009; 65:153–159 discussion 159–160.

Shiraki K, Fujikawa K, Sugimoto K, Ito T, Yamanaka T, Suzuki M, Yoneda K, Takase K, Nakano T. Cellular apoptosis susceptibility protein and proliferation in human hepatocellular carcinoma. Int J Mol Med 2006; 18:77–81.

Shull, A.Y., et al., Novel somatic mutations to PI3K pathway genes in metastatic melanoma. PLoS One, 2012. 7(8): p. e43369.

Smalley KS, McArthur GA. The current state of targeted therapy in melanoma: this time it's personal. Semin Oncol. 2012 Apr;39(2):204-14. doi: 10.1053/j.seminoncol.2012.01.008. PMID: 22484192; PMCID: PMC3322364.

Soderholm JF, Bird SL, Kalab P, Sampathkumar Y, Hasegawa K, Uehara-Bingen M, Weis K, Heald R. Importazole, a small molecule inhibitor of the transport receptor importin-β. ACS Chem Biol. 2011 Jul 15;6(7):700-8. doi: 10.1021/cb2000296. Epub 2011 Apr 21. PMID:

Song D, Liang H, Qu B, Li Y, Liu J, Zhang Y, Li L, Hu L, Zhang X, Gao A. Ivermectin inhibits the growth of glioma cells by inducing cell cycle arrest and apoptosis in vitro and in vivo. J Cell Biochem. 2019 Jan;120(1):622-633. doi: 10.1002/jcb.27420. Epub 2018 Sep 14. PMID: 30596403.

Song, C., Wang, L., Xu, Q. et al. Targeting BMK1 Impairs the Drug Resistance to Combined Inhibition of BRAF and MEK1/2 in Melanoma. Sci Rep 7, 46244 (2017). https://doi.org/10.1038/srep46244.

Stawerski P, Wagrowska-Danilewicz M, Stasikowska O, Danilewicz M. Immunoexpression of CAS protein is augmented in high grade serous ovarian tumors. Pol J Pathol 2010; 61:219–223

Stecca B, Rovida E. Impact of ERK5 on the Hallmarks of Cancer. Int J Mol Sci. 2019 Mar 21;20(6):1426. doi: 10.3390/ijms20061426. PMID: 30901834; PMCID: PMC6471124.

Sugo, N., Morimatsu, M., Arai, Y. et al. Single-Molecule Imaging Reveals Dynamics of CREB Transcription Factor Bound to Its Target Sequence. Sci Rep 5, 10662 (2015). https://doi.org/10.1038/srep10662.

Tatake, R.J., et al., Identification of pharmacological inhibitors of the MEK5/ERK5 pathway. Biochem Biophys Res Commun, 2008. 377(1): p. 120-5.

through paracrine mechanisms. Cancer Res. 2006 Jan 15;66(2):794-802. doi: 10.1158/0008-5472.CAN-05-1716. PMID: 16424011.

Titus-Ernstoff L, Perry AE, Spencer SK, Gibson JJ, Cole BF, Ernstoff MS. Pigmentary characteristics and moles in relation to melanoma risk. Int J Cancer. 2005 Aug 10;116(1):144-9. doi: 10.1002/ijc.21001. PMID: 15761869.

Tsao H, Chin L, Garraway LA, Fisher DE. Melanoma: from mutations to medicine. Genes Dev. 2012 Jun 1;26(11):1131-55. doi: 10.1101/gad.191999.112. PMID: 22661227; PMCID: PMC3371404

Tubita A, Lombardi Z, Tusa I, Dello Sbarba P, Rovida E. Beyond Kinase Activity: ERK5 Nucleo-Cytoplasmic Shuttling as a Novel Target for Anticancer Therapy. Int J Mol Sci. 2020 Jan 31;21(3):938. doi: 10.3390/ijms21030938. PMID: 32023850; PMCID: PMC7038028.

Tung CL, Chao WY, Li YZ, Shen CH, Zhao PW, Chen SH, Wu TY, Lee YR. Ivermectin induces cell cycle arrest and caspase-dependent apoptosis in human urothelial carcinoma cells. Int J Med Sci. 2022 Sep 11;19(10):1567-1575. doi: 10.7150/ijms.76623. PMID: 36185334; PMCID: PMC9515697.

Tusa, I.; Cheloni, G.; Poteti, M.; Gozzini, A.; DeSouza, N.H.; Shan, Y.; Deng, X.; Gray, N.S.; Li, S.; Rovida, E.; et al. Targeting the Extracellular Signal-Regulated Kinase 5 Pathway to Suppress Human Chronic Myeloid Leukemia Stem Cells. Stem Cell Rep. 2018, 11, 929–943

Tusa, I.; Gagliardi, S.; Tubita, A.; Pandolfi, S.; Urso, C.; Borgognoni, L.; Wang, J.; Deng, X.; Gray, N.S.; Stecca, B.; et al. ERK5 is activated by oncogenic BRAF and promotes melanoma growth. Oncogene 2018, 37, 2601–2614.

Van der Watt PJ, Maske CP, Hendricks DT, Parker MI, Denny L, Govender D, Birrer MJ, Leaner VD. The Karyopherin proteins, Crm1 and Karyopherin beta1, are overexpressed in cervical cancer and are critical for cancer cell survival and proliferation. Int J Cancer 2009; 124:1829–1840.

Van der Watt PJ, Ngarande E, Leaner VD. Overexpression of Kpnbeta1 and Kpnalpha2 importin proteins in cancer derives from deregulated E2F activity. PLoS One 2011;6:e27723. Vemurafenib induces senescence features in melanoma cells. J Invest Dermatol 2013.

Voskoboynik, M. and H.T. Arkenau, Combination therapies for the treatment of advanced melanoma: a review of current evidence. Biochem Res Int, 2014. 2014

Wagstaff KM, Rawlinson SM, Hearps AC, Jans DA. An AlphaScreen®-based assay for high-throughput screening for specific inhibitors of nuclear import. J Biomol Screen. 2011

Feb;16(2):192-200. doi: 10.1177/1087057110390360. PMID: 21297106.

Wagstaff KM, Sivakumaran H, Heaton SM, Harrich D, Jans DA. Ivermectin is a specific inhibitor of importin α/β-mediated nuclear import able to inhibit replication of HIV-1 and dengue virus. Biochem J. 2012 May 1;443(3):851-6. doi: 10.1042/BJ20120150. PMID: 22417684; PMCID: PMC3327999.

Wang B, Kohli J, Demaria M. Senescent cells in cancer therapy: friends or foes? Trends Cancer 2020; 6:838–57.

Wang J, Erazo T, Ferguson FM, Buckley DL, Gomez N, Muñoz-Guardiola P, Diéguez-Martínez N, Deng X, Hao M, Massefski W, Fedorov O, Offei-Addo NK, Park PM, Dai L, DiBona A, Becht K, Kim ND, McKeown MR, Roberts JM, Zhang J, Sim T, Alessi DR, Bradner JE, Lizcano JM, Blacklow SC, Qi J, Xu X, Gray NS. Structural and Atropisomeric Factors Governing the Selectivity of Pyrimido-benzodiazipinones as Inhibitors of Kinases and Bromodomains. ACS Chem Biol. 2018 Sep 21;13(9):2438-2448. doi: 10.1021/acschembio.7b00638. Epub 2018 Aug 31. PMID: 30102854; PMCID: PMC6333101.

Wang K, Gao W, Dou Q, Chen H, Li Q, Nice EC, Huang C. Ivermectin induces PAK1-mediated cytostatic autophagy in breast cancer. Autophagy. 2016 Dec;12(12):2498-2499. doi: 10.1080/15548627.2016.1231494. Epub 2016 Sep 22. PMID: 27657889; PMCID: PMC5173258.

Wang X, Tournier C. Regulation of cellular functions by the ERK5 signalling pathway. Cell Signal. 2006 Jun;18(6):753-60. doi: 10.1016/j.cellsig.2005.11.003. Epub 2006 Jan 6. PMID: 16376520.

Weeraratna, A.T., et al., Wnt5a signaling directly affects cell motility and invasion of metastatic melanoma. Cancer Cell, 2002. 1(3): p. 279-88.

Weldon CB, Scandurro AB, Rolfe KW, Clayton JL, Elliott S, Butler NN, Melnik LI, Alam J, McLachlan JA, Jaffe BM, Beckman BS, Burow ME. Identification of mitogen-activated protein kinase kinase as a chemoresistant pathway in MCF-7 cells by using gene expression microarray. Surgery. 2002 Aug;132(2):293-301. doi: 10.1067/msy.2002.125389. PMID: 12219026.

Wellmann A, Krenacs L, Fest T, Scherf U, Pastan I, Raffeld M, Brinkmann U. Localization of the cell proliferation and apoptosis-associated CAS protein in lymphoid neoplasms. Am J Pathol 1997.

Williams CA, Fernandez-Alonso R, Wang J, Toth R, Gray NS, Findlay GM. Erk5 Is a Key Regulator of Naive-Primed Transition and Embryonic Stem Cell Identity. Cell Rep. 2016 Aug16;16(7):1820-8. doi: 10.1016/j.celrep.2016.07.033. Epub 2016 Aug 4. PMID: 27498864; PMCID: PMC4987282.

Xu L, Massagué J. Nucleocytoplasmic shuttling of signal transducers. Nat Rev Mol Cell Biol. 2004 Mar;5(3):209-19. doi: 10.1038/nrm1331. PMID: 14991001.

Yan C, Luo H, Lee JD, Abe J, Berk BC. Molecular cloning of mouse ERK5/BMK1 splice variants and characterization of ERK5 functional domains. J Biol Chem. 2001 Apr

6;276(14):10870-8. doi: 10.1074/jbc.M009286200. Epub 2001 Jan 3. PMID: 11139578.

Yang L, Hu B, Zhang Y, Qiang S, Cai J, Huang W, Gong C, Zhang T, Zhang S, Xu P, Wu X, Liu J. Suppression of the nuclear transporter-KPNβ1 expression inhibits tumor proliferation in hepatocellular carcinoma. Med Oncol. 2015 Apr;32(4):128. doi: 10.1007/s12032-015-0559-1. Epub 2015 Mar 21. PMID: 25794490.

Yang Q, Deng X, Lu B, Cameron M, Fearns C, Patricelli MP, et al. Pharmacological inhibition of BMK1 suppresses tumor growth through promyelocytic leukemia protein. Cancer Cell 2010; 18:258–67

Yang Q, Liao L, Deng X, Chen R, Gray NS, Yates JR 3rd, Lee JD. BMK1 is involved in the regulation of p53 through disrupting the PML-MDM2 interaction. Oncogene. 2013 Jun 27;32(26):3156-64. doi: 10.1038/onc.2012.332. Epub 2012 Aug 6. PMID: 22869143; PMCID: PMC3493705.

Yang SNY, Atkinson SC, Wang C, Lee A, Bogoyevitch MA, Borg NA, Jans DA. The broad spectrum antiviral ivermectin targets the host nuclear transport importin α/β1 heterodimer. Antiviral Res. 2020 May; 177:104760. doi: 10.1016/j.antiviral.2020.104760. Epub 2020 Mar 3. PMID: 32135219.

Yang, Q., et al., Pharmacological inhibition of BMK1 suppresses tumor growth through promyelocytic leukemia protein. Cancer Cell, 2010. 18(3): p. 258-67

Yao Y, Dong Y, Lin F, Zhao H, Shen Z, Chen P, Sun YJ, Tang LN, Zheng SE. The expression of CRM1 is associated with prognosis in human osteosarcoma. Oncol Rep 2009; 21:229–23

Yoon, S.; Seger, R. The extracellular signal-regulated kinase: multiple substrates regulate diverse cellular functions. Growth Factors 2006, 24, 21–44, doi:10.1080/02699050500284218.

Yoshimoto S, Loo TM, Atarashi K, Kanda H, Sato S, Oyadomari S, Iwakura Y, Oshima K, Morita H, Hattori M, Honda K, Ishikawa Y, Hara E, Ohtani N. Obesity-induced gut microbial metabolite promotes liver cancer through senescence secretome. Nature. 2013 Jul 4;499(7456):97-101. doi: 10.1038/nature12347. Epub 2013 Jun 26. Erratum in: Nature. 2014 Feb 20;506(7488):396. Hattori, Masahisa [corrected to Hattori, Masahira]. PMID: 23803760.

Zeng B, Hu J, Yuan R, Hu L, Zhong L, Kang K. Increased expression of importin13 in endometriosis and endometrial carcinoma. Med Sci Monit 2012;18:CR361–CR367.

Zhang P, Zhang Y, Liu K, Liu B, Xu W, Gao J, Ding L, Tao L. Ivermectin induces cell cycle arrest and apoptosis of HeLa cells via mitochondrial pathway. Cell Prolif. 2019 Mar;52(2): e12543. doi: 10.1111/cpr.12543. Epub 2018 Dec 4. PMID: 30515909; PMCID: PMC6496724.

Zhou, G., Z.Q. Bao, and J.E. Dixon, Components of a new human protein kinase signal transduction pathway. J Biol Chem, 1995. 270(21): p. 12665-9

Published OnlineFirst November 19, 2021; DOI: 10.1158/0008-5472.CAN-21-0993

Inhibition of ERK5 Elicits Cellular Senescence in Melanoma via the Cyclin-Dependent Kinase Inhibitor p21

Alessandro Tubita[1], Zoe Lombardi[1], Ignazia Tusa[1], Azzurra Lazzeretti[1], Giovanna Sgrignani[1], Dimitri Papini[1], Alessio Menconi[1], Sinforosa Gagliardi[2], Matteo Lulli[1], Persio Dello Sbarba[1], Azucena Esparís-Ogando[3], Atanasio Pandiella[3,4], Barbara Stecca[2], and Elisabetta Rovida[1]

ABSTRACT

Melanoma is the deadliest skin cancer with a very poor prognosis in advanced stages. Although targeted and immune therapies have improved survival, not all patients benefit from these treatments. The mitogen-activated protein kinase ERK5 supports the growth of melanoma cells *in vitro* and *in vivo*. However, ERK5 inhibition results in cell-cycle arrest rather than appreciable apoptosis. To clarify the role of ERK5 in melanoma growth, we performed transcriptomic analyses following ERK5 knockdown in melanoma cells expressing BRAFV600E and found that cellular senescence was among the most affected processes. In melanoma cells expressing either wild-type or mutant (V600E) BRAF, both genetic and pharmacologic inhibition of ERK5 elicited cellular senescence, as observed by a marked increase in senescence-associated β-galactosidase activity and p21 expression. In addition, depletion of ERK5 from melanoma cells resulted in increased levels of CXCL1, CXCL8, and CCL20, proteins typically involved in the senescence-associated secretory phenotype. Knockdown of p21 suppressed the induction of cellular senescence by ERK5 blockade, pointing to p21 as a key mediator of this process. *In vivo*, ERK5 knockdown or inhibition with XMD8–92 in melanoma xenografts promoted cellular senescence. Based on these results, small-molecule compounds targeting ERK5 constitute a rational series of prosenescence drugs that may be exploited for melanoma treatment.

Significance: This study shows that targeting ERK5 induces p21-mediated cellular senescence in melanoma, identifying a prosenescence effect of ERK5 inhibitors that may be exploited for melanoma treatment.

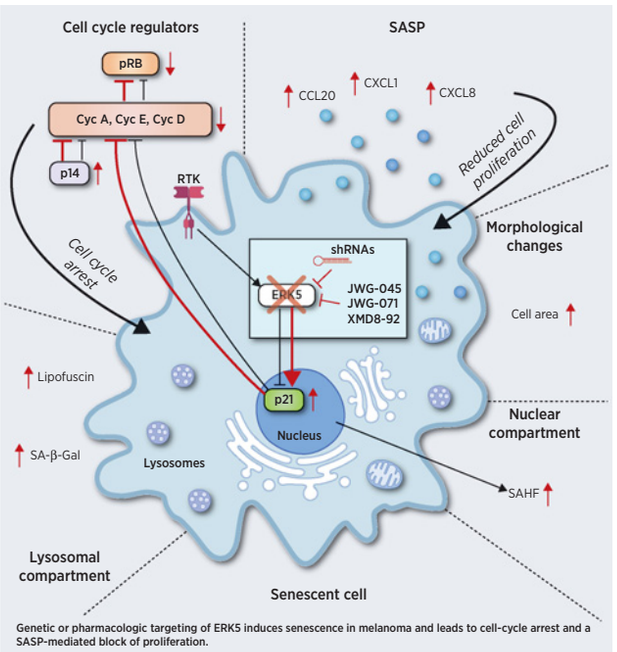

Genetic or pharmacologic targeting of ERK5 induces senescence in melanoma and leads to cell-cycle arrest and a SASP-mediated block of proliferation.

Introduction

Malignant melanoma is one of the most aggressive cancer and its incidence is increasing worldwide. Early-stage disease can be cured in the majority of cases, while late-stage melanoma is a highly lethal disease (1). Genomic sequencing studies of melanomas have found mutations in BRAF, NRAS, and NF1 that hyperactivate the mitogen-activated protein kinases (MAPK) extracellular signal-regulated kinase 1 and 2 (ERK1/2), thus supporting cell proliferation (2, 3). These findings allowed the development of BRAF- and MEK1/2-targeting drugs that, together with immunotherapy, increased the overall survival of melanoma patients (4). However, either the lack of responsiveness to immunotherapy or the presence of intrinsic and acquired resistance to BRAF-MEK1/2 inhibitors limit the benefits of available therapies (5, 6).

ERK5 is involved in cell survival, antiapoptotic signaling, proliferation and differentiation of several cell types, as well as angiogenesis (7), and plays a relevant role in the biology of cancer (8). ERK5 activation is achieved through MEK5-dependent phosphorylation, that stimulates ERK5 nuclear translocation, a key event for cell proliferation (9, 10).

Cellular senescence, a permanent state of cell-cycle arrest, is widely recognized as a potent tumor-suppressive mechanism (11, 12),

[1]Department of Experimental and Clinical Biomedical Sciences "Mario Serio", University of Florence, Florence, Italy. [2]Core Research Laboratory - Institute for Cancer Research and Prevention (ISPRO), Florence, Italy. [3]Instituto de Biología Molecular y Celular del Cáncer (IBMCC-CIC), Instituto de Investigación Biomédica de Salamanca (IBSAL), CIBERONC, Salamanca, Spain. [4]CSIC, Salamanca, Spain.

Note: Supplementary data for this article are available at Cancer Research Online (http://cancerres.aacrjournals.org/).

A. Tubita, Z. Lombardi, and I. Tusa equally contributed to the article.

Corresponding Author: Elisabetta Rovida, Department of Experimental and Clinical Biomedical Sciences, Università di Firenze, Viale G.B. Morgagni, 50, Firenze 50134, Italy. Phone: 3905-5275-1320; E-mail: elisabetta.rovida@unifi.it

Cancer Res 2022;82:447–57

doi: 10.1158/0008-5472.CAN-21-0993

Published OnlineFirst November 19, 2021; DOI: 10.1158/0008-5472.CAN-21-0993

so that induction of senescence is included among the possible strategies to fight cancer (12, 13). Melanoma is frequently characterized by the loss of the pathways supporting cellular senescence that would prevent tumor growth and progression (14). We previously showed that ERK5 inhibition reduces the growth of melanoma, determining a block of the cell cycle rather than inducing apoptosis (15). Because MAPK are frequently involved in cellular senescence (16, 17), we investigated the effects of ERK5 targeting on senescence with the aim to identify a novel therapeutic strategy for melanoma.

Materials and Methods

Cells and cell culture

A375 melanoma cells (18) were obtained from ATCC; SK-Mel-5 melanoma cells (19) were kindly provided by Dr. Laura Poliseno (CRL-ISPRO, Pisa, Italy). SSM2c melanoma cells were already described (Supplementary Table S1; ref. 20). Cells were maintained in DMEM supplemented with 10% heat-inactivated fetal bovine serum (FBS), 2 mmol/L glutamine, 50 U/mL penicillin, and 50 mg/mL streptomycin (EuroClone). Cell lines were yearly authenticated by cell profiling (Promega PowerPlex Fusion System Kit; BMR Genomics s.r.l). Presence of *Mycoplasma* was periodically tested by PCR.

Drugs

ERK5 inhibitor XMD8–92 (21) and MEK5 inhibitor BIX02189 (22) were from MedChemExpress LLC.

Cell lysis and Western blotting

Total cell lysates and nuclear–cytoplasmic fractions were obtained using Laemmli buffer or hypotonic buffer, respectively, as reported

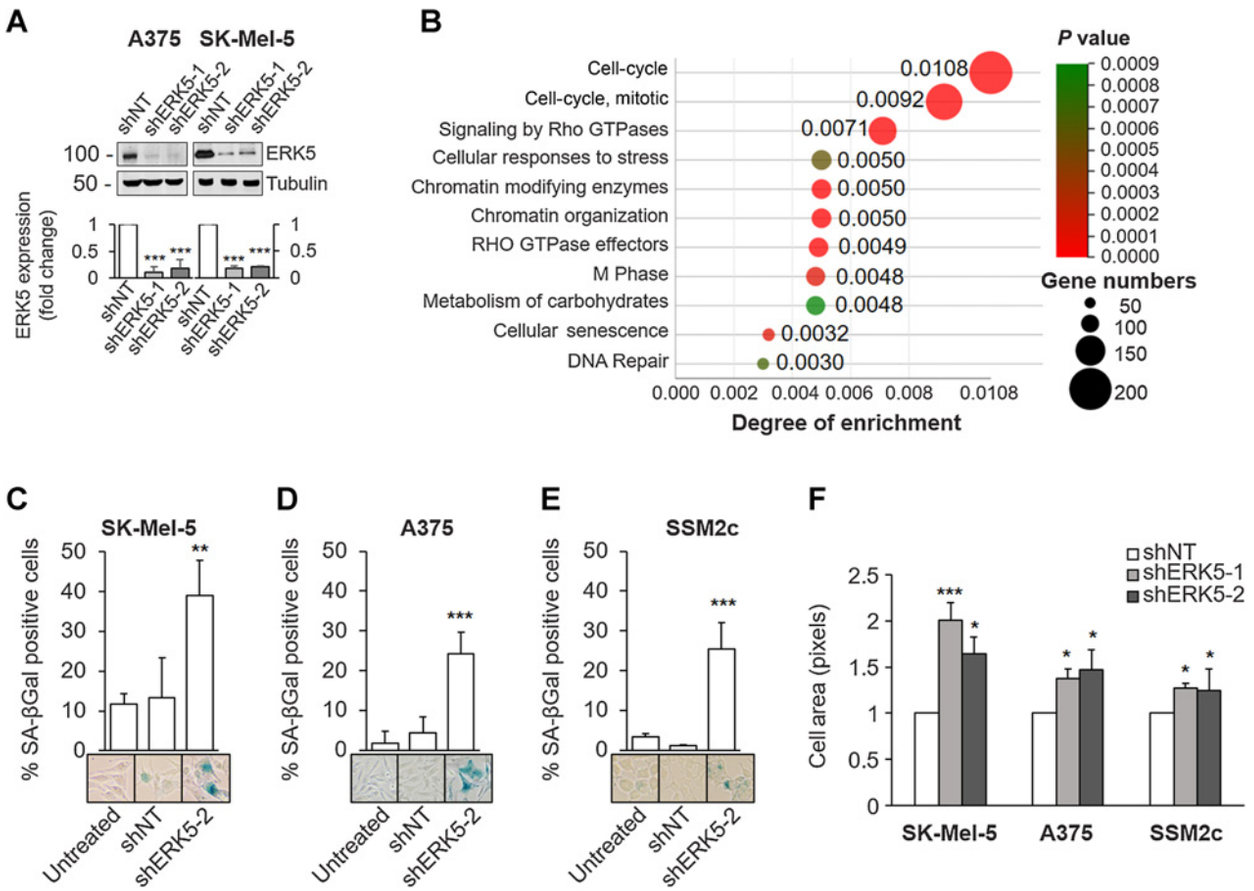

Figure 1.

ERK5 inhibition induces cellular senescence in melanoma cells. **A,** Genetic inhibition of ERK5. Cells were lysed after infection with lentiviral vectors carrying control nontargeting shRNA (shNT) or ERK5-specific shRNA (shERK5–1 and shERK5–2). Western blotting was performed with the indicated antibodies. Migration of molecular weight markers is indicated on the left (kDa). The graphs show average densitometric values of ERK5 protein levels normalized for tubulin content from three independent experiments. **B,** Transcriptomic analysis in A375 and SK-Mel-5 cells upon ERK5 KD. WebMeV analysis was performed on transcriptomic data after infection with lentiviral vectors carrying control or ERK5-specific shRNA. Data obtained from the two shRNA targeting ERK5 were averaged (A375, $n = 4$; SK-Mel-5, $n = 3$). Shown are the first eleven most impacted pathways based on degree of enrichment. Size of circles indicate the number of genes that are upregulated or downregulated in each pathway. **C–E,** ERK5 KD increased SA-βGal positivity in melanoma cells. Untreated cells or cells transduced with lentiviral vectors carrying control (shNT) or ERK5-specific shRNA (shERK5–2) were cultured for 72 hours. The percentage of SA-βGal–positive cells (blue ones) with respect to total number of cells/well was evaluated in three independent experiments. Representative images from each condition are shown. **F,** ERK5 KD induces an increase of melanoma cell area. Cell area was evaluated with ImageJ software. *P* values refer to differences with respect to shNT; *, $P < 0.05$; **, $P < 0.01$; ***, $P < 0.001$.

Table 1. Senescence and SASP-associated genes significantly deregulated in SK-Mel-5 and A375 melanoma cells upon ERK5 genetic inhibition. Data for shERK5 referred to average results from shERK5–1 and shERK5–2.

	A375		SK-Mel-5	
Gene symbol	Fold change shNT/shERK5	*P* value	Fold change shNT/shERK5	*P* value
HIST1H3B	−2.36	0.0178	−9.57	0.0252
HIST1H3F	−3.41	0.007	−5.96	0.0223
HIST1H4B	−2.61	0.0045	−2.25	0.0094
HIST1H4D	−1.7	0.0106	−4.7	0.0091
HIST1H4E	−2.45	0.0197	−2.35	0.0025
HIST1H4H	−2.85	0.0053	−2.13	0.0279
HIST1H4J	−1.88	0.0271	−2.9	0.0046
HIST1H4K	−1.75	0.0411	−2.9	0.0311
HIST2H3D	−1.8	0.0189	−1.7	0.0318
HIST2H4A	−1.8	0.0023	−9	0.0249
HIST2H4B	−1.88	0.0011	−4.3	0.0369
RBL1	−1.6	0.0389	−2.25	0.0159
LAMA1	−1.55	0.0306	−1.7	0.0194
CDC25A	−4.9	0.0063	−4.2	0.0022
LIN9	−1.6	0.004	−2.1	0.0078
CDKN1B	1.8	0.0136	2.04	0.05
CXCL1	6.7	0.0432	3.8	0.0496
CXCL8	20.3	0.0389	54.57	0.0434
CCL20	2	0.046	9.9	0.012
IGFBP7	7	0.0229	1.3	0.05
TP53	3.5	0.0189	1.6	0.028
RRAS	2.85	0.0000456	2.7	0.05
AKT3	2	0.008	1.96	0.03

previously (23, 24). Proteins were separated by SDS-PAGE and transferred onto Hybond PVDF (GE Healthcare) by electroblotting. Infrared imaging (Odyssey, Li-Cor Bioscience) was performed. Images were quantified with ImageJ software. Antibodies are in Supplementary Table S2.

RNA interference

TRC1.5-pLKO.1-puro lentiviral vectors (Supplementary Table S3) were produced in HEK293T cells as reported previously (25). Transduced cells were selected with 2 μg/mL puromycin for at least 72 hours.

Transcriptomic analysis

Total RNA was isolated using RNeasy Mini Kit (Qiagen), and mRNA expression evaluated with Affymetrix Clariom-S Human Genechip following the manufacturer's instructions. Transcriptome analysis console (TAC) software was used (fold change >1.5/<−1.5 and $P \leq 0.05$) to identify differentially expressed genes (DEG). Most enriched pathways were identified by Meta-analysis of DEG using WebMeV (Multiple Experiment Viewer).

Quantitative real-time PCR

Total RNA was isolated using TRIzol (Life Technologies). cDNA synthesis was carried out using ImProm-II Reverse Transcription System, while quantitative PCR (qPCR) was performed using GoTaq qPCR Master Mix (Promega Corporation). For primer sequences see Supplementary Material. QPCR was performed using CFX96 Touch Real-Time PCR Detection System (Bio-Rad). mRNA expression was normalized to GAPDH and 18S mRNA.

Flow cytometry

Cell-cycle phase distribution (propidium iodide staining) was determined as previously reported using a FACSCanto (Beckton Dickinson; ref. 26).

Chemokines determination in conditioned media

Fourteen days after lentiviral transduction, medium was replaced with DMEM/10% FBS. Conditioned media (CM) were harvested after 72 hours. Chemokine expression was measured in CM using RayBiotech Quantibody array (RayBiotech) following the manufacturer's instructions. Each antigen was measured in quadruplicate and relative fluorescence intensity determined using ImageJ software. Results were normalized for protein content in lysates.

Cell viability assay and neutralization experiments

Cell viability was measured by 3-(4,5-dimethylthiazol-2-yl)-3,5-diphenyltetrazolium bromide (MTT) assay. Cells were seeded in 96-well plate in DMEM/10% FBS. After 24 hours, medium was replaced with CM and cells further incubated for 72 hours. MTT (0.5 mg/mL) was added during the last 4 hours. Plates were read at 595 nm using a Microplate reader-550 (Bio-Rad). For neutralization experiments, control isotype IgG or neutralizing antibodies (Supplementary Table S2) were added to CM prior to administration to cells.

Determination of cellular senescence by senescence-associated βGal staining and of cell area

Cells were incubated for 72 hours and then fixed (2% formaldehyde, 10 minutes, room temperature). After washing, senescence-associated (SA) βGal staining solution (X-gal 1 mg/mL, 40 mmol/L citric acid, 5 mmol/L $C_6FeK_4N_6$, 5 mmol/L $C_6N_6FeK_3$, 150 mmol/L NaCl and 2 mmol/L $MgCl_2$; pH 6.1 -SK-Mel-5- or 5.9 -A375, SSM2c; ref. 27) was added (16 hours, 37°C). Senescent cell quantification was performed by counting SA-βGal–positive (blue) cells in 10 random images/well taken using a brightfield microscope. An average of 800 cells/condition were counted. In other experiments, cell area was evaluated with ImageJ software.

Immunohistochemistry and determination of cellular senescence *in vivo*

Formalin-fixed paraffin-embedded (FFPE) sections from archival xenografts established with shNT or shERK5–2 A375 or SSM2c cells, or with A375 cells from XMD8–92 (25 mg/kg)- or vehicle (2-hidroxypropyl-β-cyclodextrin 30%)-treated mice were used (15). Experiments had been approved by the Italian Ministry of Health (authorization no. 213/2015-PR) and were in accordance with the Italian ethic guidelines and regulations. Sections (3 μmol/L thick) were deparaffinized and stained with Sudan Black Blue (SBB; Bio-Optica) to reveal lipofuscin (28, 29), and counterstained with Nuclear Fast Red (NFR, Bio-Optica). Immunohistochemistry (IHC): After citrate buffer antigen retrieval, staining was performed with the UltraVision LP Detection System HRP Polymer Kit (Thermo Fisher Scientific) following the manufacturer's instructions. Sections were incubated overnight at 4°C with primary antibodies (Supplementary Table S2) and (3,3′-diaminobenzidine; Thermo Fisher Scientific; DAB) used as a chromogen. Sections were counterstained with hematoxylin.

Published OnlineFirst November 19, 2021; DOI: 10.1158/0008-5472.CAN-21-0993

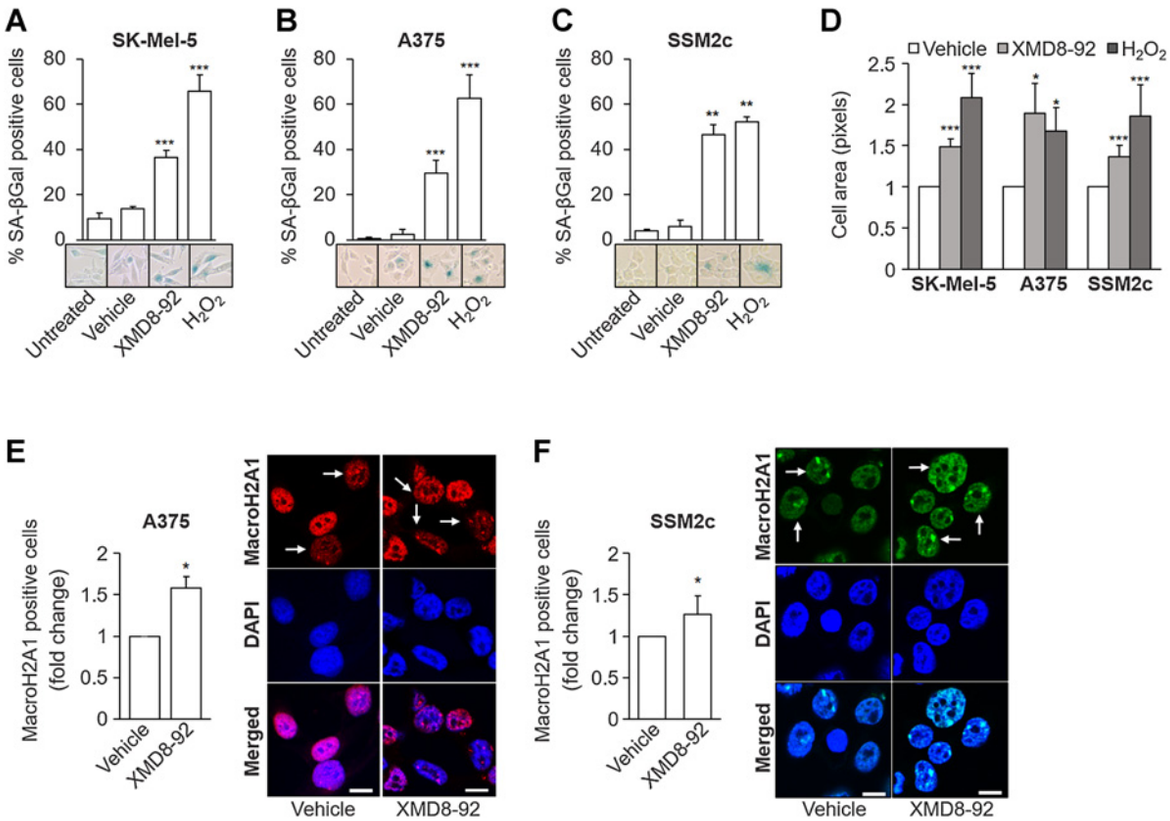

Figure 2.

Pharmacologic inhibition of ERK5 induces senescence in melanoma cells. **A–C,** Cells were left untreated or treated with DMSO (vehicle) or with 5 μmol/L XMD8–92 for 72 hours. Treatment with 300 nmol/L H_2O_2 during the first 2 hours was used as a positive control. The percentage of SA-βGal–positive cells (blue) with respect to the total number of cells/well was evaluated in three independent experiments. Representative images from each condition are shown. *P* values refer to differences with respect to vehicle-treated samples. **, $P < 0.01$; ***, $P < 0.001$. **D,** Pharmacologic inhibition of ERK5 induces an increase of melanoma cell area. The area of the cells was evaluated with ImageJ software. *P* values refer to differences with respect to shNT. *, $P < 0.05$; ***, $P < 0.001$. **E** and **F,** Pharmacologic inhibition of ERK5 induces an increase in macroH2A1-positive foci formation. Cells were treated with DMSO (vehicle) or with 5 μmol/L XMD8–92 for 72 hours and then stained for macroH2A1. Confocal images were analyzed to quantify macroH2A1-positive cells. *P* values refer to differences with respect to vehicle-treated cells. *, $P < 0.05$. Scale bar, 10 μm.

Colony formation assay

Cells were treated for 72 hours and then seeded in p60 dishes in DMEM 10% FBS. Colonies (i.e., more than 50 cells) were counted following crystal violet staining after 7 (A375) or 10 (SSM2c) days.

Immunofluorescence analysis

Cells were plated on glass coverslips and incubated for 72 hours in DMEM/2,5%FBS, and fixed with 4% paraformaldehyde (10 minutes, room temperature). Cells were permeabilized (0.2% Triton X-100) and saturated with 10% horse serum in PBS/1% BSA for 45 minutes. Incubation with primary antibody (overnight, 4°C) and with Cy2- or Cy3-labeled secondary antibodies was performed. Cell nuclei were labelled with DAPI (Invitrogen). Images were analyzed with a confocal inverted microscope equipped with a Nikon S Fluor 60× immersion oil objective (Nikon Instruments).

Statistical analysis

Data represent mean or ± SD values calculated on at least three independent experiments. *P* values were calculated using Student *t* test (two groups) or one-way ANOVA (more than two groups). $P < 0.05$ was considered statistically significant.

Results

ERK5 inhibition induces cellular senescence in melanoma cells and xenografts

We previously showed that ERK5 inhibition reduces proliferation of melanoma cells *in vitro* and growth of melanoma xenografts *in vivo* (15). To deepen the role of ERK5 in melanoma growth, we performed transcriptomic experiments in BRAFV600E A375 and SK-Mel-5 melanoma cells after ERK5 KD with two different shRNAs (**Fig. 1A**). DEG analysis showed that the most impacted pathways dealt with cell-cycle regulation. Interestingly, cellular senescence was the tenth most impacted pathway (0.0032 degree of enrichment; **Fig. 1B**; Supplementary Table S4). We also identified several senescence-related genes, whose expression was significantly changed upon ERK5 KD (**Table 1**).

We then verified whether ERK5 inhibition elicits cellular senescence. Both SK-Mel-5 and A375 ERK5-KD cells showed a marked increase (20%–30%) of SA-βGal–positive cells, when compared with naïve or to control nontargeting shRNA-transduced cells (**Fig. 1C** and **D**). The same effects were observed in triple wild-type SSM2c cells (**Fig. 1E**). In all three cell lines, ERK5 KD determined an increase of the cell area (**Fig. 1F**), a morphologic change typical of senescent cells (16). Importantly, the ERK5 inhibitors XMD8–92 (**Fig. 2A–C**)

Published OnlineFirst November 19, 2021; DOI: 10.1158/0008-5472.CAN-21-0993

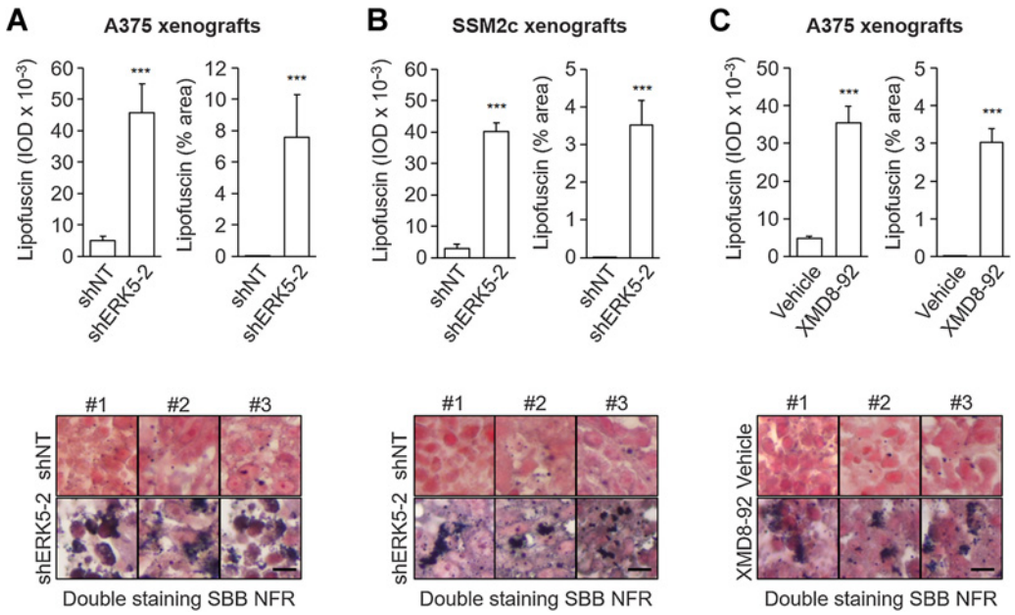

Figure 3.

Genetic inhibition of ERK5 induces senescence in human melanoma xenografts. **A–C,** FFPE sections from A375 (**A**) and SSM2c (**B**) shNT and shERK5–2 xenografts or A375 xenografts obtained from mice treated with vehicle or XMD8–92 (**C**) were stained with Sudan Black B (SBB) to evaluate lipofuscin content and Nuclear Fast Red (NFR). Integrated optical density (IOD; left graphs) or percentage (%) of area of positively stained tissues (right graphs) was used to quantify the amount of lipofuscin. The integrated optical density and percent area was calculated from six different ×40 magnified fields from three xenografts. Representative images are shown. Scale bar, 40 μm. ***, $P < 0.001$.

and JWG-045 (Supplementary Fig. S1A and S1B), used at concentrations with negligible off-target effects (15), as well as JWG-071 (Supplementary Fig. S1A), a more specific inhibitor of ERK5 over bromodomain-containing proteins (30, 31), were able to induce cellular senescence. Interestingly, the MEK5 inhibitor BIX02189 did not induce cellular senescence (Supplementary Fig. S1A–S1C). Pharmacologic inhibition of ERK5, which lasted for the entire duration of the experiments (Supplementary Fig. S1D), determined an increase of cell area (**Fig. 2D**), and of senescence-associated heterochromatin foci (SAHF)-positive cells (**Fig. 2E** and **F**). The latter effect was also observed after ERK5 KD (Supplementary Fig. S1E). The BRAFV600E inhibitor vemurafenib, but not the MEK1/2 inhibitor trametinib, determined an increase of senescent cells similarly to XMD8–92, and in combination with the latter further increased the percentage of senescent cells (Supplementary Fig. S1F).

The occurrence of cellular senescence *in vivo* was then investigated performing lipofuscin staining on archival xenografts of A375 and SSM2c cells transduced with shNT- or shERK5-encoding lentiviral vectors, the latter of which drastically reduced tumor growth (Supplementary Fig. S2A and S2B; ref. 15). In A375 and SSM2c xenografts, the amount of lipofuscin and the percentage of lipofuscin-stained area were markedly higher in ERK5-KD than in control xenografts (**Fig. 3A** and **B**). Similarly, systemic administration of XMD8–92, which induced a marked reduction of tumor growth (Supplementary Fig. S2C; ref. 15), determined a robust increase of lipofuscin in A375 xenografts with respect to vehicle-treated mice (**Fig. 3C**).

ERK5 inhibition impairs cell-cycle progression and affects cell-cycle regulators in melanoma cells

We then deepened the effects of ERK5 inhibition on cell-cycle progression that is impaired in senescent cells characterized by an irreversible block of proliferation. ERK5 KD determined an increase of cells in G_0–G_1 or G_2–M phase in A375 or SSM2c cells, respectively (**Fig. 4A** and **B**). This increase is robust when taking into consideration that 20% to 30% of the population undergoes senescence upon ERK5 KD (**Fig. 1C–E**). ERK5 KD determined a reduction of PCNA protein, in keeping with a reduced proliferation (Supplementary Fig. S3). Moreover, exposure to mitogens (i.e., 10% FBS), that increased the percentage of vehicle-treated cells in S phase, did not affect cell-cycle phase distribution in XMD8-92–treated cells (**Fig. 4C** and **D**). Of note, XMD8–92 blocked cell-cycle progression with a significant increase of cells in G_0–G_1 or G_2–M phase in A375 and SSM2c cells, respectively, in line with ERK5-KD cell results (**Fig 4A** and **B**) and with our previous data (15). Colony assay experiments using 72 hours XMD8-92–treated cells demonstrated their irreversible inability to proliferate (**Fig. 4E** and **F**).

The cyclin-dependent kinase inhibitor p21 mediates cellular senescence induced by ERK5 inhibition

To deepen the impact of ERK5 inhibition on cell-cycle regulators involved in senescence, we first revealed that ERK5 KD determined a reduction of RB phosphorylation and an increase of the cyclin-dependent kinase inhibitor (CDKi) p21 protein level in A375 and SSM2c cells (**Fig. 5A**), both representing the most used markers of cellular senescence. Furthermore, we found a reduced expression of cyclin E, D1, and A2 (**Fig. 5A**), in keeping with a reduced proliferation. Interestingly, either genetic (**Fig. 5A** and **B**) or pharmacologic (**Fig. 5C** and **D**) ERK5 inhibition increased the amount of the CDKi p14 protein. The increased protein levels of p21 (**Fig. 5E** and **F**) and of p14 (**Fig. 5G** and **H**) upon ERK5 KD were confirmed *in vivo* using A375 and SSM2c xenografts. Of note, the increase in the percentage of p14 positive cells in ERK5-KD A375 xenografts, although significant,

Published OnlineFirst November 19, 2021; DOI: 10.1158/0008-5472.CAN-21-0993

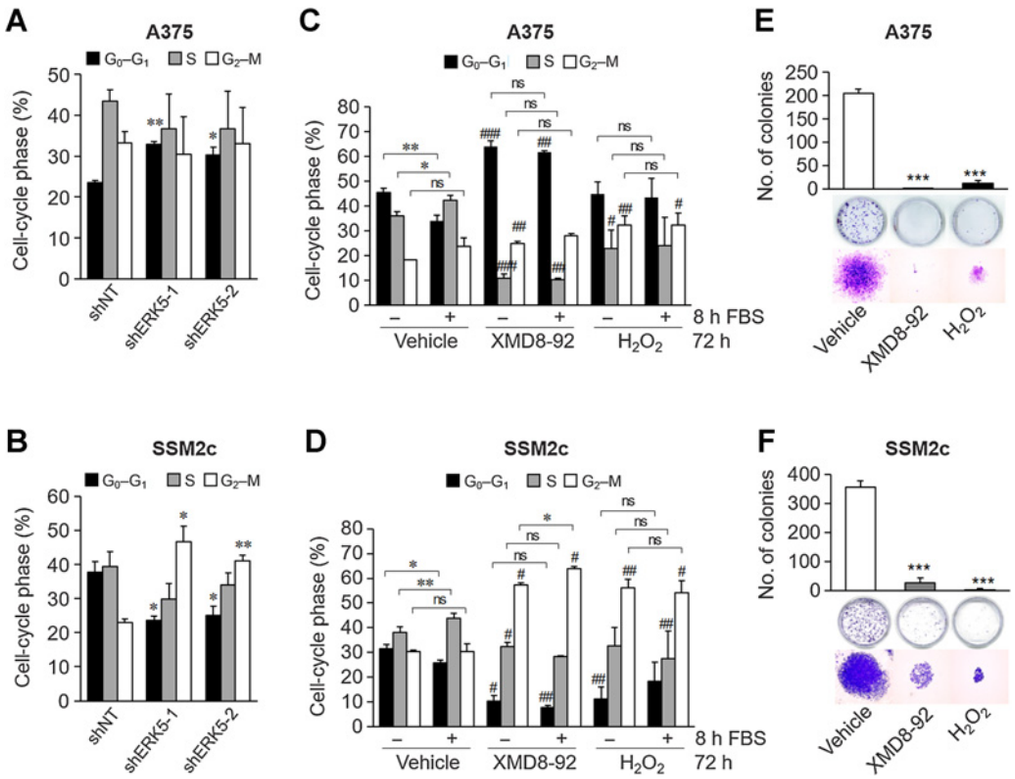

Figure 4.

Effects of ERK5 inhibition on cell-cycle progression and colony formation ability. **A** and **B,** Cells were transduced with lentiviral vectors carrying control (shNT) or ERK5-specific shRNA (shERK5–1 or shERK5–2) and were cultured for 72 hours. Cell-cycle phase distribution was then determined in three independent experiments. *P* values refer to differences with respect to shNT cells. *, $P < 0.05$; **, $P < 0.01$. **C** and **D,** Cells were treated with vehicle or 5 μmol/L XMD8–92 for 72 hours. Treatment with 300 nmol/L H_2O_2 during the first 2 hours was used as a positive control. After 72 hours, cells were treated with 10% FBS for 8 hours or left untreated. Cell-cycle phase distribution was then determined in three independent experiments. **#**, $P < 0.05$; **##**, $P < 0.01$; **###**, $P < 0.001$ refer to differences with vehicle-treated samples; *, $P < 0.05$; **, $P < 0.01$. **E** and **F,** Cells were treated with vehicle or 5 μmol/L XMD8–92 for 72 hours. Treatment with 300 nmol/L H_2O_2 during the first 2 hours was used as a positive control. After 72 hours, colony-forming assay was performed. *P* values refer to differences with respect to vehicle-treated cells. ***, $P < 0.001$. ns, nonsignificant.

was relatively low (**Fig. 5G**), and, accordingly, the increased amount of p14 protein was appreciable in nuclear extracts only (**Fig. 5A–C**). Consistently, we observed an increase of p21 and a decrease of PCNA-positive A375 cells after treatment with XMD8–92 *in vivo* (Supplementary Fig. S4A and S4B). Upon ERK5 KD, we also confirmed the increase of p27 and p53 protein levels, and the reduction of RBL-1 mRNA, identified by the transcriptomic analysis (**Table 1**). Moreover, the increased phosphorylation of CDK1 at Y15 seems to support the observed reduction of phosphatase CDC25a expression (Supplementary Fig. S4C–S4E).

Among the cell-cycle regulators, whose expression is markedly deregulated upon ERK5 inhibition, we focused on p21 in order to deepen the mechanism of ERK5 KD-associated senescence. Of note, p53 was found increased in the transcriptomic data (and confirmed at the protein level), and p21 is the effector of the majority of p53-induced biological effects including cellular senescence. Genetic inhibition of p21 using two different shRNAs (**Fig. 6A**) halved the percentage of A375 cells undergoing cellular senescence following treatment with XMD8-92 or H_2O_2 (**Fig. 6B**), revealing a key role of p21 in ERK5-dependent cellular senescence. The observed reduction of the percentage of cells undergoing senescence upon p21 KD was robust, taking into consideration that XMD8-92 induced a slight but significant increase of p21 protein level in p21 KD cells (**Fig. 6C**; compare lanes 5 and 6 vs. 2 and 3, respectively). In this respect, the lack of effect of BIX02189 on cellular senescence (Supplementary Fig. S1A–S1C) is in keeping with the ineffectiveness of this compound in increasing p21 protein level (15), while XMD8-92 induced a dose dependent increase of cellular senescence and p21 protein (Supplementary Fig. S5A–S5C). The above data indicate that cellular senescence induced by ERK5 inhibition in melanoma cells relies, at least in part, on p21.

ERK5 inhibition induces the senescence-associated secretory phenotype

One of the key features of senescent cells is the senescence-associated secretory phenotype (SASP; ref. 32). Transcriptomic data showed that SASP (0.0020 degree of enrichment, Supplementary Table S4) and SASP-related genes (**Table 1**) were significantly modulated upon ERK5 KD. Among the latter, transcriptomic analysis indicated that CXCL1/GROalpha and CXCL8/IL8, two of the most prominent SASP products (33), and CCL20/MIP3alpha mRNA were significantly upregulated in both A375 and SK-Mel-5 ERK5-KD cells (**Fig. 7A**). IL6, another key component of the SASP, was not altered upon ERK5 KD (**Fig. 7A**). QPCR experiments confirmed that lack of increase of IL6 mRNA in the same experimental settings in which CXCL8 mRNA was significantly increased in A375, SK-Mel-5, and SSM2c ERK5-KD cells (**Fig. 7B**). Importantly, protein array in CM

Published OnlineFirst November 19, 2021; DOI: 10.1158/0008-5472.CAN-21-0993

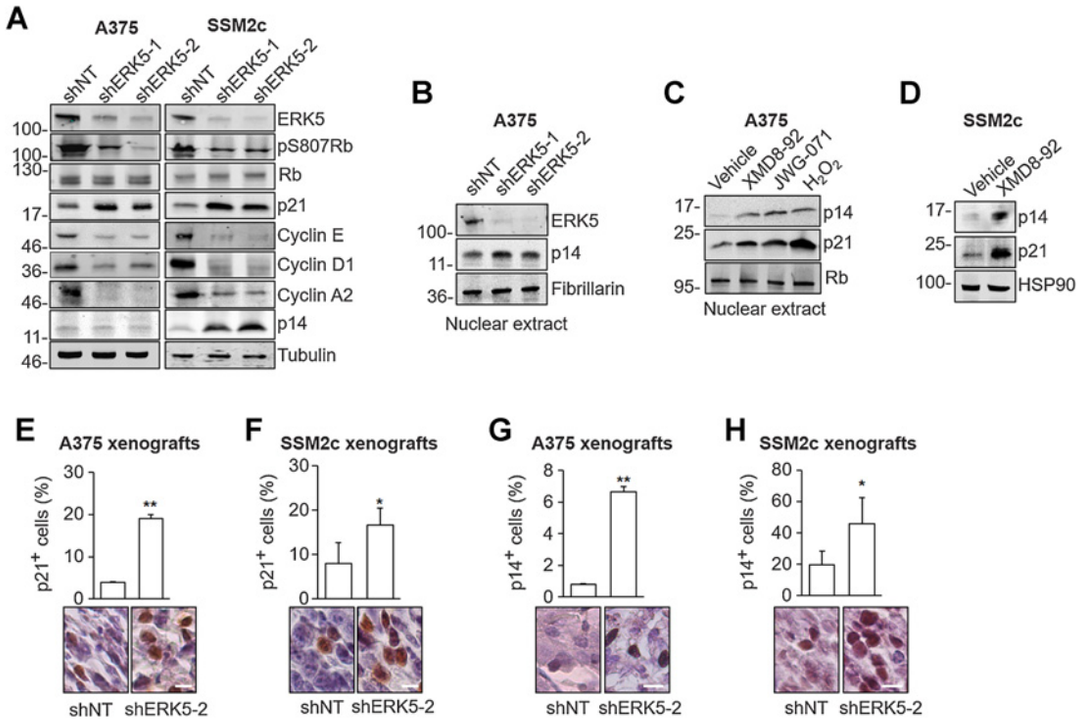

Figure 5.

Effects of ERK5 inhibition on signaling molecules involved in cell cycle and senescence. **A,** Cells transduced with control nontargeting shRNA (shNT) or ERK5-specific shRNAs (shERK5–1 and shERK5–2) were lysed, and Western blotting was performed with the indicated antibodies. Images are representative of three independent experiments showing similar results. Migration of molecular weight markers is indicated on the left (kDa). **B,** Cells transduced with control nontargeting shRNA (shNT) or ERK5-specific shRNAs (shERK5–1 and shERK5–2) were lysed, and Western blotting was performed on nuclear extracts with the indicated antibodies. Images are representative of three independent experiments showing similar results. Migration of molecular weight markers is indicated on the left (kDa). **C,** Cells were treated with DMSO (vehicle) or with the indicated drugs (5 μmol/L) for 72 hours. Treatment with 300 nmol/L H_2O_2 during the first 2 hours was used as a positive control. Cells were lysed, and Western blotting was performed on nuclear extracts with the indicated antibodies. Migration of molecular weight markers is indicated on the left (kDa). **D,** Cells were treated with DMSO (vehicle) or with XMD8–92 (5 μmol/L) for 72 hours. Cells were lysed, and Western blotting was performed with the indicated antibodies. Images are representative of three independent experiments showing similar results. Migration of molecular weight markers is indicated on the left (kDa). **E–H,** IHC detection of p21 (**E** and **F**) or p14 (**G** and **H**) proteins in shNT- or shERK5–2 xenografts. Hematoxylin counterstaining was performed. Bar plots of percentage (%) of p21 (**E** and **F**)- or p14 (**G** and **H**)-positive cells are shown. The percentage of positive cells was calculated from six different ×40 magnified fields from three shNT and three shERK5–2 tumors. Representative photographs are shown (original magnification, ×40). Scale bar, 40 μm.

(**Fig. 7C**) confirmed that CXCL1, CXCL8, and CCL20 protein levels were significantly increased in ERK5-KD A375 cells. Interestingly, publicly available datasets from the cBioPortal for Cancer Genomics (34, 35) confirmed the coexpression of the above-mentioned SASP products in patients with melanoma (Supplementary Fig. S6A and S6B). Indeed, the amount of CXCL1/GROalpha mRNA showed a robust positive correlation with that of CXCL8 (0.58 Spearman correlation; $P = 6.68e^{-41}$), and with that of CCL20 (0.49 Spearman correlation; $P = 1.34e^{-27}$; Skin Cutaneous Melanoma TCGA, Pan-Cancer Atlas; Supplementary Fig. S6A). The positive correlation between the mRNA level of CXCL1/GROalpha and of CXCL8 was confirmed (0.35 Spearman correlation; $P = 0.028$) in another data set (Metastatic Melanoma, DFCI, Science 201; Supplementary Fig. S6B; ref. 36).

SASP products may elicit either pro- or antiproliferative effects on tumor cells (29). To discriminate between these possible opposite outcomes, we tested CM from A375 and SK-Mel-5 cells and found that CM recovered from ERK5-KD cells markedly reduced the viability of either A375 or SK-MEL-5 cells with respect to CM from shNT cells (**Fig. 7D**). The proof that CXCL1, CXCL8, and CCL20 are among the SASP products responsible for the reduced proliferation was obtained using neutralizing antibodies (**Fig. 7E**). Indeed, each blocking antibody was able to partially rescue melanoma cell proliferation.

Discussion

Cellular senescence is considered a potent suppressive mechanism of tumorigenesis, and therapies that enhance senescence, besides promoting a stable cell growth arrest, may stimulate the activation of the antitumor immune response. Based on that, prosenescence molecules are actively sought after in view of their potential use as antineoplastic treatments (12, 13). In this study, we demonstrated a prominent role of ERK5 in cellular senescence in human melanoma. In BRAF-mutated and wild-type melanoma cells and xenografts, ERK5 inhibition induced indeed marked cellular senescence and production of several soluble mediators involved in the SASP. Mechanistically, we demonstrated that ERK5-dependent senescence is mediated by the CDKi p21.

The induction of cellular senescence upon ERK5 inhibition was demonstrated using different approaches. Senescence emerged first, in transcriptomic experiments, as one of the most impacted pathways upon ERK5 KD in BRAFV600E-mutated melanoma cells. Besides

Published OnlineFirst November 19, 2021; DOI: 10.1158/0008-5472.CAN-21-0993

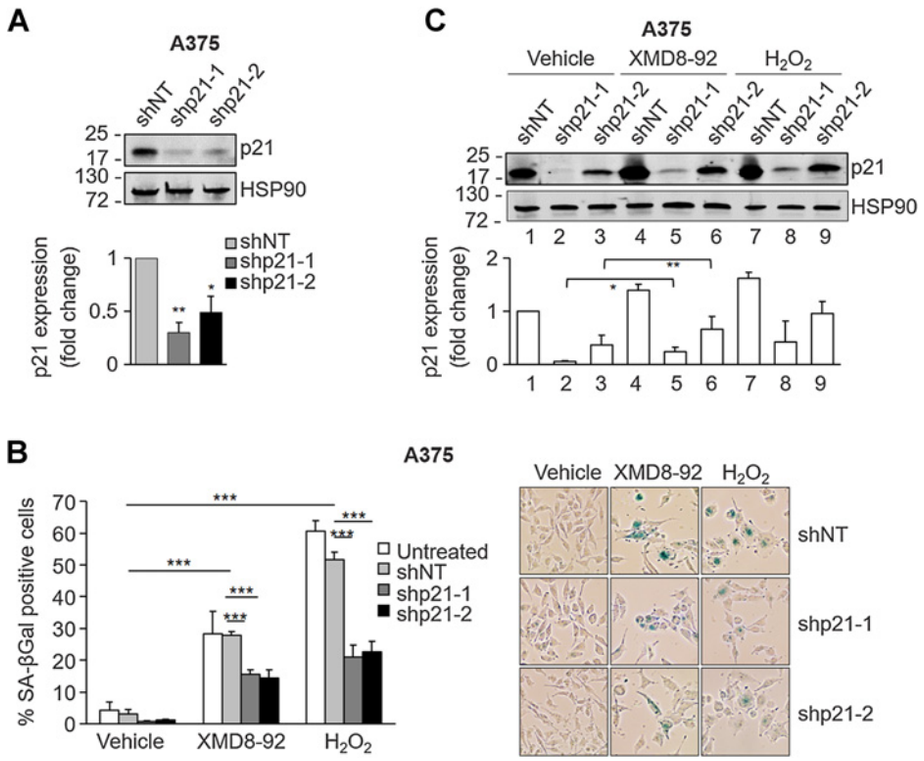

Figure 6.

Genetic inhibition of p21 prevents cellular senescence induced by ERK5 inhibition in A375 cells. **A,** Genetic inhibition of p21. Cells transduced with control nontargeting shRNA (shNT) or p21-specific shRNA (shp21–1 and shp21–2) were lysed, and Western blotting was performed with the indicated antibodies. Migration of molecular weight markers is indicated on the left (kDa). The graph shows average densitometric values of p21 protein normalized for HSP90 content from three independent experiments. **B,** Parental A375 (untreated) or A375 infected with lentiviral vectors carrying shNT, shp21–1, or shp21–2 were treated with DMSO (vehicle) or with XMD8–92 (5 μmol/L) for 72 hours. Treatment with 300 nmol/L H_2O_2 during the first 2 hours was used as a positive control. The percentage of SA-βGal-positive cells with respect to the total number of cells/well was evaluated in three independent experiments. Representative images from each condition are shown. **C,** A375 cells infected with lentiviral vectors carrying shNT, shp21–1, or shp21–2 were treated with DMSO (vehicle) or 5 μmol/L XMD8–92 for 72 hours and H_2O_2 (300 nmol/L for 2 hours) and then lysed. p21 expression was evaluated by Western blotting. Blots are representative of three independent experiments showing similar results. The graph shows average densitometric values of p21 protein normalized for HSP90 content. *, $P < 0.05$; **, $P < 0.01$; ***, $P < 0.001$.

cellular senescence, ERK5 inhibition significantly impacted oxidative stress induced senescence and the SASP. In this respect, ERK5 had been previously reported to be activated in colorectal adenocarcinoma cells undergoing methotrexate-induced senescence (37). We demonstrated the occurrence of cellular senescence by showing that both genetic and pharmacologic inhibition of ERK5 determined a marked increase of SA-βGal positivity in melanoma cells harboring wild-type or oncogenic BRAF, as well as of cellular area and of SAHF. In addition, we found that the expression of a number of genes known to regulate cell cycle and cellular senescence, including CDC25a, RBL-1, p27, and p53, was altered upon ERK5 KD.

Cellular senescence upon ERK5 inhibition was also demonstrated *in vivo*. Indeed, in A375 and SSM2c xenografts, ERK5 KD determined a robust increase of lipofuscin, an indicator of cellular senescence *in vivo* (28). More importantly in view of a possible translation to the clinics, similar effects were observed in melanoma xenografts of XMD8-92–treated mice. The occurrence of a block of cell-cycle progression, an event invariably linked to cellular senescence (16), was supported by the fact that ERK5-KD cells underwent an accumulation in G_0–G_1 or G_2–M phase, depending on the cell line, and cells treated with XMD8-92 showed reduced ability to respond to mitogens and did not form colonies upon replating. Consistently, ERK5 inhibition determined a reduction of RB phosphorylation and cyclin protein levels, as well as an increase of p21 protein. This CDKi was identified as a prominent player of ERK5-dependent cellular senescence. Indeed, the amount of p21 protein was increased following ERK5 pharmacologic inhibition, whereas p21 genetic inhibition reverted the prosenescence effect of XMD8-92 treatment. While the involvement of p21 in ERK5-mediated biological effects has been widely reported (21, 38), the role of p21 in ERK5-mediated cellular senescence is a novel finding.

Cellular senescence may be accompanied by the SASP, which consists of secretion of a number of soluble factors in the surrounding microenvironment. SASP determines both beneficial and deleterious biological outcomes, which makes of senescence a double-edged sword with respect to cancer onset and development (32, 39). In this work, we identified a number of SASP-related chemokines, including CXCL1, CXCL8, and CCL20, that are markedly increased in CM of ERK5-KD cells undergoing cellular senescence. Our data showed that these CM markedly reduced the viability of melanoma cells, and that the treatment with neutralizing antibodies for each of the above chemokines rescued the proliferation of melanoma cells. In this respect, despite the growth-promoting functions of CXCL8, CXCL1, and CCL20 reported so far (40–44) may appear in contrast with the

Published OnlineFirst November 19, 2021; DOI: 10.1158/0008-5472.CAN-21-0993

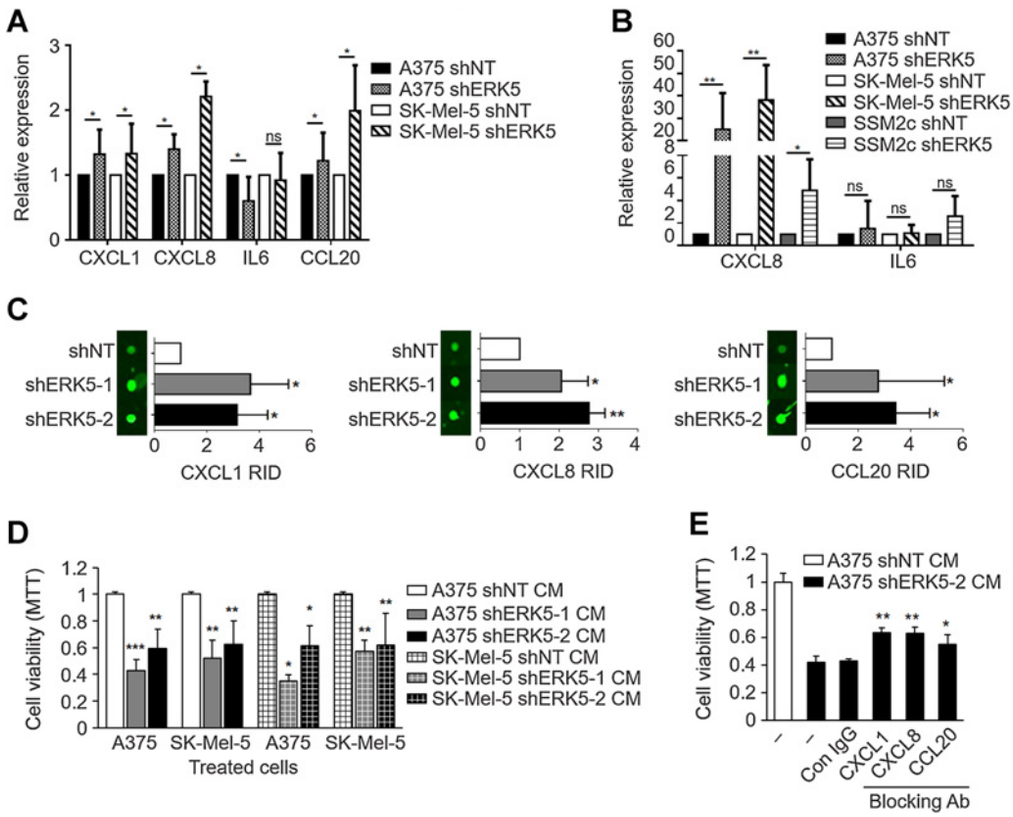

Figure 7.

ERK5 KD increases SASP soluble factors. **A,** mRNA expression profiles were determined using TAC software. Data shown for shERK5 are mean (±SD) of pulled data from shERK5–1 and shERK5–2 (A375, $n = 4$; SK-Mel-5, $n = 3$). *, $P < 0.05$ as determined using one-way ANOVA. **B,** CXCL8 and IL6 mRNA levels determined by qPCR in ERK5 KD cells. Data shown for shERK5 are mean (±SD) of pulled data from shERK5–1 and shERK5–2 (A375, $n = 6$; SK-Mel-5, $n = 6$). **C,** Chemokines expression in CM from ERK5-KD (shERK5–1 and shERK5–2) A375 cells was analyzed using Quantibody Human Array (#QAA-CUST-SW; RayBiotech). Each antigen was measured in quadruplicate from three independent experiments and the relative fluorescence intensity (RID) was determined using ImageJ software (NIH). The obtained results were normalized for protein content in cell lysates. Data shown are mean ± SD. Representative fluorescent dots are shown. **D,** MTT was performed in A375 or SK-Mel-5 cells treated with CM harvested from A375 or SK-Mel-5 cells 14 days posttransduction with shNT or shERK5 (shERK5–1 or shERK5–2) lentiviral vectors. Data shown are mean ± SD from three independent experiments. **E,** MTT was performed on A375 cells treated with CM harvested from shNT (white column) or shERK5–2 (dark columns) A375 cells in the presence of 10 μg/mL of the indicated blocking antibodies or control IgG. Data shown are mean ± SD from three independent experiments. *, $P < 0.05$; **, $P < 0.01$; ***, $P < 0.001$ as determined by Student t test. ns, nonsignificant.

antiproliferative effects elicited by CM from ERK5-KD cells, it has been demonstrated that senescent cells may activate a self-amplifying secretory network in which CXCR2-binding chemokines (i.e., CXCL1 and CXCL8) reinforce growth arrest (45). As regard the link between ERK5 inhibition and SASP occurrence, multiple different nuclear and cytoplasmic factors have been shown to trigger SASP, including chromatin remodeling and SAHF formation. In this respect, it is worth pointing out that ERK5 KD determined a profound remodeling of the mRNA levels of a number of histone variants, as well as SAHF increase. However, the molecular mechanism linking ERK5 KD to chemokine regulation remains to be investigated.

Another relevant finding of our study is the identification of prosenescence drugs that may be exploited for cancer treatment. Indeed, XMD8-92, JWG-045, and JWG-071 elicited robust senescence in melanoma cells. The fact that XMD8-92, extensively showed to reduce tumor growth *in vitro* and *in vivo* (8), has off-target effects (46) does not reduce the possibility to exploit this small-molecule inhibitor as a prosenescence drug. Interestingly, the prosenescence effect of XMD8-92 was increased when used in combination with vemurafenib, that we found able to induce senescence in melanoma cells, in keeping with a previous report (47). Thus, combined targeting of BRAF and ERK5, besides reducing tumor growth more efficiently than single treatments (15), supports prosenescent signals. These effects are in line with the well-established fact that, either chemo and radio, as well as targeted therapies engage a senescence response as part of the outcome (13). However, if this combination is more effective in preventing resistance mechanisms with respect to BRAF/MEK inhibitors alone remains to be investigated.

Authors' Disclosures

No disclosures were reported.

Authors' Contributions

A. Tubita: Data curation, formal analysis, investigation, writing–original draft, writing–review and editing. **Z. Lombardi:** Data curation, formal analysis, investigation, methodology, writing–original draft, writing–review and editing. **I. Tusa:** Data curation, formal analysis, supervision, writing–original draft, writing–review and editing. **A. Lazzeretti:** Formal analysis, methodology. **G. Sgrignani:** Formal analysis. **D. Papini:** Formal analysis. **A. Menconi:** Formal analysis. **S. Gagliardi:**

Published OnlineFirst November 19, 2021; DOI: 10.1158/0008-5472.CAN-21-0993

Investigation. **M. Lulli:** Data curation, investigation. **P. Dello Sbarba:** Resources, writing–review and editing. **A. Esparís-Ogando:** Resources, writing–review and editing. **A. Pandiella:** Resources, writing–review and editing. **B. Stecca:** Investigation, writing–review and editing. **E. Rovida:** Conceptualization, resources, data curation, formal analysis, supervision, funding acquisition, investigation, writing–original draft, project administration, writing–review and editing.

Acknowledgments

The work in E. Rovida's lab was supported by grants from Associazione Italiana per la Ricerca sul Cancro (AIRC, IG-15282 and IG-21349), by Ente Fondazione Cassa di Risparmio di Firenze (ECRF), and Università degli Studi di Firenze (Fondo di Ateneo ex-60%). A. Tubita was supported by a "Carlo Zanotti" Fondazione Italiana per la Ricerca sul Cancro (FIRC)-AIRC fellowship (ID-23847).

The costs of publication of this article were defrayed in part by the payment of page charges. This article must therefore be hereby marked *advertisement* in accordance with 18 U.S.C. Section 1734 solely to indicate this fact.

Received April 10, 2021; revised October 6, 2021; accepted November 15, 2021; published first November 19, 2021.

References

1. Balch CM, Gershenwald JE, Soong SJ, Thompson JF, Atkins MB, Byrd DR, et al. Final version of 2009 AJCC melanoma staging and classification. J Clin Oncol 2009;27:6199–06.
2. Hodis E, Watson IR, Kryukov GV, Arold ST, Imielinski M, Theurillat JP, et al. A landscape of driver mutations in melanoma. Cell 2012;150:251–63.
3. Cohen ED, Mariol MC, Wallace RMH, Weyers J, Kamberov YG, Pradel J, et al. DWnt4 regulates cell movement and focal adhesion kinase during drosophila ovarian morphogenesis. Dev Cell 2002;2:437–48.
4. Chapman PB, Hauschild A, Robert C, Haanen JB, Ascierto P, Larkin J, et al. Improved survival with vemurafenib in melanoma with BRAF V600E mutation. N Engl J Med 2011;364:2507–16.
5. Samatar AA, Poulikakos PI. Targeting RAS-ERK signalling in cancer: promises and challenges. Nat Rev Drug Discov 2014;13:928–42.
6. Tubita A, Tusa I, Rovida E. Playing the whack-a-mole game: ERK5 activation emerges among the resistance mechanisms to RAF-MEK1/2-ERK1/2- targeted therapy. Front Cell Dev Biol 2021;9:647311.
7. Drew BA, Burow ME, Beckman BS. MEK5/ERK5 pathway: the first fifteen years. Biochim Biophys Acta 2012;1825:37–48.
8. Stecca B, Rovida E. Impact of ERK5 on the hallmarks of cancer. Int J Mol Sci 2019;20:1426.
9. Gomez N, Erazo T, Lizcano JM. ERK5 and cell proliferation: nuclear localization is what matters. Front Cell Dev Biol 2016;22; 4:105.
10. Tubita A, Lombardi Z, Tusa I, Dello Sbarba P, Rovida E. Beyond kinase activity: ERK5 nucleo-cytoplasmic shuttling as a novel target for anticancer therapy. Int J Mol Sci 2020;21:938.
11. Campisi J. Cellular senescence as a tumor-suppressor mechanism. Trends Cell Biol 2001;11:S27–31.
12. Acosta JC, Gil J. Senescence: a new weapon for cancer therapy. Trends Cell Biol 2012;22:211–9.
13. Nardella C, Clohessy JG, Alimonti A, Pandolfi PP. Pro-senescence therapy for cancer treatment. Nat Rev Cancer 2011;11:503–11.
14. Gray-Schopfer V, Wellbrock C, Marais R. Melanoma biology and new targeted therapy. Nature 2007;445:851–7.
15. Tusa I, Gagliardi S, Tubita A, Pandolfi S, Urso C, Borgognoni L, et al. ERK5 is activated by oncogenic BRAF and promotes melanoma growth. Oncogene 2018; 37:2601–14.
16. Muñoz-Espín D, Serrano M. Cellular senescence: from physiology to pathology. Nat Rev Mol Cell Biol 2014;15:482–96.
17. Anerillas C, Abdelmohsen K, Gorospe M. Regulation of senescence traits by MAPKs. Geroscience 2020;42:397–408.
18. Giard DJ, Aaronson SA, Todaro GJ, Arnstein P, Kersey JH, Dosik H, et al. In vitro cultivation of human tumors: establishment of cell lines derived from a series of solid tumors. J Natl Cancer Inst 1973;51:1417–23.
19. Carey TE, Takahashi T, Resnick LA, Oettgen HF, Old LJ. Cell surface antigens of human malignant melanoma: mixed hemadsorption assays for humoral immunity to cultured autologous melanoma cells. Proc Natl Acad Sci U S A 1976;73: 3278–82.
20. Pandolfi S, Montagnani V, Penachioni JY, Vinci MC, Olivito B, Borgognoni L, et al. WIP1 phosphatase modulates the hedgehog signaling by enhancing GLI1 function. Oncogene 2013;32:4737–47.
21. Yang Q, Deng X, Lu B, Cameron M, Fearns C, Patricelli MP, et al. Pharmacological inhibition of BMK1 suppresses tumor growth through promyelocytic leukemia protein. Cancer Cell 2010;18:258–67.
22. Tatake RJ, O'Neill MM, Kennedy CA, Wayne AL, Jakes S, Wu D, et al. Identification of pharmacological inhibitors of the MEK5/ERK5 pathway. Biochem Biophys Res Commun 2008;377:120–5.
23. Rovida E, Spinelli E, Sdelci S, Barbetti V, Morandi A, Giuntoli S, et al. ERK5/BMK1 is indispensable for optimal colony-stimulating factor 1 (CSF-1)-induced proliferation in macrophages in a src-dependent fashion. J Immunol 2008;180: 4166–72.
24. Barbetti V, Morandi A, Tusa I, Digiacomo G, Riverso M, Marzi I, et al. Chromatin-associated CSF-1R binds to the promoter of proliferation-related genes in breast cancer cells. Oncogene 2014;33:4359–64.
25. Rovida E, Di Maira G, Tusa I, Cannito S, Paternostro C, Navari N, et al. The mitogen-activated protein kinase ERK5 regulates the development and growth of hepatocellular carcinoma. Gut 2015;64:1454–65.
26. Barbetti V, Tusa I, Cipolleschi MG, Rovida E. Dello sbarba P. AML1/ETO sensitizes via TRAIL acute myeloid leukemia cells to the pro-apoptotic effects of hypoxia. Cell Death Dis 2013;4:e536.
27. Zhao J, Fuhrmann-Stroissnigg H, Gurkar AU, Flores RR, Dorronsoro A, Stolz DB, et al. Quantitative analysis of cellular senescence in culture and *in vivo*. Curr Protoc Cytom 2017;79:9.51.1–9.51.25.
28. Georgakopoulou EA, Tsimaratou K, Evangelou K, Fernandez Marcos PJ, Zoumpourlis V, Trougakos IP, et al. Specific lipofuscin staining as a novel biomarker to detect replicative and stress-induced senescence. a method applicable in cryo-preserved and archival tissues. Aging 2013;5: 37–50.
29. Evangelou K, Gorgoulis VG. Sudan black B, the specific histochemical stain for lipofuscin: a novel method to detect senescent cells. Methods Mol Biol 2017;1534: 111–9.
30. Wang J, Erazo T, Ferguson FM, Buckley DL, Gomez N, Muñoz-Guardiola P, et al. Structural and atropisomeric factors governing the selectivity of pyrimido-benzodiazipinones as inhibitors of kinases and bromodomains. ACS Chem Biol 2018;13:2438–48.
31. Williams CA, Fernandez-Alonso R, Wang J, Toth R, Gray NS, Findlay GM. Erk5 is a key regulator of naive-primed transition and embryonic stem cell identity. Cell Rep 2016;16:1820–8.
32. Coppé JP, Desprez PY, Krtolica A, Campisi J. The senescence-associated secretory phenotype: the dark side of tumor suppression. Annu Rev Pathol 2010;5:99–118.
33. Coppé JP, Patil CK, Rodier F, Sun Y, Muñoz DP, Goldstein J, et al. Senescence-associated secretory phenotypes reveal cell-nonautonomous functions of oncogenic RAS and the p53 tumor suppressor. PLoS Biol 2008;6:2853–68.
34. Cerami E, Gao J, Dogrusoz U, Gross BE, Sumer SO, Aksoy BA, et al. The cBio cancer genomics portal: an open platform for exploring multidimensional cancer genomics data. Cancer Discov 2012;2:401–4.
35. Gao XJ, Potter CJ, Gohl DM, Silies M, Katsov AY, Clandinin TR, et al. Specific kinematics and motor-related neurons for aversive chemotaxis in drosophila. Curr Biol 2013;23:1163–72.
36. Van Allen EM, Miao D, Schilling B, Shukla SA, Blank C, Zimmer L, et al. Genomic correlates of response to CTLA-4 blockade in metastatic melanoma. Science 2015;350:207–1.
37. Dabrowska M, Skoneczny M, Rode W. Functional gene expression profile underlying methotrexate-induced senescence in human colon cancer cells. Tumour Biol 2011;32:965–76.
38. Perez-Madrigal D, Finegan KG, Paramo B, Tournier C. The extracellular-regulated protein kinase 5 (ERK5) promotes cell proliferation through the down-regulation of inhibitors of cyclin dependent protein kinases (CDKs). Cell Signal 2012;24:2360–8.
39. Wang B, Kohli J, Demaria M. Senescent cells in cancer therapy: friends or foes? Trends Cancer 2020;6:838–57.

40. Green D, Eyre H, Singh A, Taylor JT, Chu J, Jeys L, et al. Targeting the MAPK7/MMP9 axis for metastasis in primary bone cancer. Oncogene 2020;39:5553–69.
41. Finegan KG, Perez-Madrigal D, Hitchin JR, Davies CC, Jordan AM, Tournier C. ERK5 is a critical mediator of inflammation-driven cancer. Cancer Res 2015;75:742–53.
42. Pereira DM, Gomes SE, Borralho PM, Rodrigues CMP. MEK5/ERK5 activation regulates colon cancer stem-like cell properties. Cell Death Discov 2019;5:68.
43. Bar-Eli M. Role of interleukin-8 in tumor growth and metastasis of human melanoma. Pathobiology 1999;67:12–18.
44. Samaniego R, Gutiérrez-González A, Gutiérrez-Seijo A, Sánchez-Gregorio S, García-Giménez J, Mercader E, et al. CCL20 expression by tumor-associated macrophages predicts progression of human primary cutaneous melanoma. Cancer Immunol Res 2018;6:267–75.
45. Acosta JC, O'Loghlen A, Banito A, Guijarro MV, Augert A, Raguz S, et al. Chemokine signaling via the CXCR2 receptor reinforces senescence. Cell 2008;133:1006–18.
46. Lin EC, Amantea CM, Nomanbhoy TK, Weissig H, Ishiyama J, Hu Y, et al. ERK5 kinase activity is dispensable for cellular immune response and proliferation. Proc Natl Acad Sci U S A 2016;113:11865–70.
47. Haferkamp S, Borst A, Adam C, Becker TM, Motschenbacher S, Windhövel S, et al. Vemurafenib induces senescence features in melanoma cells. J Invest Dermatol 2013;133:1601–9.

Published OnlineFirst November 19, 2021; DOI: 10.1158/0008-5472.CAN-21-0993

Cancer Research
The Journal of Cancer Research (1916–1930) | The American Journal of Cancer (1931–1940)

AACR American Association for Cancer Research

Inhibition of ERK5 Elicits Cellular Senescence in Melanoma via the Cyclin-Dependent Kinase Inhibitor p21

Alessandro Tubita, Zoe Lombardi, Ignazia Tusa, et al.

Cancer Res 2022;82:447-457. Published OnlineFirst November 19, 2021.